Design and Simulation of a Circulating Tumor Cell Detector

by

Zhixi Qian

A dissertation submitted to the Graduate Faculty of
Auburn University
in partial fulfillment of the
requirements for the Degree of
Doctor of Philosophy

Auburn, Alabama
May 8, 2016

Keywords: magnetic cell separation, circulating tumor cell, Fluent, point-of-care device

Copyright 2016 by Zhixi Qian

Approved by

Thomas Hanley, Chair, Professor of Chemical Engineering
Allan David, Professor of Chemical Engineering
Robert Chambers, Professor of Chemical Engineering
Mark Byrne, Professor of Chemical Engineering
Paul Todd, Professor in Techshot

Abstract

Recent advances in magnetic cell selection have enhanced the possibility of isolating cells of interest from mixtures. The detection of fetal cells in maternal blood, circulating stem cells and circulating tumor cells will soon be a technology that can be transferred to point-of-care (POC) diagnosis. As a component of a POC portable rare cell analyzer a three-stage magnetic trap for magnetically labeled rare cells was designed and tested. The trap design consists of a pair of horizontal flow channels with three bends and a permanent magnet positioned at the outer curve of each bend. Magnetic labeling of cells entering the trap is performed by the automated addition of sample and reagent into a static mixer coupled directly to the inlet of the trap. Findings are reported on the computational fluid dynamic analysis of the design, testing with model commercial magnetic beads used in cell labeling, and testing with cultured lymphoma cells immunomagnetically labeled in the presence of whole blood. The computational results provide cell flow data along stream lines as a function of position in the trap. The measurements of field profiles of the magnets were used to determine forces applied as a function of position in the trap. Testing with 3.27 μm diameter standard magnetic beads (Seragen) indicated that at least 99.998% of these strongly magnetic particles are captured within the trap, most in the first stage at a flow rate of 1.0 ml/min. The laboratory test used Bursa Lymphoma of Chicken (Gallus gallus) as target cell, and the coupled labeling and separation test proved the device is able to label and separate the target cells from whole blood. The test proved the static mixer has at least equal labeling performance to a standard shaker table used in laboratories, and the magnetic trap captured 60-80% of labeled cell input. Thus, the combined device was demonstrated to be effective in cell magnetic labeling and separation.

Acknowledgments

First, I should sincerely thank my advisor, Dr. Thomas R. Hanley, as he provided great help and support all the time. Also, I should thank Dr. Paul W. Todd (Techshot) for his support on the model set up and calculation. Dr. Todd provides a lot of helpful materials for my project. I also thank Dr. Gene Boland (Techshot) for his support in my laboratory work.

I also would like to thank Mr. Byron Guernsey (IKOTECH) for supporting the magnetophoretic mobility measurements, Mr. Sam Logan (Techshot) for design and construction of the magnetic trap, Lisa Reece (Purdue) for assisting me in maintaining and preparing the melanoma cells and Drs. Rungkiet Kamondetdacha and John Nyenhuis (Purdue) for providing data that formed the basis for Figure 3.3.

I should thank Bobby Holland (Techshot) for his support of my laboratory work and daily life. I should thank Dr. Zhongliang Lu, as he gave me a lot of help in my life working in Indiana. Lastly, I will give my sincere thanks to my family and Yinyin. I'm proud of you!

This research was supported by the U. S. Department of Health and Human Services, the National Institutes of Health, the National Cancer Institute Small Business Innovation Research (SBIR) contract HHSN261201000067C to Techshot, Inc. and by Auburn University.

Table of Contents

List of Figures

List of Tables

Chapter 1

Introduction

Cancer is the second major cause of death in the United States. In 2015, about 589,430 Americans are expected to die of cancer, or about 1,620 people per day.[3] One in six Americans develops skin cancer at some point. Skin cancer accounts for one third of all cancers in the United States. Among cancers, melanoma is responsible for the most deaths of all skin cancers, with nearly 9,000 people dying from it each year [61]. It is also one of the most common types of cancer among U.S. adolescents and young adults. Annually, about $3.3 billion of skin cancer treatment costs are attributable to melanoma.

Early detection is a key issue in cancer treatment, greatly reducing the cost of treatment and increasing the life expectancy of patients. Detecting a circulating tumor cell (CTC) in blood samples would greatly improve both diagnosis and early cancer treatment, as the cancer cells can be identified and characterized before they spread beyond the tissue of origin. Two major types of separation is used today. Immune affinity capture method is based on interaction between antibody and antigen to capture target cells, and magnetic capture method is based on magnetophoretic force applied on particles. The magnet capture method proves to be economical, effective and widely applicable to other cells.

However, early detection today is both difficult and expensive. Today CTC detection requires complex, expensive equipment as well as highly trained technicians to perform and interpret the analysis. Current CTC detection is limited to a few laboratories and is inadequate to meet current needs, considering the large number of patients each year.

A point-of-care CTC detection device that is both accurate and affordable would greatly improve early cancer detection. This device should be capable of providing accurate results

quickly using low cost analytical reagents and minimally trained technical support. Ideally, patients could be tested in any location with results available in a matter of hours.

The primary objective of this research is to design, simulate and test an accurate, cost-effective, user-friendly point-of-care CTC detection device. The preliminary design includes three syringes for sample, buffer and reagents, a static mixer, a magnetic filter, a microfluidic "chip" and a waste receptor. The device is smaller and cheaper than traditional detection devices. Also, device operation is easier with only one operator required. The device can be used in clinics, nursing homes or residences allowing earlier detection of most fatal cancers, including pancreatic cancer, ovarian cancer and melanoma.

Specifically, this research employs computational fluid dynamics (CFD) software to

- simulate flow patterns in the static mixer. This analysis includes the mixing of the blood sample, buffer and reagents as well as the effects of Reynolds number and fluid viscosity,

- simulate flow patterns in the magnetic filter, incorporating magnetic particle mobilities and reaction kinetics, results of the simulations direct the optimization of the design of the static mixer and the magnetic filter.

Results of the simulations direct the optimization of the design of the static mixer and the magnetic filter.

Laboratory experiments using blood samples with CTC's present are employed to verify the effectiveness of the device over a range of operating conditions to develop protocols for future application.

Chapter 2

Literature Review

2.1 Abstract

The concept of early detection finding tumors early, before they spread and become incurable has tantalized cancer-control researchers for many years. Until now, a few early-detection approaches have proven sufficiently effective and practical for mass use. Recent advances in genomics have altered the landscape of early detection, promising to vastly expand the pool of potentially useful screening tests. (Etzioni etc. al 2007)[1].

Meanwhile, although advances in conventional diagnostic strategies have provided some improvements in the detection of disease, they still do not reach the sensitivity and specificity that are needed to reliably detect early-stage disease. In many cases, cancer is not diagnosed and treated until cancer cells have already invaded surrounding tissues and metastasized throughout the body. Over 60 per cent of patients with breast, lung, colon and ovarian cancer have hidden or overt metastatic colonies at presentation and most conventional therapeutics are limited in their success once a tumor has spread beyond the tissue of origin. (Wulfkuhle et al. 2003)[2]

For the improvement of cancer's early detection, the appliance of point-of-care devices will help in expand the coverage of general population. Local clinics and neighborhood health centers would be essential sites for early cancer indicators. These institutions, however, lack both complex and expensive analytical devices as well as qualified technicians. To expand early detection's coverage, testing would have to be inexpensive and well accepted by the population targeted for screening.

A fully-functional circulating tumor cell (CTC) detection system requires biomarkers to ensure the targeted CTCs be marked, a separation system using various techniques (magnetic

separation, for example) to separate CTCs from other cells and a detection system to identify and count the CTCs in the sample. Researchers' work is to develop and optimize such a system.

2.2 Background information

2.2.1 CTCs and cancer development

In medical field, people use different stages to express the size and extension of the tumor. The development of prostate cancer is a typical example. In stage 1, tumors are so small that they can't be detected during a digital rectal exam (DRE) or seen with imaging such as trans-rectal ultrasound. In stage 2 tumors can be detected during a DRE but appear to be confined to the prostate gland. In stage 3 tumors have begun to grow and spread outside the prostate and may involve the seminal vesicles. During this stage the CTCs would be released into blood flow. In stage 4 tumors have grown into tissues next to the prostate (other than the seminal vesicles). Patients with stage 3 tumors have AJCC Stage III (regional stage disease) and those with stage 4 tumors are considered to have AJCC Stage IV (distant stage disease). [3]

Recent research has indicated that CTCs have important clinical implications and can serve as new diagnostic, prognostic and predictive markers. Gallagher et al. (2009)[4] discussed the detection of metastatic urothelial cancer cells. The author used the CellSearch^{tm} System to check the patient's peripheral blood sample. As a result, the CTC evaluations were carried out in 33 patients with metastatic urothelial cancer. In the test, 14 of 33 patients (44 per cent; 95 per cent confidence interval 27 per cent to 59 per cent) had a positive assay (range 0 to 87 cells/7.5 ml of blood) with 10 patients (31 per cent) having five or more CTCs. The results indicated that CTCs can be utilized for early detection of urothelial cancer.

Antibodies are widely used for the detection of CTCs. Wang etc. al (2012) [12] studied on the detection of CTCs among breast cancer (BC) patients, as well as to explore their

clinical relevance. CTCs can be selected first with the fluorescent antibody against CD45 to delete the contamination of leukocytes. Following that, fluorescent antibody targeted at EPCAM (epithelial-cell adhesion molecule) was used to select EPCAM positive cells. CTCs were CD45 negative and EPCAM positive cells. The authors used estrogen receptor (ER) as a reference; during the test they found that CTC levels were statistically relevant to histology stages, ER status and PR status. In summary, ER could potentially be a new maker for CTCs' detection.

Cohen et al. (2008) [5] studied the relationship between CTCs and tumor response. In a multi-center study, CTCs were enumerated in the peripheral blood of 430 patients with metastatic colorectal cancer at baseline and after starting first, second, or third-line therapy. The patients were stratified into unfavorable and favorable prognostic groups based on CTC levels of three or more or less than three CTCs/7.5 mL, respectively. A comparison of the groups indicated that unfavorable patients had shorter median progression-free survival (PFS; 4.5 versus 7.9 months; P = 0.0002) and overall survival (OS; 9.4 versus 18.5 months; P <0.0001). Differences persisted at 1 to 2, 3 to 5, 6 to 12, and 13 to 20 weeks after therapy. Conversion of baseline unfavorable CTCs to favorable at 3 to 5 weeks was associated with significantly longer PFS and OS compared with patients with unfavorable CTCs at both time points (PFS, 6.2 versus 1.6 months; P=0.02; OS, 11.0 v 3.7 months; P = 0.0002). Among non-progressing patients, favorable compared with unfavorable CTCs within one month of imaging was associated with longer survival (18.8 v 7.1 months; P <0.0001). Baseline and follow-up CTC levels remained strong predictors of PFS and OS after adjustment for clinically significant factors.

Fan et al. (2009) [6] evaluated the association of invasive CTCs with the disease stage. 71 patients were undergoing evaluation for ovarian malignancy. Tumor cells were labeled by a Cell Adhesion Matrix (CAM) and distinguished from non-tumor and non-viable cells. According to the survey, 43 (60.6 per cent) patients had detectable CTCs: 0/5 benign patients, 1/10 (10 per cent) early stage, 39/52 (73.1 per cent) late stage and 3/4 (75 per

cent) unstaged patients (p-value = 0.001). CTC counts ranged from 0 to 149 CTCs/ml with stage III/IV patients exhibiting significantly higher mean counts (41.3 CTCs/ml) than stage I/II patients (6.0 CTCs/ml) and benign patients (0 CTCs/ml, p-value = 0.001).

Allard et al. (2004) [7] reported a survey of CTC system's accuracy, precision, and linearity. They applied a cell search system checking the blood samples from 199 patients with nonmalignant diseases, 964 patients with metastatic carcinomas, and 145 healthy donors. The research used the CellSearch^{tm} system (Veridex LLC) as the detection platform. The CellSearch^{tm} system consisted of a CellPrep system, a CellSearch Epithelial Cell Kit, and a CellSpotter Analyzer. According to the report, none of the healthy women and only one woman with a nonmalignant disease were found to have elevated CTCs, giving a specificity of 99.7 per cent. In contrast, the number of CTCs in their survey of metastatic cancer patients ranged from 0 to 23,618, indicating the potential of CTC identification for cancer's early detection.

Pachmann (2008) [8] focused on a specific CTC called circulating epithelial tumor cells (CETC), which proved to be a helpful indicator cell. In 25 consecutive non-metastatic primary breast cancer patients adjutant Xuorouracil/epirubicin/cyclophosphamid (FEC) or EC followed by taxane (EC-T) or cyclophosphamid/methotrexate/Xuorouracil (CMF) therapy were given. Circulating epithelial tumor cells (CETC) were quantified before and after each second cycle of the therapy regimen, between the anthracycline and the taxane block of the regimen and in some cases repeatedly during CMF treatment. The report indicated a high correlation between the response of CETC to therapy and relapse ($p < 0.0001$). Curves of both patient groups were super imposable. Multivariate analysis revealed the response of CETC to therapy to be an independent predictive marker for relapse.

Lustburg's group (2012)[9] designed a prospective trial to characterize CTCs as well as other circulating cell populations in blood samples from women with metastatic breast cancer without EpCAM-dependent enrichment and/or isolation technology. : A total of 32 patients with metastatic breast cancer were enrolled, and blood samples were processed

using a previously described negative depletion immunomagnetic methodology. The result showed that metastatic breast cancer patients have CTCs circulating in their blood.

Yukako et al. (2016)[10] analyzed CTCs in metastatic breast cancer (MBC) patients and With a CTC cut-off value of 1, there were 53 (54.1 %) CTC-negative patients and 45 (45.9 %) CTC-positive patients. Patients in the CTC-positive group had worse survival than those in the CTC-negative group ($p< 0.0001$). The researcher found that a CTC cut-off value of 1 is appropriate in patients with advanced/metastatic breast cancer, and CTCs proved to be a useful early signal for cancer detection.

The rapid evolution of new and more reliable technology combined with an increasingly expanding array of potential markers makes it likely that the field of molecular diagnostics of cancer is going to continue to expand. At long-term study, these advances will probably impact the way that we understand, diagnose, and treat cancer in ways that we are only beginning to understand and foresee. Despite the tantalizing potential of these diagnostic tools, it is clear for each that further work is needed to establish reproducible assays that allow for accurate detection prior to application in the patient care arena. Long-term prospective studies with large patient enrollments are ongoing and have the potential to address some of the initial clinical questions. (Baker et al. 2003) [11]

All these studies proved the relationship between CTCs and tumors, the level of CTCs in blood can predict the cancer progress. As tumor cells begin to circulating in body, the detaching CTCs would flow along blood vessels and thus be able to function as a predictor of cancer development.

2.3 Methods for CTC capture and separation

Several methods have been developed for the detection of CTCs. Reverse transcriptase polymerase chain reaction (RT-PCR) is a commonly used one. During the process, a RNA strand is reverse transcribed into its DNA complement (complementary DNA, or cDNA) using the enzyme reverse transcriptase, and the resulting cDNA is amplified using PCR.

Bossolasco et al. (2002)[13] used RT-PCR detected the CTCs in bone marrow and peripheral blood. The specificity of the RT-PCR used in this study was tested by examining myeloid (K562, AR230, KG1a, RWLeu4, HL60) and lymphoid (Jurkat J6, Daudi, TK6TGR) leukemia cell lines, samples from healthy donors and samples from patients with diseases. The positive cases included 23.6 per cent of the patients with and 9 per cent of those without metastasis. Only 4 of 60 negative controls analyzed were positive by PCR. Results showed high specificity and a good correlation with disease status.

New systems have been put into practical use. Recent technical advancements in CTC detection and characterization include three types: image-based approaches like classic immunocytochemistry (ICC), such as the CellSearch$^{\text{tm}}$ system (Veridex), the Ariol system, and laser-scanning cytometry. Imaging approaches are based on the characterization of isolated cells as CTCs through fluorescently labeled antibodies mainly against epithelial antigens such as CK-19. A limited number of other protein markers have also been used for this reason.

Another system is molecular assays based on nucleic acid analysis of CTCs, such as the highly sensitive RT-qPCR methods, multiplex reverse transcription PCR (RT-PCR) assays, or a combination of molecular and imaging methods; molecular assays are based mainly on the analysis of gene expression in CTCs. The third type is a protein-based assay like the EpiSpot assay, which will detect tumor-specific proteins released by CTCs. By use of these two approaches the presence of a small number of CTCs can be shown through the highly sensitive detection of epithelial markers such as CK-19 in the presence of millions of peripheral blood mononuclear cells. However, it's only able to detect whether CTCs exists or not, and the number of CTCs contains in sample can't be evaluated.

A challenge today is the force analyze of nanoparticles used during the cell detection process. Ruan et al. (2010)[20] discussed the controlled motion of nanomaterials. The authors divided the factors affecting particle motions to two critical features in controlled motion of nanomaterials are providing a sufficient force for movement and a visualization scheme to

track that motion. They demonstrated a "nano-conveyer-belt" technology that permited simultaneous transport and tracking of multiple individual nanospecies in a selected direction. The technology consisted of two components: nanocontainers, which encapsulate the nanomaterials transported, and nanoconveyer arrays, which used magnetic force to manipulate individual or aggregate nanocontainers.

Recently, there has been interest in using techniques that take advantage of similar scales of microscale technologies and intrinsic properties of cells for increased automation and decreased cost. The area with the potential for improved, cost-effective biomedicine are discussed. To detect the development of cancer, varies of detection methods have been applied. A simple approach for detection is based on the physical properties of the CTCS.

One established method for the collection of CTCs is sucrose or CsCl density gradient centrifugation (DGC) which relies on the physical characteristics of density and size to separate mononuclear cells and CTCs which have a density of less than 1.077 g/ml, from red blood cells, and granulocytes, which have a density greater than 1.077 g/ml. However, as the cell's density difference is not significant, the efficiency of separation is unsatisfying.([95])

Zhou's research group (2015)([96]) provides a good alternative method in cell separation. A key issue is separation of cells in a steamline. With the adjustment of devices, force applied on target cells will separate tumor cells from others. It can be a simple, fast, efficient, sensitive, and reproducible method. However, the specificity of the system was hampered by the fact that the tumor cell's expression pattern was varied making it difficult to find a universal cell marker.

In conclusion, all studies required a highly-sensitive CTC detection method. Recent CTC detection technology still requires further improvement.

2.3.1 Immune affinity capture methods

CTCs can be separated from normal blood cells based on surface markers. Immune affinity capture methods, or affinity mediated immunoassays, are first demonstrated by coating

the microparticle with anti-EpCAM antibodies. A well-designed device can increase the separation efficiency.

The presence of tumor cells in the bone marrow was first identified using conventional imaging techniques. Building on this work, detecting tumor cells in the circulation was attempted using simple hematoxylin and eosin staining. This exhaustive method consisted of visually identifying large numbers of gradient-separated cells and comparing them with primary tumor cells morphologically. Cytometric methods isolated and enumerated individual cells based on their antigen expression, using, for example, monoclonal antibodies directed against epithelium-specific antigens.

Molloy et al.(2011) [21] developed a multimarker QPCR-based platform which utilizes a panel of four tumor marker genes: cytokeratin 19 (CK19), human secretory protein p1.B (p1B), human epithelial glycoprotein (EpCAM; here: EGP) and mammaglobin (MmGl). In this study, the author used an improved platform for CTC detection in a prospective cohort of patients with early-stage breast cancer in an effort to detect the presence of CTCs at diagnosis. These data were then correlated to disease outcome. In addition, they used the platform in two control groups, advanced breast cancer patients and healthy volunteers . A total of 82 women with early-stage breast cancer were included, and a peripheral blood sample was obtained before surgery and before initiating adjuvant therapy. Circulating tumor cells were detected in 16 of 82 (20%) patients with early-stage breast cancer and in 13 out of 16 (81%) with advanced breast cancer. The specificity was 100%. The median follow-up time was 51 months (range: 1760).

Rosenbach et al. (2011) [22] studied the immune affinity's effect on cell separation. The target cell was a T- Lymphocyte cell which influences the body's initial inflammatory response after the traumatic injuries. They used a quantitative real-time polymerase chain reaction (PCR) measuring the RNA levels of numerous cytokines, including IFN-γ, IL-2, IL-4, and IL-10. From a 0.5-mL whole blood sample, the microfluidic devices captured high purity T lymphocytes from healthy volunteers and burn-injury patients. The primary aim of

this work was to demonstrate the feasibility of T lymphocyte isolation and RNA extraction (suitable for downstream gene-expression analysis) using a microfluidics platform. However, due to the limited sample scale (only 5 patients involved), the number of patients and time points were insufficient to postulate any mechanistic or clinical correlates. A further study with a larger and clinically stratified patient population would be necessary.

Farlow et al. (2010)'s aim is to develop a convenient serum assay capable of unambiguously identifying patients with NSCLC (Nonsmall cell lung cancer) [23], Standard immunoproteomic method was used to assess differences in circulating autoantibodies among lung adenocarcinoma patients relative to cancer-free controls. Candidate autoantibodies identified by these discovery phase studies were translated into Luminex-based "direct-capture" immunobead assays along with 10 autoantigens with previously reported diagnostic value. As a result, thirteen of the 25 analytes tested showed statistical significance (Mann-Whitney P $<.05$ and a receiver operator characteristic "area under the curve" over 0.65) when evaluated against a second patient cohort. Multivariate statistical analyses identified a six-biomarker panel with only a 7% misclassification rate.

Punnoose et al. (2010) [24]focused on CTC applied in cancer focus detection. They developed a CellSearch platform using immunomagnetic beads coated with antibodies to a Epithelial Cell Adhesion Molecule (EpCAM) used for detection of non smallcell lung cancer (NSCLC), prostate cancer and metastatic breast cancer. Researchers used the EpCAM biomarker analysis which proved effective in detection of various types of cancer cells. The system enables CTCs to be present in sufficient numbers to allow molecular characterization in the majority of patients. The authors reported an average CTC count of 0.50 CTC/ml and that 100% of patients across multiple indications showed .5 CTCs/mL of blood, a significantly higher prevalence and number than are typically described for the CellSearch platform. Also, captured cells must be amenable to commonly used biomarker assay formats such as IF, FISH, mutation detection, and qRT-PCR. The authors found that captured CTCs were amenable to quantitative IF scoring for both EGFR and HER2 on the standard

CellSearchH platform, and that the levels of spiked tumor cells isolated from blood were generally reflective of expression levels in the parent cell line.

Stott et al. (2010) [25] developed a microvortex-generating herringbone-chip which provides an enhanced platform for CTC isolation. The microfluidic device was made of PDMS bonded to glass substrates using soft lithography techniques. It consisted of a 1" * 3" glass slide bonded to a polydimethylsiloxane (PDMS) structure, containing eight micro-channels with patterned chevrons or herringbones on their upper surface. Devices were functionalized with epithelial cell adhesion molecule (EpCAM, R and D Systems) antibody using avidin-biotin chemistry. Blood samples from 15 patients at various stages of treatment for metastatic prostate cancer were processed with the HB-Chip. The authors also processed blood from healthy individuals as controls (n = 10). Cells were immunostained with primary antibodies, either a rabbit polyclonal antibody to PSA (DAKO), monoclonal antibody against cytokeratin 7/8 (CAM 5.2 clone, BD Biosciences), or a monoclonal mouse IgG2b antibody to PSMA (Santa Cruz Biotechnology). Following, the appropriately matched secondary AlexaFluor 488-conjugated antibody (Invitrogen) was used to identify epithelial cells. Nuclei were stained with DAPI. All samples were counterstained with mouse IgG1 antihuman anti-CD45 (Clone H130, BD Biosciences), followed by Alexa Fluor 594 fluorophore (Invitrogen) to identify any bound leukocytes.

Shan etc. al (2012) [26] worked on urine-derived human genomic DNA (gDNA)'s extraction using carboxylated magnetic nanoparticles (CMNPs) as solid-phase adsorbents. Adding10 mM EDTA and subsequent pH modification (pH 6.07.1) can re-dissolve urine sediments. Purified gDNA ranged from around 0.1 kb to more than 23 kb. The CMNP gDNA extraction technique proved to be simple, rapid, sensitive and environmentally friendly, with application for routine laboratory use and potentially within automated urine extraction platforms.

Khleif et al. (2010) [27] aim to modernize the drug development process by incorporating new techniques that can predict the safety and effectiveness of new drugs faster, with more

certainty, and at lower cost. Researchers bring together disparate stakeholders to clearly delineate these barriers, to develop recommendations for integrating biomarkers into the cancer drug development enterprise, and to set in motion the necessary action plans and collaborations to see the promise of biomarkers come to fruition, efficiently delivering quality cancer care to patients.

Cho etc al. (2010) [28] discussed the integration of microfluidic selection with high throughput DNA sequencing technology for rapid and efficient discovery of nucleic acid aptamers. As a demonstration, Cho's group have identified aptamers that specifically bind to PDGF-BB protein with Kd $<$ 3 nM within 3 rounds. Furthermore, it's shown that the aptamers identified by Quantitative Selection of Aptamers through Sequencing have $\sim$3-8-fold higher affinity and $\sim$2-4-fold higher specificity relative to those discovered through conventional cloning methods.

Long et al. (2011)[15] reported an envanescent wave DNA-based biosensor for rapid and very sensitive Hg^{2+} detection based on a direct structure-competitive detection mode. A DNA probe covalently immobilized onto a fiber optic sensor contains a short common oligonucleotide sequences that can hybidize with a fluorescently labeled complementary DNA. The DNA probe also comprises a sequence of TT mismatch pairs that binds with Hg^{2+} to form a $THg^{2+}T$ complex by folding of the DNA segments into a hairpin structure. With a structure-competitive mode, a higher concentration of Hg^{2+} leads to less fluorescence-labeled cDNA bound to the sensor surface and thus to lower fluorescence signal.

Tong X.'s research group (2007) [16]developed a repeatable enrichment process that included a flow-through immunomagnetic cell separation system. The system was operated in a negative mode of operation by immunomagnetically targeting normal human peripheral blood lymphocytes (PBL) through the CD45 surface marker. The tumor cell has a recover rate around 80%.

Qian X. etc al. (2008)[17] discussed the development of biocompatible nanoparticles for in vivo molecular imaging and targeted therapy. Based on pegylated gold nanoparticles

and surface-enhanced Raman scattering (SERS), colloidal gold has been safely used to treat rheumatoid arthritis for 50 years, and has recently been found to amplify the efficiency of Raman scattering by 1415 orders of magnitude. When conjugated to tumor-targeting ligands such as single-chain variable fragment (ScFv) antibodies, the conjugated nanoparticles were able to target tumor biomarkers such as epidermal growth factor receptors on human cancer cells and in xenograft tumor models.

Lustberg's research group (2012)[9] developed a negative depletion CTC enrichment strategy that relies on the removal of normal cells using immunomagnetic separation in the blood of cancer patients. Negative depletion is a CTC pre-enrichment method by depletion of normal cells prior to separation. It can increase the efficiency to identify uncommon cells. As tradition method relies on biomarkers to find target cells, some mutated tumor cells will be missed. However, a negative selection methodology is difficult to obtain a high enough enrichment to be able to identify the "abnormal cells" or CTCs which exist in the specimen. The depletion process will raise the risk of contamination during the process as well.

Wu Y. et al (2013)[18] presented a negative depletion process and discussed which consists of red blood cell (RBC) lysis and the subsequent removal of CD45 expressing cells through immunomagnetic depletion. Using this optimized assembly on 120 whole blood specimens, different types of rare non-hematopoietic cells were found in these enriched peripheral blood samples and a wide range of external and internal markers had been characterized, which demonstrated the range and heterogeneity of the rare cells.

Subramaniam D. R. etc al. (2013)[19] studies on the innate immune response which includes rolling-adhesion, firm-adhesion, chemotaxis, and transmigration. The researchers initially demonstrated the model for cellcell collisions occurring near a planar substrate, and for cellsubstrate adhesive interactions. The adhesion studies provide a new perspective of the contribution of Hertzian contact mechanics toward variations in contact area at the cell-substrate interface. The results confirm that interfacial contact area will increase as a result of the contact formulation and that this mechanism may enhance cell rolling interactions for

cells driven toward endothelium by cellcell collisions. As a result of cell compliance, rolling velocity may decrease significantly, compared to non-compliant cells. In general, methods for CTC detection can be divided into cytometric (i.e., whole-cell based) and nucleic-acid based techniques. Both techniques usually include an enrichment step where CTCs are gathering and a detection step (Mostert et al. (2009).

Based on the antibody-antigen binding process, the immuno affinity methods has a good selectivity for target cells. However, the method is limited by the relatively slow transport of target cells to the capture surface. Also, it's difficult to remove non-target cells during the process. ([98])

2.3.2 Magnetic capture methods and magnetic field analyse

Magnetic separation technology has received considerable attention offering unique advantages over other techniques (Haun et al., 2010). [29] Magnetic separation devices are relatively inexpensive to produce, physically and chemically stable, biocompatible and environmentally safe. In addition, biological samples exhibit virtually no magnetic background, and thus highly sensitive measurements can be performed in turbid or otherwise visually obscured samples without further processing. In these days the antibody-coated magnetic beads have been developed, now they can offer a wide range of chemical and surface properties that will provide several different solid phase separations for cell separations and cell modification. (Kildew, 2002) [30]

There're two ways to apply magnetic field in the device, one is use electric magnet, the other is use static magnetic poles. The electric magnet is good in adjusting field strength, and it's ideal for devices needs a changing magnetic field. However, the electric device will give out heat, in microfluidic device, the extensive heat will be harmful. Also, the field strength of electric magnet field is less than static magnetic poles. What's more, the cost of static magnetic poles is much lower than electric magnet, so the researcher's device are mainly use static poles.

Cristofanilli, M. et. al (2004) [14] used the technology tested 177 patients with measurable metastatic breast cancer for levels of circulating tumor cells both before the patients were to start a new line of treatment and at the first follow-up visit. The author used a commercial device Cellsearch system for the isolation and enumeration of circulating tumor cells. It consists of a semiautomatic system for the preparation of a sample, enriches the sample for cells expressing the epithelial-cell adhesion molecule with antibody coated magnetic beads, and it labels the cells with the fluorescent nucleic acid dye. Circulating tumor cells were defined as nucleated cells lacking CD45 and expressing cytokeratin. It's found that patients in a training set with levels of circulating tumor cells equal to or higher than 5 per 7.5 ml of whole blood, as compared with the group with fewer than 5 circulating tumor cells per 7.5 ml, had a shorter median progression-free survival and shorter overall survival. At the first follow up visit after the initiation of therapy, this difference between the groups persisted and the reduced proportion of patients (from 49 percent to 30 percent) in the group with an unfavorable prognosis suggested that there was a benefit from therapy.

Issadore et al. (2011) [31] studied a magnetic separator developed from a compact and inexpensive microfluidic chip. A microfluidic channel was built directly above a self-assembled NdFeB magnet, the strongest known permanent magnetic material. To test the cell separation ability, the samples were prepared by mixing a known amount of leukocytes and tumor cells. The researchers integrated these strong magnets with a microfluidic channel, and demonstrated that very large sorting efficiencies (over 105) can be achieved. The efficiency was attained even at moderately high flow rates of 1 mL/h. Also, the self-assembled magnetic filter again showed high capturing efficiency, enriching the population of tumor cells to leukocytes by a factor of >103, outperforming the benchmark system (LD Column, 130-042-901, Miltenyi) which had an enrichment of 100. The device also performs well in detecting rare cells in blood: for suspensions with initial concentration ratios of 1/10, 1/100, and 1/1000 (tumor/leukocytes). The self-assembled magnetic filter effectively depleted the

leukocytes from the suspension, enabling sparse tumor cells to be separated and concentrated for facile detection.

Afshar et al. (2011) [32] developed a novel integrated chip-based separation system that comprises an arrangement of distinct magnetic microtips adjacent to a microfluidic channel. The system demonstrated a precise dosing amount and continuous separation in the sample flow with high resolution as well as controllable release process. The magnetic actuation system comprised an electromagnet (coil), a magnetic yoke and soft-magnetic poles, integrated with the microfluidic chip. Two distinct configurations of these magnetic poles with different shapes are placed close to the sidewalls of the fluidic channel. They are magnetized via a magnetic yoke by an external electromagnet. To test the device's separation ability, two different types of magnetic beads (d = 1.05μm and 2.83μm) were used. About 70 to 80% of a specific particle can be found at the location of a corresponding 20 mm wide virtual outlet channel. This size distribution is relatively narrow, indicating that reliable separation of particles in this size range is feasible.

Chung et al. (2011) [33] developed a semi-integrated electrical biosensor for the detection of rare circulating tumor cells in blood. Most of the current methods, such as the CellSearch$^{\text{tm}}$ system and flow cytometer, are based on fluorescence. They rely on high resolution optical characterization via fluorescent staining, which requires labor-intensive sample manipulation and the detailed qualification of each individual cell. Commercial CellSearch$^{\text{tm}}$ systems even require a trained professional to interpret and classify the images obtained to arrive at a number of CTCs. The research group used a two-module system based on the electronic detection of rare circulating tumor cells from large blood samples through a combination of immunomagnetic isolation and size filtration in a convenient syringe-based device, coupled to a microchip specifically detecting cancer cells by impedance measurement. Using MCF7 cell from a human breast cancer tumor, the cell enrichment efficiency as well as the detection of target cells by impedance was tested. The cell trapping efficiency was calculated as the number of cells trapped over the total number of cell input. Results show that an average

of 90% of MCF7 cells was trapped. Three levels of spiked CTC number (30±2, 124±29, 273±23) were distinguished by impedance change ($P < 0.05$, one-way ANOVA) which proved the device's detection ability.

Considering the low number of CTCs contain in blood, Zheng et al. (2007) [34] developed a parylene membrane microlter device used for capture and electrolysis of circulating tumor cells in human blood. The authors have two designs for membrane filters without integrated electrodes. Both designs are 1 cm by 1 cm square sheets with effective filter area of 0.6 cm by 0.6 cm. For design one, each pore is consisted of 10 μm diameter circular holes with center to center distance between adjacent pores of 20 μm. Design two uses oval shaped pores that were formed by etching rectangular masks of 14 μm by 8 μm with 12 μm edge to edge distance. With a back-pressure up to 3.45 kPa and adding electrical field strength of 0.3105 V/m, the device achieved the CTC capture on filter with the recovery rates for both circular ($87.3 \pm 7.0\%$) and oval designs ($89.1 \pm 7.0\%$) within 10 min.

Xu et al. (2011) [35] developed a sensitive and specific isolation and enumeration system for circulating tumor cells in patients with hepatocellular carcinoma (HCC). The system was used to detect CTCs in 5 mL blood. Blood samples spiked with Hep3B cells (ranging from 10 to 810 cells) were used to determine recovery and sensitivity. Prevalence of CTCs was examined in samples from HCC patients, healthy volunteers, and patients with benign liver diseases or non-HCC cancers. CTC samples were also analyzed by FISH with an average recovery of 61% or more at each spiking level. No healthy, benign liver disease or non-HCC cancer subjects had CTCs detected. CTCs were identified in 69 of 85 (81%) HCC patients and the CTC amount was an average of 19 ± 24 CTCs per 5 ml.

Choi et. al (2001) [36] focus on the controllable capture of magnet beads. The separator is composed of micromachined semi-encapsulated spiral electromagnets and fluid channels, which have been separately fabricated and then bonded. The device was tested with super-paramagnetic beads of mean diameter 1 m which were suspended in a buffered solution.

Using this separator, cells or cell fragments and magnetic beads bonded with protein or enzyme suspended in bio-buffer solutions can be successfully separated from their suspensions, envisaging a filterless bio-separator.

Jarrige et al. (2010) [37] developed a point-of-care system on the detection of intra-operative parathyroid hormone (ioPTH) which predicts the body's reaction after surgery. The device is an ioPTH point-of-care (POC) assay on Philips handheld magnotech system. Initially-PTH is captured by magnetic particles coated with anti-N-terminal-PTH antibodies. Then magnetic particles are collected by magnetic forces at sensor surface coated with anti-Cterminal-PTH antibodies. The POC test is able to give accurate results in less than 10 minutes, using 25 μL of whole blood.

For the research on magnetic capture methods, the research and analyze of magnet field strength distribution within systems would be necessary.

Li et al (2010) [38] studies the impact of a static magnetic field on the electricity production of Shewanella-inoculated microbial fuel cells. The electricity production of Shewanella-inoculated microbial fuel cells (MFCs) under magnetic field (MF) exposure was investigated in different reactor systems. Application of a 100-mT static MF to the MFCs improved electricity production considerably, with an increase in the maximum voltage by 20-27% in both single- and two-chamber MFCs, while a more conspicuous improvement in the electricity generation was observed in a three-electrode cell. The MF effects were found to be immediate and reversible, and adverse effects seemed to occur when the MF was suddenly removed. The improvement in the electricity production of MFCs underMFwas mainly attributed to the enhanced bioelectrochemical activity, possibly through the oxidative stress mechanism. An accelerated cell growth under MF might also contribute to the enhanced substrate degradation and power generation.

Haverkort et al. (2009) [39] discussed the Magnetic Drug Targeting (MDT), with computational simulations performed of blood flow and magnetic particle motion in a left coronary artery and a carotid artery, using the properties of presently available magnetic carriers and

strong superconducting magnets. For simple tube geometries it is deduced theoretically that the particle capture efficiency scales as

$$\eta \sim \sqrt{Mnp}$$

, with Mnp the characteristic ratio of the particle magnetization force and the drag force. This relation is found to hold quite well for the carotid artery. For the coronary artery, the presence of side branches and domain curvature causes deviations from this scaling rule

$$\eta \sim Mn_p^{\beta}$$

, with η>1/2. The simulations demonstrate that approximately a quarter of the inserted 4 lm particles can be captured from the bloodstream of the left coronary artery, when the magnet is placed at a distance of 4.25 cm.

Wiwatanapataphee et al.(2007) [40] worked on the fluid-solid flow phenomena. The author presents a mathematical model and a finite element method, based on the Arbitrary Lagrangian Eulerian approach, for studying blood-magnetic particle flow in small vessels. Four models with one, three, five, and nine particles are used to analyze the flow pattern and pressure distribution along the flow direction. Effects of magnetic force on the blood-particle flow are investigated. And thus created a model can simulate the flow of particles toward the targeted region.

Habibi et al (2010) [41] investigated the effect of a magnetic field on the volume concentration of magnetic nanoparticles of a non-Newtonian biofluid (blood) as a drug carrier. The effect of particles on the flow field is considered. The governing non-linear differential equations, concentration and Naviar-stokes are coupled with the magnetic field. A finite volume based code is developed and utilized. The results show accumulation of magnetic nanoparticles near the magnetic source until it looks like a solid object. The accumulation of

nanoparticles is due to the magnetic force that overcomes the fluid drag force. As the magnetic strength and size of the magnetic particles increase, the accumulation of nanoparticles increases as well.

A lot of red blood cells exist inside the patient's blood sample, to improve the quality for sample analyze, it's necessary to remove red blood cells before further process. Cell lysing is a commonly used method for sample treatment. However, traditional method used for cell lysing will cost a considerable mass loss, which will probably affect target cells. Moreover, RBC centrifugation and lysis are not well adapted to the emerging diagnostic applications, relying on microfluidics and micro-scale total analytical systems. Moore's research group designed, fabricated, and tested a magnetic red blood cell separator. (Moore et al. 2013)[42] Four flat-faced magnet poles surround a 2mm∗2mm separation area. With two diagonal switching valves, the system can control the flow ratio and direction, 80% of target cells are recovered during the separation.

2.3.3 Other cell separaton technologies

A challenge in CTCs' detection is to separate marked cells from other blood cells, i.e. RBC and WBC, with a similar size, it's necessary to find an effective method separating the target cells.

For CTCs, studies have been done on the identification of them among blood cells. As the amount of CTCs in blood sample is rather low, high assay efficiency and highly standardized preparation protocols are an absolute necessity. (Lianidou etc. al, 2011) [43]

Commonly used detection systems include image-based methods, genetic methods and protein-based methods.

Image-based methods are classic approach, such as CellSearch^{tm} system or laser-scanning cytometry, they're widely used and proved be reliable.

However, for classic ICC techniques, if many samples are to be analyzed the needed time would be very long. So the increase of analyze speed is necessary.

A possible solution is adding some sensitive factors to increase the speed. Balic et al. (2011) [44] have developed a method for multimarker image analysis for CTCs by employing novel DyLight technology. Using breast cancer cell lines, the authors developed a method optimized for multimarker analysis by employing novel DyLight Technology. Using multiple antibodies, three of the markers, CD44, ALDH1, and cytokeratin have been directly conjugated with DyLight dyes. This method showed effective in the analyze of particular therapeutic targets' expression.

Molecular assays for CTC detection and enumeration such as PCR has a satisfying analytical sensitivity and specificity. Based on the isolation of total RNA from viable CTCs, the success of detection will require the use of appropriate mRNA markers. However, the fact that CTCs are very rare and the amount of available sample is very limited presents tremendous analytical and technical challenges.

Markou A etc. al (2011) [45] developed a multiplexed PCR-coupled liquid bead array to detect the expression of multiple genes (KRT19, ERBB2, MAGEA3, SCGB2A2, and TWIST1) in CTCs. The assay was specific for each gene in complex multiplexed formats and could detect the expression of each gene at the level of a single SK-BR-3 cell. The result showed the expression of multiple genes in CTCs can be measured simultaneously and reliably, thus saving precious sample and reducing the costs and time of analysis. This assay forms an efficient basis for a multiplex approach to study the expression of up to 100 genes in CTCs.

Today's CTC detection mainly based on the using of an antibody that binds to the protein EpCAM (epithelial cell adhesion molecule), which is often present on the surface of malignant epithelial cells but not of blood cells. However, different type of tumor cells have different antibodies, and the protein at the surface of tumor cell will change in different stages as well, thus this method is limited to certain type of tumor cells and stages. (Zeliadt, 2014) [89]

Lin's research group [90] focus on the physical difference between tumor cells and blood cells, they developed a microfluidic chip with a spiral channel that isolates CTCs from blood based on their size. At a high speed, interplay between the inertial and centrifugal forces makes larger cell stay at inner side of channel while drift small cells towards outer side of the wall. At the outlet of the chip, the channel bifurcates, and the cells travelling along the outer wall flow into a waste container, while those near the inner wall pass into a collection chamber for further analysis. The device is good at keep tumor cells intact for further analysis and reduce time for separation, however, the size of tumor cells varies as well, which will reduce the capture ratio for tumor cells.

Gascoyne etc al. (2014) [91] focus on Dielectrophoresis (DEP) methods for cancer separation. Dielectrophoresis is the movement of particles caused by asymmetrical displacement of electric fields. DEP method has a wider selectivity than traditional antibody-antigen methods, when an alternating electric field is applied to a suspension of viable cells, the cell membrane exteriors accumulate surface charges from the ionic medium that tend to repel electric field lines so that ion currents flow around the cells. The DEP responses of cancer and normal blood cells expressed in terms of the reciprocal cell dielectric phenotype. The author reported that all of the cell lines derived from solid tumors have a much lower DEP responses than normal cells. Based on this result, new device can developed for cancer detection. However, as CTC is rather rare in patient's blood, it is necessary to process blood specimens of 10 mL or more to isolate sufficient CTCs for meaningful analysis. The challenge now is to develop a system able to process with large numbers of cells with sufficient discrimination in a reasonable time for clinical users.

2.4 Point-of-care (POC) device and its application

Hsieh et al. (2006) [46] developed a new scanning technology which can locate CTCs at a rate that is 500-times faster than conventional automated digital microscopy. The fiber-optic array scanning technology (FAST) technology is the core of this system. The scan rate

(100 lines per second) results from a fast laser raster. A 10 megawatt argon ion laser excites fluorescence in labeled cells that are collected in optics with a large (50 mm) field-of-view which is enabled by an optical fiber bundle. Because larger volumes of peripheral blood can be analyzed than using conventional microscopy in the same time, purification or enrichment steps are avoided, which reduces the risk of cell loss. The authors tested the repeatability of the system using a model sample of peripheral blood spiked with cells from the HT-29 colorectal cancer cell line. In future testing the average automated digital microscopy image acquisition time would be reduced to below 20 minutes for a 10 ml sample. To check the efficiency of the system, the authors prepared three samples each containing HT-29 cells in the range of 1021 cells. The authors scanned each sample 10 times with the FAST cytometer and then took high resolution images of all the objects. In each case, the FAST cytometer detected exactly the same cells in the same locations, with conventional microscope scanning producing similar results.

The Laser Scanning Cytometer (LSC) (Compucyte Corporation, Cambridge, MA) was developed to improve scanning of fluorescent cells. Pachmann et al. (2008) [47] used the scanning system to detect the breast cancer cells. The microscope recognizes all white cells by light scattering and measures the fluorescence of each cell. The enrichment of epithelial cells using a magnet and analysis with the cytometer enabled relocation of cells for visual examination of vital epithelial cells. CTCs may be identified through the detection of (epi) genetic alterations that are specific for cancer cells. Alterations in DNA such as mutations in proto-oncogenes or tumor suppressor genes, microsatellite instability and sequences of oncogenic viruses may be detected.

Detection of mRNA of factors that are overexpressed or mutated in breast cancer using RT-PCR is a more widely used alternative. As RNA disappears quickly from the blood after cell death, detection of RNA is likely due to the presence of a whole tumor cell, not cell fragments or free RNA. In RT-PCR, after cDNA synthesis, the gene of interest is amplified using oligonucleotide primers specific for this gene of interest.

Sieuwerts et al. (2011) [48] identified 55 mRNAs and 10 miRNAs more abundantly expressed in samples from 32 patients with at least 5 CTCs in 7.5 mL of blood compared with samples from 9 patients without detectable CTCs and HBDs. From 61 patients with metastatic breast cancer, two 7.5 mL blood samples were taken for CTC enumeration and isolation prior to initiation of systemic therapy for metastatic disease. Clustering analysis resulted in four different patient clusters characterized by five distinct gene clusters. Twice the number of patients from cluster 2 to 4 had developed both visceral and non-visceral metastases. Comparing transcript levels in CTCs with those measured in corresponding primary tumors showed clinically relevant discrepancies in estrogen receptor and HER2 levels. visceral and non-visceral metastases. Comparing transcript levels in CTCs with those measured in corresponding primary tumors showed clinically relevant discrepancies in estrogen receptor and HER2 levels.

Zheng et al. (2011) [49] reported a novel three dimensional microfilter device that can enrich viable circulating tumor cells from blood. The fabricated 3D microfilter is a 1* 1 cm^2 device with two layers of parylene on a silicon substrate. Using human prostate adenocarcinoma cell line (LNCaP) and human breast adenocarcinoma cell line (MCF-7) as cell samples, the authors tested the device's cell capture efficiency. It's reported that here a 3D microfilter that can enrich viable CTCs with ∼86% capture efficiency in a few minutes. And the captured cells were shown to be viable and metabolically active even after 2 weeks of cell culture on the device.

Hsieh et al. (2011) [50] developed a rapid and sensitive method for detecting cancer cells at low concentration. The coupling of immunomagnetic-bead-captured cells with Quantum dots (QDs) as markers for fluorescence analysis was employed, as QDs have the advantages of brightness, low photobleaching, broad excitation spectra and narrow emission bandwidth. The researchers used Human Jurkat cells (T-help cells) (ATCC TIB-152) and Human C1R cells (B cells) (ATCC CRL-1993) as targets. The intensity of fluorescence increases linearly with the frequency of T-help cells from 10^{-7} to 10^{-3}, and neither B cells nor red blood cells

interfere with the detection of T-help cells. Moreover, the total detection time is less than 15 minutes, even though the frequency of specific T-help cells is as low as $5*10^{-7}$.

Nagrath et al. (2007) [51] designed a microfluidic device (the 'CTC-chip') that can efficiently and reproducibly isolate CTCs from the blood of patients with common epithelial tumors. The CTC-chip consisted of an array of microposts that were made chemically functional with anti-epithelial-celladhesion-molecule (EpCAM, also known as TACSTD1) antibodies. To determine the efficiency of capture, the authors spiked non-small-cell lung cancer (NSCLC) cells (NCI-H1650) into phosphate buffered saline (PBS) at 100 cells ml21 and captured the spiked cancer cells using the CTC-chip. The calculated capture efficiency was 65% and decreased significantly at flow rates above 2.5 ml/h. For clinical test, a total of 116 samples from 68 patients with epithelial cancers including NSCLC (n555), prostate (n526), pancreatic (n515), breast (n510) and colon (n510) were studied. CTCs were identified in 115 of 116 (0.99%) patient samples analyzed, with the single negative specimen being a small volume sample (0.9 ml) from a patient with colorectal cancer.

Zhao C. etc al (2011) [52] present a microfluidic device to continuously purify bio-nanoparticles from cells based on their different intrinsic movements on the microscale. A biological sample is layered on top of a physiological buffer, and both fluids are transported horizontally at the same flow rate in a straight channel under laminar flow. While the micron sized particles such as cells sediment to the bottom layer with a predictable terminal velocity, the nanoparticles move vertically by diffusion. As their vertical travel distances have a different dependence on time, the micro- and nanoparticles can preferentially reside in the bottom and top layers respectively after certain residence time, yielding purified viruses.

Seo et al.(2010) [53] designed a hybrid cell sorter that combines hydrodynamics and magnetophoresis. It consisted of a magnetic alignment channel and a virtual impactor. The aim is to separate polystyrene beads, Jurkat cells as well as WBCs from RBCs in blood. The authors performed the experiment at a flow rate of 1ml/min with a classification efficiency of red blood cells increasing from 75.2% to 86.8% with the application of a magnetic field.

Also, the classification efficiency of white blood cells decreased from 83.8% to 70.9% with an applied magnetic field. The higher flow rate made the separation efficiency relatively lower.

Han et al. (2006) [54] developed a microsystem for separating suspended breast cancer cells in peripheral blood and for sorting them based on their electrophysiological characteristics. The core of the system is consisted of a magnetophoretic micro-separator and a μ-EIS. The micro-separator has one inlet and three outlets. The magnetic particles placed near the ferromagnetic wire experience a magnetophoretic force created by the high gradient magnetic field which will make deoxyhemoglobin RBCs and other biological components move in opposite directions due to the force created by the high gradient magnetic field. The deoxyhemoglobin RBCs and BCCs can be separated continuously as the BCC-spiked blood sample passes through the microchannel of the microseparator. The experimental results show that the PMC micro-separator separates out 94.8% of the BCCs from the outermost outlets at 0.05 mm/s flow velocity. The efficiency of cell the flow rate required (2.5 to 20 μl/h) is relatively low to efficiently isolate cancer cells from raw peripheral blood. Improvements can be made from a ferromagnetic wire with a higher permeability, using a higher external magnetic flux, increasing the microchannel length, and designing new channel structures (e.g., cascade structure).

Cui et al. (2011) [55] examined the feasibility of a microfluidics chip for cell capturing and pairing with a high efficiency. The chip was fabricated by the polydimethylsiloxane-based soft-lithography technique and contained two suction duct arrays set in parallel on both sides of a main microchannel. Cells were captured and paired by activating two sets of suction ducts one by one with the help of syringe pumps along with switching the cell suspensions inside the main microchannel correspondingly. The present chip was capable of creating 1024 pairs of two different cell populations in parallel. The preliminary experimental results showed that the cell capturing efficiency was 100% and the pairing one was 88% with an optimal suction rate of 5 l/min in the chip in the 2 m-sized suction duct chip.

Warkiani et al. (2016) [56] described detailed procedures for the production and use of a label-free spiral microfluidic device. The system allowed size-based isolation of viable CTCs using hydrodynamic forces that are present in curvilinear micro-channels. The spiral microfluidic devices can be produced at an extremely low cost using standard microfabrication and soft lithography techniques, and it can be used experimentally in a broad range of potential genomic and transcriptomic applications.

Kuczenski (2011)'s [57] study is on the diagnosis of sepsis. Sepsis is a whole body inflammatory response often caused by microbial infections of the blood. The diagnosis is a model system for pursuing the advantages of microfluidic devices over traditional diagnostic protocols. The author designed a microfluidic chip using dielectrophoresis to sort and concentrate the target microbe from a flowing blood sample. This design was optimized using the applicable electrokinetic and hydrodynamic theories. The researcher quantified the sorting efficiency of this device using growth-based assays which show 30% of injected microbes are recovered viable, consistent with the electroporation of target cells by the dielectrophoretic cell sorters. Finally, the results illustrate the device is capable of a five-fold larger microbe concentration in the target analyzed stream compared to the waste stream at a continuous sample flow rate of 35 μl/h.

Contract to traditional methods separating CTCs from blood cell, Toner's team use an opposite method by separating blood cells from CTCs. [92] The researchers first mix a blood sample with antibody-coated magnetic microbeads that bind a protein on the surface of white blood cells. Then, they pump the sample into their microfluidic device which will separate red blood cells and platelets from CTCs. In theory, the device can separate any types of CTCs regardless of its type and shape. Meanwhile, the challenge is to increase the separation efficiency of white blood cells. For every mL of blood analyzed, the device also captured an average of 32,000 white blood cells.

Kuhn's research group developed an automated fluorescence microscopy-based platform for picking out CTCs in a sample of blood on a microscope slide.[93] The researchers have

established a fluid phase biopsy approach that identifies circulating tumor cells (CTCs) without using surface protein-based enrichment and presents them in sufficiently high definition (HD) to satisfy diagnostic pathology image quality requirements. The key innovative aspects of this assay are its simplicity, with minimal processing to the blood specimen, and its ability to enable professional morphologic interpretation with diagnostic pathology/cytopathology quality imagery. However, it's still a time-consuming to identify tumor cells from huge amounts of blood cells. For a 7.5ml sample, it will take days to finish the analyze process.

2.5 Melanoma cells and CTC

One in six Americans develops skin cancer at some point. Skin cancer accounts for one third of all cancers in the United States. Most patients with skin cancer develop non-melanoma skin cancer. (Jerant A 2000) [58]

Melanoma is less common than other skin cancers. However, it is much more dangerous and causes the majority (75%) of deaths related to skin cancer. According to a WHO report, about 48,000 melanoma related deaths occur worldwide per year. (Lucas etc. 2006) [59]

Braam et al. (2012) [60] works on analyzing the risk factors for SMN (second malignant neoplasm) after childhood cancer. And it's found that of 151,575 CCS, 4,010 (2.6%) children developed an SMN, 212 of which were melanoma (5.3% or 0.14% of all CCS). The risk factors for malignant melanoma as SMN were identified: radiotherapy, or the combination alkylating agents and anti-mitotic drugs. Melanomas are most frequently observed after Hodgkin disease, hereditary retinoblastoma, soft tissue sarcoma, and gonatumors.

A foremost deleterious attribute of CMM is the high tendency to metastasize to distant organs or tissues leading to melanoma-related death. CMM is a highly aggressive form of cancer with a metastatic potential that is considerably greater than other solid tumours.2 Moreover, CMM has a high resistance to chemotherapy once the metastatic process has begun, which dramatically reduces the life expectancy of those afflicted with this disease. (Nezos etc. 2011) [61]

2.5.1 melanoma cell detection

Ma etc. al (2010) [62] provided evidence for the existence of circulating melanoma cells that are capable of causing tumor initiation and metastatic disease progression, considerably strengthening the rationale for ongoing clinical evaluations of melanoma CTC as a biomarker for disease progression, prognosis and outcome. Using a mRNA expression for human GAPDH and/or ATP-binding cassette subfamily B member 5 (ABCB5), a marker of malignant melanoma-initiating cells previously shown to be associated with metastatic disease progression in human patients.

De Giorgi, V etc. al (2010) [63] focus on a filtration- and Isolation-by-Size technique for the detection of CTCs, in which tumor cells are collected by filtration because of their large size in comparison with peripheral blood leukocytes, to ensure the sensitivity of methods, real time RT-PCR and the ISET method were both used. 140 subjects were included during the experiment, among them, CTCs were neither detected in the controls nor in the in situ melanoma group. While in 62.5% of metastatic melanoma patients CTCs were shown, only 29% of patients with primary invasive melanoma has a CTCs positive response, indicating a high false-negative result.

Recently immunomagnetic capture is the most commonly used technique for CTC collection. For melanomas, the Antigen-Melanoma Associated Chondroitin Sulphate Proteoglycan (HMW-MAA/MCSP) monoclonal antibody is a commonly used for specifically recognizes Circulating Melanoma Cells (CMCs). Still the immune capture is not reliable in sensitivity and specificity, also the cost is too high for wider use. (Georgieva J etc. 2002) [64]

The CellSearch Platform is also taken into research task recently. Using anti-epCAM as the capture method, as reported by researchers (Steen S etc. 2008) [65], this technique has recently been proved to be applicable for the detection of CMCs at least for some cases of malignant melanoma patients.

2.5.2 biomarkers for melanoma

As antibodies have a good efficiency in detecting and attaching cancer cells, the usage of antibody reaction has been applied for a long time. To detect the pleiotropic cyto/lymphokine tumor necrosis factor (TNF), Hans etc. al, (2009) [66] used two sets of monoclonal antibodies (mAbs) against TNF-binding proteins from the HL-60 (htr-mAb series) and U-937 (utr-mAb series) cell lines. Flow cytometry studies show that mAbs htr-9 and utr-1 detect two distinct TNF-binding sites on human cell lines. Immunologic blot and immunoprecipitation analyses indicate that mAbs htr-9 and utr-1 recognize proteins of 55 kDa and 75 kDa, respectively. These data provide evidence for the existence of two distinct TNF receptor molecules that contribute to varying extent to the TNF binding by different human cells. Up till now, technologies using antibodies for cell binding has become a well-developed technology.

Tierling S. etc. al (2012) [69] developed a new method in detection of KRAS protein, which was active in the development of colorectal cancers. The method is based on multiplexed primer extension reactions coupled to HPLC separation. They present a primer extension-based approach with subsequent IP/RP-HPLC separation that detects selectively all 12 clinically relevant variants known for codons 12 and 13 of the KRAS gene. Compare with other traditional methods such as PCR and direct sequencing, the new approach has many advantages such as reliable, fast, cost-effective and sensitive. As the workflow can be almost entirely automatized, a minimum of human resources is required.

Maetzel etc al. (2009) [70] studies on EpCAM and its shown that regulated intramembrane proteolysis activates EpCAM as a mitogenic signal transducer in vitro and in vivo. This involves shedding of its ectodomain EpEX and nuclear translocation of its intracellular domain EpICD. In patients, EpICD was found in nuclei of colon carcinoma but not of normal tissue. Nuclear signalling of EpCAM explains how EpCAM functions in cell proliferation.

2.6 Development of Computational-Aided Design technology

2.6.1 Finite-element meshes

The classical finite element method (FEM) is a well-established tool in scientific computing and it's widely used in many areas of application. It employs a variation approach with piecewise polynomial shape functions and shows an improved geometry handling compared e.g. with the finite difference method. These features render the FEM a very versatile numerical approach and it can be regarded as a general purpose solver e.g. for the discretization of partial differential equations (PDE). (Schweitzer, 2012) [71]

Ansystm developed a series of software to solve tasks with FEM. Starts with advanced CAD/geometry readers and repair tools to allow the user to quickly progress to a variety of geometry-tolerant meshers and produce high-quality volume or surface meshes with minimal effort. Advanced mesh diagnostics, interactive and automated mesh editing, output to a wide variety of computational fluid dynamics (CFD) and finite element analysis (FEA) solvers and multiphysics post-processing tools make ANSYS ICEM CFD a complete meshing solution.

Charles et al. (2008) [72] used fluent to simulate a parallel particle model for transport of sediments, and the authors developed a sediment transport model using three different sediment suspension methods. The first method uses a modified mean for the Poisson distribution function to determine the expected number of the suspended particles in each particular grid cell of the domain over all available processors. The second method determines the number of particles to suspend with the aid of the Poisson distribution function only in those grid cells which are assigned to that processor. The third method is based on the technique of using a synchronised pseudo-randomnumber generator to generate identical numbers of suspended particles in all valid grid cells for each processor. And the result showed the second method is the best method on distributed computing systems (e.g., a Beowulf cluster), whereas the third maintains the best load distribution.

2.6.2 Relevant applications of FLUENT

Mohanty et al. (2010) [73] made a three-dimensional CFD model of a continuous to describe the performance of immunomagnetophoretic cell sorters (ICS). Based on the Navier-Stokes equations, the CFD model is used to investigate the performance of a generic continuous cell separation system. The author designed a Y-channel microfluidic device for cell capture, using the commercial CFD software FLUENT to simulate the mixing process and calculate the concentrate profile of magnetic-beaded cells in the channel. The simulation proved that the optimum position of the magnet(s) can be essential in obtaining the best design.

Marchetta et al. (2008) [74] performed a computational simulation of magnetic positive positioning (MP2), the model was set up for the cryogenic propellant reorientation in reduced gravity. a three-dimensional magnetic field and magnetic force model was developed as a feature of a commercially available fluid flow model which has been well validated. The computational tool was then improved upon to model magnetically induced flows in a transient acceleration field. Simulation predictions obtained with the enhanced model are compared to available reduced gravity experiment data. Evidence is presented and conclusions are drawn that support the continued use of the simulation as viable modeling and predictive tool in the continuing study of MP2.

Tang et al. (2012) [75] studies on the the relationship between porosity and tortuosity in porous media with cubic particles, with an assumption that the porous medium is homogeneous, the problem is converted to the micro-level over a unit cell, and geometry models of flow paths are proposed. In three-dimensional (3D) cells, the flow paths are too complicated to define. Hence, the 3D models are converted to two-dimensional (2D) models to simplify the calculation process. The author also proposed quadrate particle and interaction (QI) and quadrate and triangular particle (QT) models with cubic particles. Both models have shown good agreement with the experimental data.

Ramamurthy et al. (2013) [76] worked on the sharp open channel bend flows. A comprehensive analysis was performed to determine the best modeling parameters to study the open channel sharp bend flow. Comparisons of the simulation results were made from two commercial codes, three turbulence models, two flow domain representations, and three water surface treatments. Adequate representation of counter-rotating secondary flow cells in the channel downstream of the bend requires both the appropriate treatment of the channel free surface and a turbulence model that can resolve the anisotropy of turbulence.

Hamidipour et al. (2012) [77] studies the hydrodynamics in three-phase fluidized beds. CFD simulations of gasliquidsolid fluidized beds have been performed in a full three-dimensional, unsteady multiple-Euler framework by means of the commercial software FLUENT. The simulation results were compared with experimental data obtained from laboratory scale three-phase fluidized beds. The results indicate that in order to minimize numerical diffusion artifacts and to enable valid discussions on the choice of physical models, third-order numerical schemes need to be implemented. The realizable turbulence formulation was unable to produce the expected solids gulf-stream pattern (i.e., rising solid particles in the core and descending solid particles near the wall) in three-phase fluidized beds whereas the RNG and standard ke models were able to better captured depictions of flow patterns.

Toljic et al. (2012) [78] presented a full three dimensional FLUENT numerical model of the electrostatic coating process with the embedded moving mesh capability and piecewise linear type target motion. The model includes target geometries that do not exhibit symmetry. All the dominant mechanical and electrical phenomena are taken into account. Mechanical phenomena include shaping air effects, downdraft effects and the motion of the polydispersed particles. It was demonstrated that the numerical model can accurately mimic the type of the motion used in real world applications.

Xin et al. (2012)'s [79] simulation project is flow field and particle trajectory of radio frequency inductively coupled plasma spheroidization. With customized CFD commercial code FLUENT software, the numerical simulation of the argon flow field of inductively

coupled plasma spheroidization system was performed by using ke turbulent model and PISO pressurevelocity coupling algorithm. The results show that the simulation values of the powder collection rates and granulometric parameters of the spheroidized powders are close to the experimental data, which indicates the numerical simulation of the argon flow field and injected TiAl alloy powder particle trajectories of inductively coupled plasma spheroidization system is reliable.

Xu J.'s research group (2012)[80] optimized the magnetic separation and analysis technology. With a developed cell tracking velocimetry (CTV). Three types of commercially available, and commonly used, magnetic particles were studied. The researcher found out different kinds of magnet particles commercially available have a pretty different size distribution and magnet mobility distribution. It will be important to choose a proper magnet beads for a desired result.

2.6.3 CFD for blood samples and its special problems

In recent years, many researchers have used computational design to help in the development of point-of-care devices. Plouffe et al. (2011) [81] produced a design analysis which provided a rational basis to select the operating conditions, including chamber and wire geometry, flow rates, and applied currents, for a magnetic-microfluidic cell separation device. The author analyzed factors affected the drag force on magnetic particles in fluid and developed a formula describing the velocity pattern of the particles. Based on the set model, different geometric layouts were investigated. The author made an optimized design considering microbead and cell parameters, such as diameter, magnetic susceptibility, and particle binding characteristics as well.

The particle interaction within the system is also a task for researchers. Cichocki and Felderhof (1990) [82] studied diffusion in a dilute system of Brownian particles with hydrodynamic interaction and hard core repulsion. It's assumed that the hard core has a radius larger than the hydrodynamic one. The short-time and long-time self-diffusion coefficient, as

well as the collective diffusion coefficient, are calculated exactly to first order in the volume fraction. And the authors showed that hydrodynamic interactions are important even when the hard core radius is several times larger than the hydrodynamic one.

Habibi et al. (2011) [41] investigated the effect of a magnetic field on the volume concentration of magnetic nanoparticles of a non-Newtonian biofluid (i.e. blood) as a drug carrier. The authors set up a series of non-linear differential equations, and a finite volume-based code was developed and utilized. The calculation showed among factors affect the nanoparticle absorption, particle size is the most important one. Also, the distance between the magnet source and the blood flow would affect the absorption process significantly. The authors report that the particles accumulated in the channel would greatly increase the wall shear stress.

2.7 Need for Improvement

Today, researchers have developed many CTC detection methods effective in detecting tumor cells in blood; however, these system are still inadequate for the application of point-of-care detection. Current methods still require complex operation , and development is needed before the CTC detector is operational with a relatively simple structure applicable for clinical use. Some applicable designs are still not practical in use. A key factor is the separation progress. The flow rate should be low enough to provide adequate time to make the labeling and capturing of CTCs successful, with current devices unable to satisfy the balance between efficiency and accuracy. The cost for both device and operation can be reduced as well.

2.7.1 Mixing for reactions between particles

Before the analyze process, a necessary part is the preparation of blood samples, where blood samples would be mixed with reagents thus the magnet particles could be "labeled" on targeted CTCs. As CTCs are fragile and tend to degrade within a few hours when collected

in standard evacuated blood collection tubes, specific designed containers would be needed for shipment if samples can't be analyzed locally. The effect of mixing is undetermined if samples and reagents were mixed manually, while the specific designed sample mixing system is mainly for laboratory work. For the point-of-care system, the aim is to make the cell labeling successful with a minimum requirement of resource. It's necessary to obtain further data of sample and mixture in the mixer. Thus a simulation of system is in need for optimizing the mixer system.

2.7.2 Magnetic capture

The labeled CTCS would be captured by the separation system, a varies design of magnet traps have been mentioned, for the design of new device, it's necessary to evaluate the capture efficiency of CTCs, in practice, the overall amount of samples and reagents are usually up to 20∼30 ml, thus the control of flow rate is essential as a balance between analyze speed and capture ability is necessary. Also, the magnetic field analyze is also an essential part in the design of system, and the shape of magnet pole would affect the magnet field strength as well. This is a necessary part in the design of new point-of-care device when the simulation task as well as laboratory experiment would be expected.

Today the magnetic separation method has played a significant rone in cancer's detection and treatment. However, the separation device we have today still can't provide satisfying performance for studies and widely clinical use. Also, the bulky size and low portability restricts the usage of POC device.

2.7.3 Cell detection

Right now some CTC detection systems have been put into commerce product, such as the CellSearch^{tm} system, developed by veridex, llc., which has been widely used in medical research as well as biology laboratory and had contributed to several research works. However, the system requires a specified preparing system as well as the analyzer, both take a

large volume of space, along with the CTC control kits as well as containers for reagents, it's necessary to set up a laboratory to support the system.

Another problem is the specify of cell types. Based on the detection of EpCAM on the surface of circulating tumor cells for cell isolation, the CellSearch isolation method, did not recognize, in particular, normal-like breast cancer cells that in general have aggressive features thus new tests are needed that include antibodies that specifically recognize normal-like breast tumor cells but not cells of hematopoietic origin. (Sieuwerts et al. 2009) [83]

Also, the Ikotech inc. developed a IsoFlux System which is a platform designed for sensitive applications. Using a revolutionary microfluidic technology, the instrument isolates rare cells from a variety of different biological samples and prepares the samples for down-stream analysis. It works with a wide range of samples - blood, cultures, tissue dissociations, etc. Also, the system can analyze samples in low volume (10-20μL), which is optimized for cellular and molecular analysis.

Chapter 3

Computational Fluid Dynamic Analysis and Testing of a Multistage Magnetic Trap for the Capture of Rare Cells from Whole Blood

3.1 Abstract

Recent advances in magnetic cell selection have made the possibility of finding rare cells (10 cells per ml blood) in blood become more realistic. Thus the detection of fetal cells in maternal blood, circulating stem cells and circulating tumor cells will soon be a technology that can ultimately be transferred to point-of-care diagnosis. As a component of a point-of-care portable rare cell analyzer, a 3-stage magnetic trap for magnetically labeled rare cells is designed and tested. The trap design consists of a flow channel with three bends and a permanent magnet positioned at the outer curve of each bend. Findings are reported on the computational fluid dynamic analysis of its design using the FLUENT^{TM} analysis package, testing with model commercial magnetic beads used in cell labeling, and testing with immune-magnetically labeled cultured melanoma cells in the presence of whole blood.

The computational result, using a realistic range of flow rates, provides cell flow data along stream lines as a function of position in the trap. The measurements of field proles of the magnets are used to determine forces applied as a function of position in the trap. Testing with 3.27 μm diameter standard magnetic beads (Seragen^{TM}) indicated that at least 99.998% of these strongly magnetic particles are captured within the trap. Testing with cultured CRL14777 melanoma cells labeled with anti-CD146 1.5 μm diameter beads indicated that 90$\pm$10% of these are captured within the trap, most of them at the first stage. The cell trap requires no eternal power, fits within a point-of-care kit and has now been found to meet functional requirements for incorporation into a point-of-care circulating tumor cell analysis system.

Key words: point-of-care, magnetic cell separation, FLUENT, rare cells in blood

3.2 Introduction

To effectively employ cancer detection by point-of-care devices, the coverage of the general population needs to be expanded considerably. Local clinics and neighborhood health centers are effective sites for early cancer indicators. Those institutes, however, lack both the complex and expensive analytical devices as well as qualified technicians. To expand early detection, testing would have to be inexpensive and well accepted by the population targeted for screening. A mature circulating tumor cell (CTC) detection system would require a biomarkers, such as antibodies, to mark the targeted CTCs; a separation system using various techniques (magnetic separation, for example) to separate CTCs from other cells and a detection system to identify and count the CTCs in the sample. Magnetic separation technology has received considerable attention offering unique advantages over other techniques [29].

The magnetic separation devices are relatively inexpensive to produce, physically and chemically stable, biocompatible and environmentally safe. In addition, biological samples exhibit virtually no magnetic background, and thus highly sensitive measurements can be performed in turbid or otherwise visually obscured samples without further processing. What's more, chip-based separation system has been successfully developed [84] [31].

To effectively employ cancer detection by point-of-care devices, the coverage of the general population will need to expand considerably. Local clinics and neighborhood health centers would be effective sites for early cancer indicators. Local clinics, however, lack both the complex and expensive analytical devices as well as qualified technicians. To expand early detection, testing would have to be inexpensive and well accepted by the population targeted for screening. A mature circulating tumor cell (CTC) detection system would require a biomarkers, such as antibodies, to mark the targeted CTCs; a separation system

using various techniques (magnetic separation, for example) to separate CTCs from other cells and a detection system to identify and count the CTCs in the sample.

The compact system proves to be effective in precise dosing amount and continuous separation in the sample flow with high resolution as well as controllable release process [33]. With the aid of magnet separation technology, recently researchers have developed varies of detector system that houses all components for CTCs' detection in a handheld, portable device [33] [49].

3.3 Materials and methods

3.3.1 Magnetic trap design

Figure 3.1 shows the magnet trap and the mesh file set for simulation. The version of the trap used in these studies is designed with three pairs of curved trapping stations and three pairs of magnets with pole-face field strengths of 430, 470 and 520 mT. At each station the north pole of the magnet was adjacent to the channel. Thus magnets of each pair, though at some distance from one another, were matched in north-to-north configuration to maintain maximum field divergence. A photo of the trap is shown in Figure 3.1 (left). :

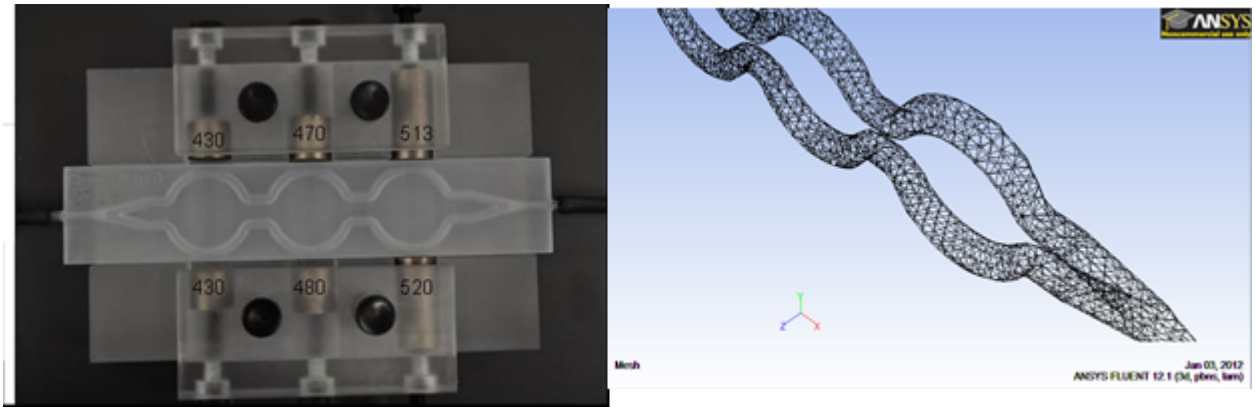

Figure 3.1: Photo of Magnet Trap

3.3.2 Computational Fluid Dynamics

Computational fluid dynamic analysis of the channel design was accomplished using the FLUENT^{TM} analysis package, which performs modeling of fluid flow and tracking particles' movement in complex geometries. With the help of ICEM CFD^{TM}, a mesh file of the channel geometry was set up (Figure 3.1, right), and a laminar flow model was deduced for calculation. For the simulation of magnetic particles, the channel was simplified to a 2-D rectangle shape. A discrete model was applied to simulate the particle movement. Tracking of particles movements was performed to show the particle trapping efficiency. A flow chart (Figure 3.2) summarizes the sequence for performing these operations.

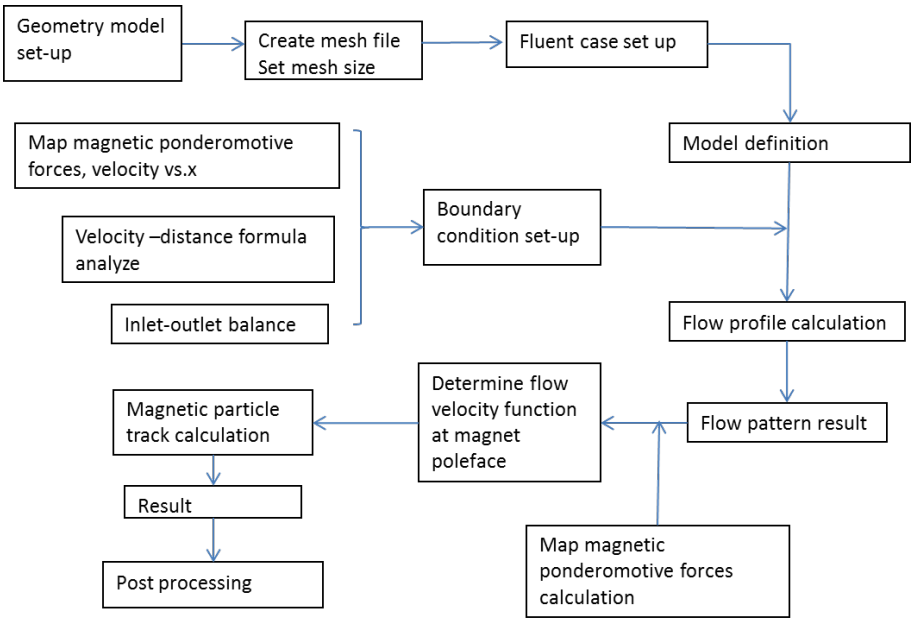

Figure 3.2: Flow Charts for Calculation

The trajectories of magnetic particles were simulated by choosing a set of coordinates within the channel and adding the flow and magnetophoretic velocity vectors as a function of position in the mesh. At each step in time the velocity is recalculated to account for simultaneous changes in streamline velocity, dy/dt and magnetophoretic velocity dx/dt. Details of this process are given in the Results section below.

3.3.3 Magnetic beads

3.27 μm diameter polystyrene beads with 14% iron oxide (Seradyn Thermo Fisher tsMGCM) were used as test particles for the magnetic trap. Magnetophoretic mobility μm = 7.47 * 10^{-12} m^3/TAs. These were diluted to 4.6 * 10^8 beads/mL to make a concentrated feed for testing. For labeling tumor cells, 1.5 μm diameter Biomag^{TM} beads coated with goat anti-mouse IgG1 from Bangs Laboratories (Cat. No. BM549) were used to react with mouse antibody sites on cells labeled with a mouse monoclonal anti-CD146 antibody cocktail containing antibody P1H12, which reacts specifically with the CD146 (MCAM, MUC18) melanoma cell biomarker. The single-bead mobility is 3.70 * 10^{-12} m^3/TAs. Based on calculations the magnetophoretic mobility of a cell carrying 10 beads would be 5.5 * 10^{-12} m^3/TAs, and one carrying 1 bead would be 0.5 * 10^{-12} m^3/TAs. The magnets must be able to capture cells within this mobility range. The magnetic labeling efficiency, under the reaction conditions used, was 90%. Magnetophoretic mobilities were measured using a magnetic particle tracking velocimeter (IKOTECH LLC, New Albany, IN).

3.3.4 Cells

The A2058 (ATCCCRL 11147) cells used in labeling and trapping experiments were obtained from American Type Culture Collection and cultivated by serial transfer and used in experiments immediately or stockpiled by slow freezing and storage at -80℃. Magnetized tumor cells were produced for these tests as follows: CRL11147 cells were harvested from culture with viability >90%. These were centrifuged at 200 g for 10 minutes, re-suspended in 1 mL Dulbecco's Phosphate Buffered Saline (PBS) and blocking buffer (6% BSA) for 5 minutes, again centrifuged at 200 g for 10 minutes and re-suspended in 500 μL PBS. To this suspension was added 10 μL of the primary antibody (Anti-MCAM, clone P1H12) and incubated at 4℃for 20 min. After addition of 10 mL PBS the cells were centrifuged at 200 g for 10 minutes and re-suspended in 500 μL PBS and secondary antibody (100 μL of 1.5 μm diameter Biomag^{TM} beads coated with Goat anti-mouse IgG) was added and incubated at

4℃for 20 min. These cells were fixed by adding 500 μL of Cyto-Chex, (Streck Innovations, Inc., Omaha, NE) and incubated for 2 hours before using in magnetic separation experiments or refrigeration for storage. They were diluted to a final feed concentration of 10^4 cells/mL in PBS.

3.3.5 Theoretical calculation of particle movement around magnets

To calculate the trajectory of a magnetic particle passing through the channel in a plane perpendicular to the pole piece we calculate the flow velocity v_x of a massless particle using the CFD results and the magnetophoretic velocity v_x from the ponderomotive force. The magnetically induced ponderomotive force is given by

$$v_x = \frac{B \bullet \nabla B}{2\mu_0}$$

Where $v_x(m/s)$ is the velocity of particles towards the magnet pole face (in the negative x direction), $\mu_m$is the magnetophoretic mobility, and μ_0 is the permeability of free space with a constant of $1.257 * 10^{-6}$ Tm/A. μ_m varies based on the properties of magnetic particles. For the 3.27 μm diameter magnetic beads, $\mu_m = 7.47 * 10^{-12}(m^3/TAs)$, for 1.5 μm diameter beads used for labeling the CRL14777 melanoma cells, $\mu_m = 3.7 * 10^{-12}(m^3/TAs)$. In our simulation task, a strong magnet bead is used, and here $\mu_m = 8.43.1 * 10^{-11}(m^3/TAs)$

For $B \bullet \nabla B$, experimental data is shown in Figure 3.3, provides the relationship between B and distance x. In this system, to simplify the calculation, we assume magnetic force only applies in the x-direction, so $B \bullet \nabla B$ can be simplified to $B \bullet dB/dx$.

From Fig. 3.3 a simplified empirical relationship between B and x was obtained by curve fitting a 2nd degree polynomial in each case (numbering magnets from left to right in Figure 1). For the three magnet profiles we obtain:

$Magnet1 : B = 5.5541x^2 - 84.2x + 425.79$

$Magnet2 : B = 4.7240x^2 - 83.642x + 463.82$

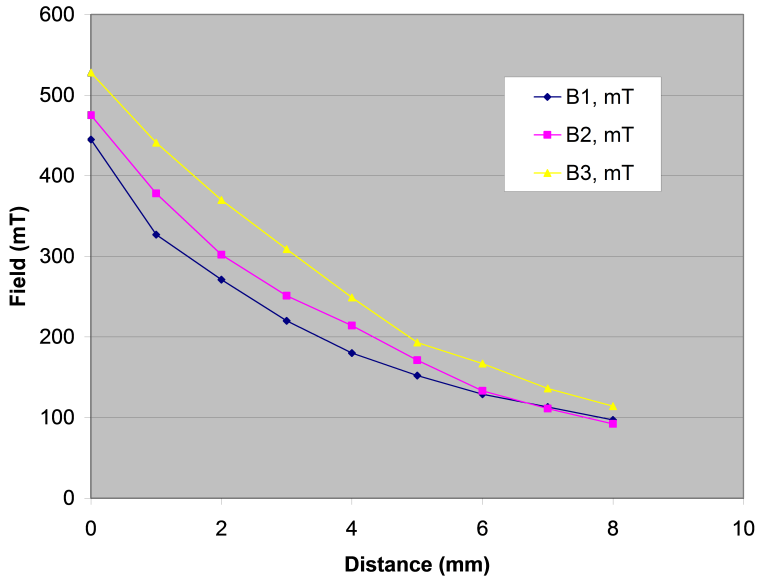

Figure 3.3: Relationship Between Field Strength and Distance

$Magnet3 : B = 4.5509x^2 - 87.957x + 527.23$

where B is in mT and x is in mm. Each of these equations is multiplied by its first derivative to obtain BdB/dx for the three magnets, and these functions are shown in Figure 3.4.

Additionally, the magnetic field magnitude is not uniform along the y direction, so the above equations apply only at the center of the poleface. At other locations they must be multiplied by a factor given by the theoretical distribution across the flat magnet pole face shown in Figure 3.5.

For calculations we consider the effective magnetic diameter be 10mm and use a channel length in the y-dimension be 20mm where magnetic force is present in.

An empirical factor function d is used to calculate B*(dB/dx) as function of y as below (formula(4)):

$d = 1.3 + 0.6y (0 \leq y \leq 0.5)$ (here y in mm)

$d = 1.6 + 0.2(y - 0.5)(0.5 \leq y \leq 1)$

$d = 0.0437y^2 - 0.4368y + 2.0952(1 \leq y \leq 9)$

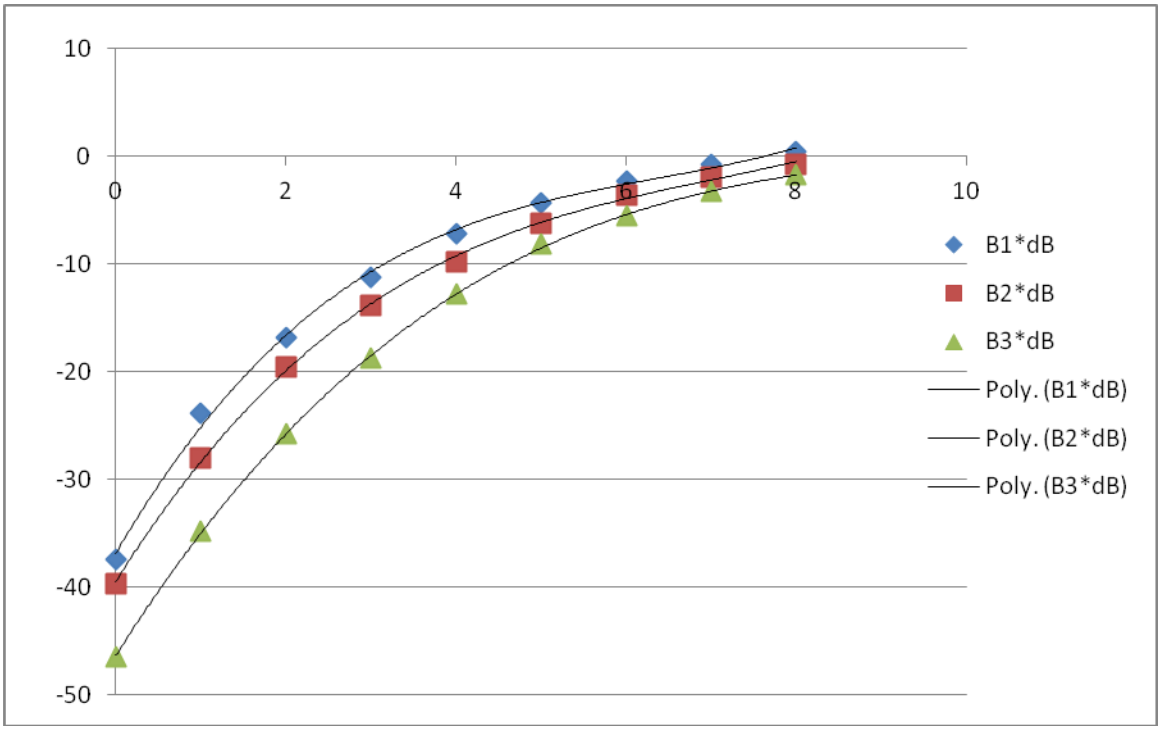

Figure 3.4: Relationship Between Ponderomotive Force and Distance

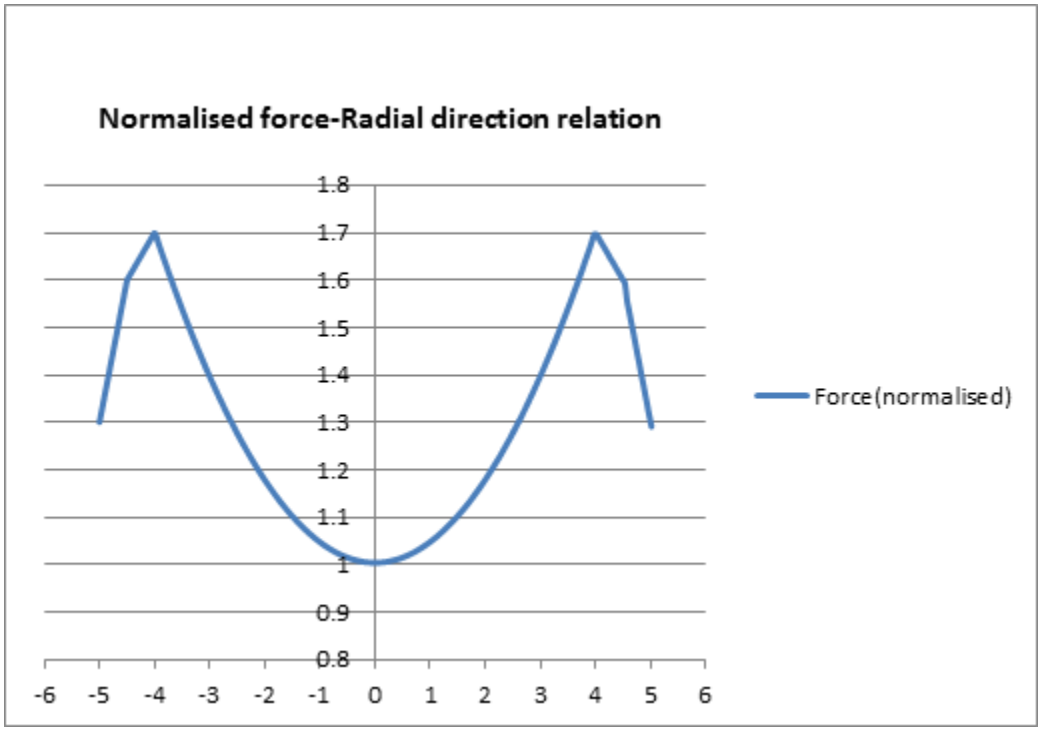

Figure 3.5: Ponderomotive Force Distribution Across the Magnet Pole

$d = 1.7 - 0.2(y - 9)(9 \leq y \leq 9.5)$

$d = 1.6 - 0.6(y - 9.5)(9.5 \leq y \leq 10)$

Then we have modified formula for v_x :

$$v_x = \mu_m d \frac{B \bullet \nabla B}{2\mu_0}$$

For magnet 1, we have:

$$v_x = 1.186 * 10^{-5} * d * (5.5541x^2 - 84.2x + 425.79) * (11.1x - 84.2)$$

For velocity v_y, with the flow rate of 1mL/min, we have: for divided channel, v=0.5mL/min, so in a channel with 5mm height and 4mm width, the average velocity =0.04cm/s=0.4mm/s. To obtain v_y the velocity profile $v_y = ax^2 + bx + c9$ is derived from the CFD simulation with boundary conditions:

At x=0.001 and 0.005 m v_y=0; at x=0.003 m, $v_y = v_m ax$; so that $v_y = v_m ax - a(x - 0.003)^2$ And as the channel can be considered as between 2 infinite planes, $v_(average) = (2/3)v_m ax$,and $v_m ax$=0.6mm/s. Thus for a total input flow rate of 1 mL/min the formula for v_y is:

$$v_y = 0.6 - (x - 3)^2 * 0.15 mm/s$$

and for the flow rate of 3mL/min:

$$v_y = 1.8 - (x - 3)^2 * 0.45$$

3.4 Results

3.4.1 Computational Fluid Dynamics

A mesh with resolution of 0.1 mm was imposed on the channel structure, and input flow rate of 1 mL/min (velocity = $5.32x10^{-}3$ m/s) was simulated. The resulting velocity pattern and distribution of Reynolds' number are shown in Figure 3-6, left and right, respectively.

The FLUENT simulation provides further details of flow pattern in the magnet trap. Figure 3.7 shows flow patterns including fluid velocity as well as flow track in the trap and in one stage of one channel.

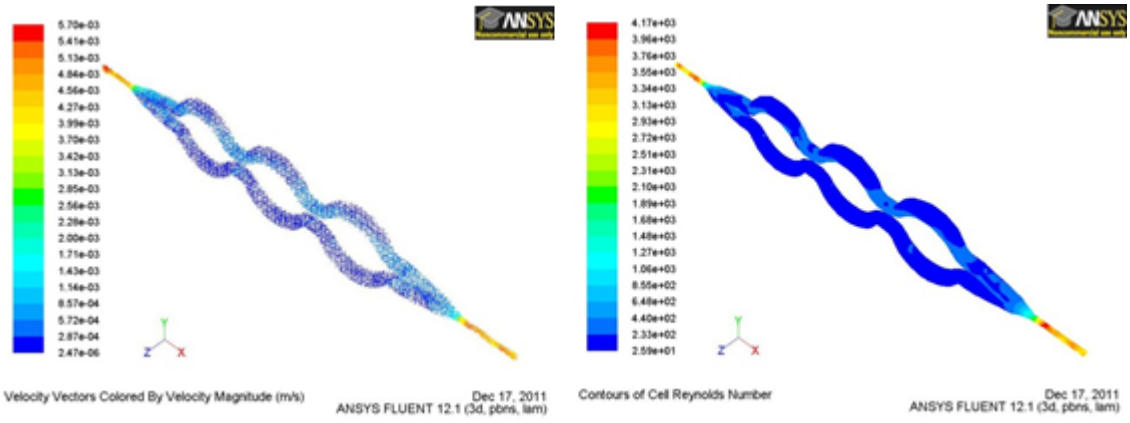

Figure 3.6: Simulation of Velocity Pattern and Reynold's Number

3.4.2 Magnetic particle track along channel

The two-dimensional distribution of the ponderomotive force for magnet 1, as given by equation (6) is shown in Figure 3-8. From these calculations we obtain the function for particle velocity in directions x and y. Using a time step of 0.1s, we obtain the track of a magnetic particles in the channel starting from three values of x when entering the magnetic field of magnet 1. These are shown in Figure 3-9. The result in figure 3-9 also showed the channel's magnetic force arrangement, as indicated by calculation, the strongest magnet force is applied at both ends of magnets, towards the magnet pole.

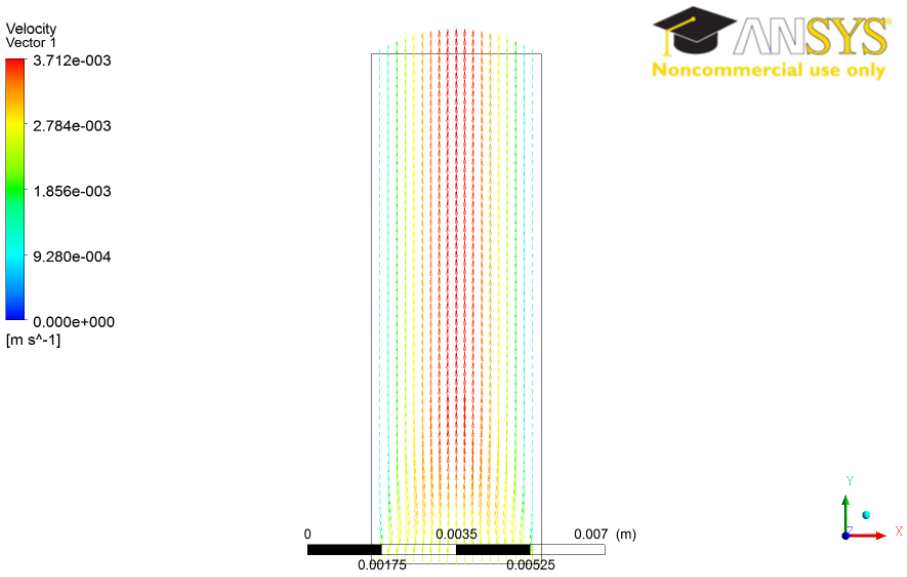

Figure 3.7: Velocity Distribution in the Magnetic Channel

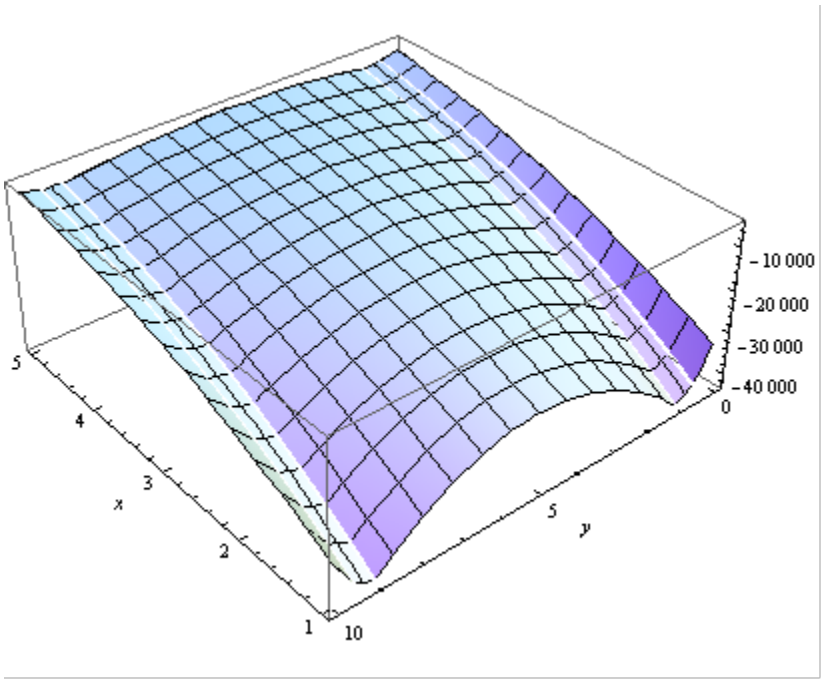

Figure 3.8: Ponderomotive Force in the Separation Area

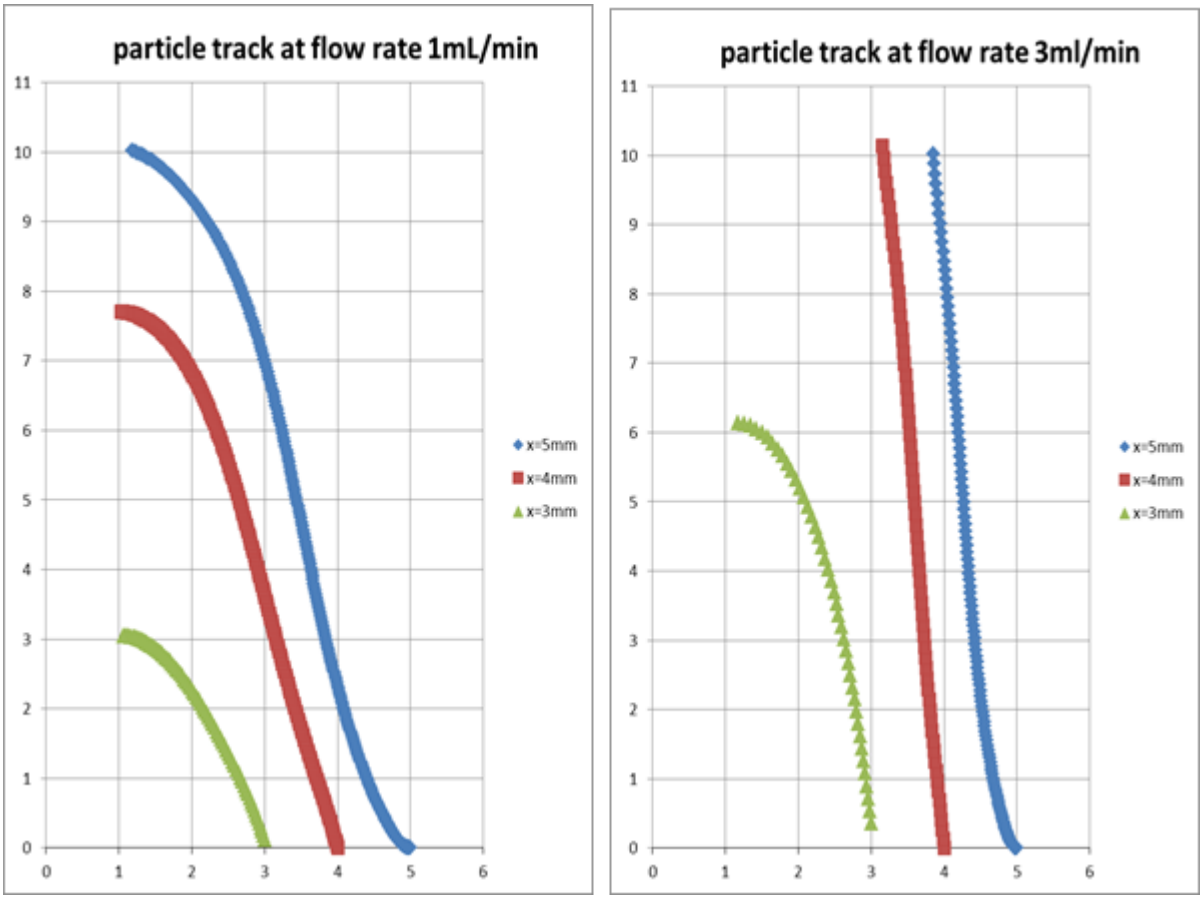

Figure 3.9: Magnetic Particle's Track at different flow rates

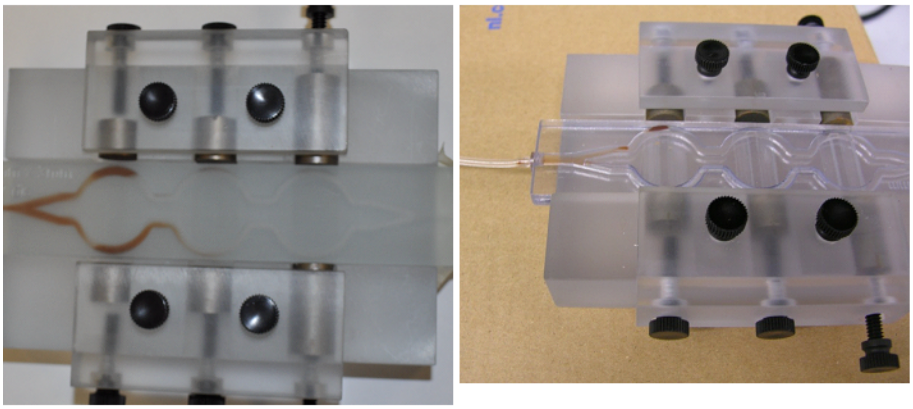

Figure 3.10: Result of Cell Capture and Magnetic Separation

3.4.3 Magnetic Bead Capture Test

In figure 3-10, on the left is a photo of captured beads in the trap. A sample of 3.27 μm diameter polystyrene beads with 14% iron oxide were suspended in 10 mL of distilled water and pumped through the magnetic filter at 1 mL/min, much faster than the final anticipated flow rate for the system. The concentration of particles entering the filter was $4.6 * 10^8$/mL, and the outflow contained <104/mL (near the detection limit). Thus, a log-10-depletion of 4.7, or 99.998% capture was demonstrated.

3.4.4 Cell capture test

In figure 3.10, at right is a photo of captured cells & beads in the trap. Magnetically labeled cells (total of 10^5) were suspended in 10mL of PBS and were pumped through the magnetic trap with a flow rate of 800 μL/minute. The labeling ratio of magnetic particles to cells was 10:1. After pumping the cell suspension through the magnetic trap, all the magnetic particles and the labeled cells were trapped in the designated areas while unlabeled cells escaped the trap and were collected at the outlet (waste). Magnetic trapping was highly efficient, $90 \pm 10\%$ of cells were counted in the trap, and $10 \pm 3\%$ (labeled and non-magnetic) were collected in waste, and the process took less than 10 minutes.

3.5 Discussion

Figure 3-6 and 3-7 showed the velocity profile of magnetic trap. As the simulation indicated, the majority of flow in the trap travels in a low velocity, this indicates a well-developed laminar flow. The stream line showed there's little turbulence among the trap which made it possible to use a 2-D model for the particle simulation. In figure 3-9 the result showed the magnet trap is able to catch all the magnetic particles with one particle, while the efficiency of capture drops with a higher flow rate, with a flow rate of 3mL/min, the capture efficiency drops to 50%, from the picture it's obvious that at x above 4mm, the magnet particle won't be caught within the magnet trap's range. The flow velocity is

essential in cell capture, as the change in v_x is smaller than change in v_y, then it's not able to simply increase flow speed for a fast detection. After all, with the recent design, the majority of magnetic beads can be captured by the first pair of magnet pole; the 3-stage design ensures the capture ability.

3.6 Conclusions

The simulations completed in this study confirm that the proposed magnetic trap design successfully traps positively labeled cells. The magnetophoretic velocity of all beads and cells analyzed to date is much greater than the fluid flow velocity in the magnetic trap and is sufficient to cause cells to be captured by the lowest-strength magnet in the current design.

As the magnetic force is strongest at edge of the magnet poles, particle movement is affected with both v_x and v_y. This prediction is collaborated by experimental tests in which strong magnetic beads and labeled cancer cells are shown to be trapped by the weakest (first) magnet in the staged multi-magnet series.

3.7 Acknowledgments

This research was supported by U. S. Department of Health and Human Services, National Institutes of Health, National Cancer Institute Small Business Innovation Research (SBIR) contract HHSN261201000067C to Techshot, Inc. and by Auburn University. We thank Mr. Byron Guernsey of IKOTECH LLC for supporting the magnetophoretic mobility measurements, Mr. Sam Logan for design and construction of the magnetic trap and John Neuienhuis of Purdue University for providing data forming the basis for Figure 3.4.

Chapter 4

Computational Fluid Dynamic Analysis and Testing of a Static Mixer

4.1 Abstract

The research on the circulating tumor cells (CTCs) requires new design and testing of a point-of-care diagnostic system for detecting and counting tumor cells in patient's blood. Computational Fluid Dynamics (CFD) technology is an effective method for the device's simulation. To improve cell labeling success rate as well as ensure a high mixing efficiency, we set up a model of static mixer for mixing blood samples containing tumor cells and reagents containing magnetic particles and quantum dots. By simulating a state of balance among diffusion, flow rate and sedimentation, we predict optimized values for mixing prior to a magnetic capture processes.

In mixing fluids, particle diffusion speed is highly dependent on particle size. The simulation result showed that after 11∼12 stages of mixing, blood sample and reagent will reach a state of mass and velocity balance, two phases will become well mixed. For a 20-stage mixer, calculation proved it will take only 0.5s for quantum dots to be mixed, but for magnetic particles the mixing time is around 70s.

We set up a model for a labeled cell and calculated its sediment rate. The rate of cell sedimentation is around $3.3 * 10^{-4}$mm/s, and it will take around 6000s for the labeled cell to reach the bottom of mixer. The result showed a 20-stage static mixer can provide adequate time for blood and reagents to be well mixed without the effect of sedimentation. the solution indicates the cells can get labeled well before sediment at a flow rate of 1ml/min through the mixer.

Key words: computer-aid design, static mixer, cell labeling, cell sedimentation, fluent simulation

4.2 Introduction

Circulating tumor cells (CTCs) are dispersed tumor cells circulating in the blood stream which can show the progress of cancer stage.[8] [4] [6] [61] [7] There're 4 stages of cancer development. In stage 4, tumor cells begin to spread inside the patient's blood stream, and will make tumors develop in other parts of the body, which can be fatal for patients if the transfer of tumor cells can't be detected in time. [3] In recent years numerous researchers are successfully using CTCs as a biomarker for cancer early detection.[1] [2] To make patients more likely to participate in detection therapy, the detection of CTC is generally a non-invasively monitor therapeutic progress; thus the refinement of detection technology would play an important role in the biomedical field (Mostert, B., 2009).[85] However, today the detection process can only be performed in specialized laboratories and the analysis requires up to four skilled technicians. Also, the device's cost could be over a million dollars, and only a few institutes can run such an expensive system(Robert Knigsberg etc. al 2010). [86] All these made the cancer detection availability very limited. It requires weeks or even months to get the analysis result, which makes it difficult to detect disease at an early stage[1].

For biochemical engineers, the task is to make the technology widely used and available to the public, by reducing the cost of manufacturing and operation. If as point-of-care (POC) device is developed for such task it can detect target CTCs in seconds, which is convenient for patients to get their result in time (Hsieh, H. B., 2006)[46]. What's more, the researchers have done a lot of work to improve the device's selectivity and efficiency, and many successful designs are reported (Zheng, S., 2011; Han S. I., 2009; Soper, S., 2006) [49] [66] [67]. Also, microfluidic technologies are widely used in POC device design, and it can perform the task of cell labeling and separation in a small and compact device (Kotz, K.T., 2010; Cui S., 2011; Kuczenski R. S., 2011) [68] [55] [57]. For CTCs, researchers have developed several devices for their separation and capture (Zhou J, 2015; Hou H. W. 2013; Nagrath, S. 2007; Stott, S. L. 2010; Zheng S 2007; Marrinucci D. 2012)[96] [97] [51] [34] [25] [99].

An important factor in cancer detection is cell labeling, where blood samples are mixed with magnetic reagents and the magnetic particles coated by antibodies could attached onto targeted CTCs. The effect of mixing is undetermined if samples and reagents are mixed manually, while the specific designed sample mixing system is mainly for laboratory work. To meet the requirement for performing cancer detection in clinics or patients' home, a point-of-care system is the solution. The system will able to perform the mixing task automatically and get the result instantly. To develop such system it's necessary to obtain further data of sample and mixture in the mixer. Many researchers have set up formulas to calculate cell labeling and interaction (Subramaniam D. R., 2013; Zhao C. 2011) [19] [52]. Also, quantum dots are applied in cell labeling process as a signal for further detection (Qian X. M. 2008) [17]. Yet the mixing process is still complicated and to help in the model set up and calculation, then a simulation system is needed for optimization.

The fluid dynamic analysis of the staged mixer is accomplished using the FLUENTTM analysis package, which performs modeling of fluid flow and tracking particles' movement in complex geometries. The fluent system has proved to be a viable modeling and predictive tool in dealing with magnetic particle movement (Marchetta J. G., 2009)[74]. In recent years, the FLUENT^{TM} code has been used to simulate the process of cell labeling and separation, models are set up based on the device designed, and with the proper simulation methods, many approaches can be achieved and various conditions may be analyzed (Khashan S. A., 2011; Mohanty, S., 2010; Plouffe, B. D., 2011)[100] [73] [81].

A static mixer is a precision engineered device for the continuous mixing of fluid materials (Paul, Edward L., 2004)[87]. Normally the fluids to be mixed are liquid, but static mixers can also be used to mix gas streams, disperse gas into liquid or blend immiscible liquids. The energy needed for mixing comes from a loss in pressure as fluids flow through the static mixer. As a widely used device in cell labeling and mixing, it's necessary to get a better knowledge of fluid mechanics inside the mixer. Many factors will affect the result of mixing (Liu M, 2011 & 2012)[101] [102], and simulation of fluid motion inside the mixer is

an essential part in POC device's design. Sedimentation is an important factor in particle mixing which can't be ignored (Richardson J.K., 1954)[103], and study of particle motion largely depends on simulation as methods for laboratory experiments are usually limited (Garcia P. D., 2013)[104]. In conclusion, to get a precise result of particle mechanics in mixing, it's necessary to consider the factor of particle sedimentation during the design of a static mixer.

4.3 Material and methods

4.3.1 device used in experimental work and simulation

Figure 4-1 shows the shape of the static mixer, the tube's diameter is 1cm and length is 15cm. inside it there are 20 buffers which will divide fluid mixture into multiple layers.

The mixer has 20 helical baffles in a cylinder tube. A mesh file has been set up and a model is used to simulate the development of flow. Based on the model a laminar flow pattern has been deduced for calculation. To simulate the separation process more clearly, the task will include the simulation of several factors: first is the multiphase mixing, second factor will be the gravity asserted on particles, which will affect the motion of blood and regent within the system. Considering the amount of inert blood cells, it'll be necessary to discuss about the effect of hindered flow within the system.

Figure 4.1: Photo of Static Mixer

After the simulation we'll set up a discrete model calculating the flow pattern of blood cells, magnetic particles and quantum dots. Also, results of the simulations will be able to direct the optimization of the design of the static mixer.

The static mixer is considered as an Interfacial Surface Generator (ISG) and we will discuss the particle diffusion inside the static mixer. The particle sedimentation is also an

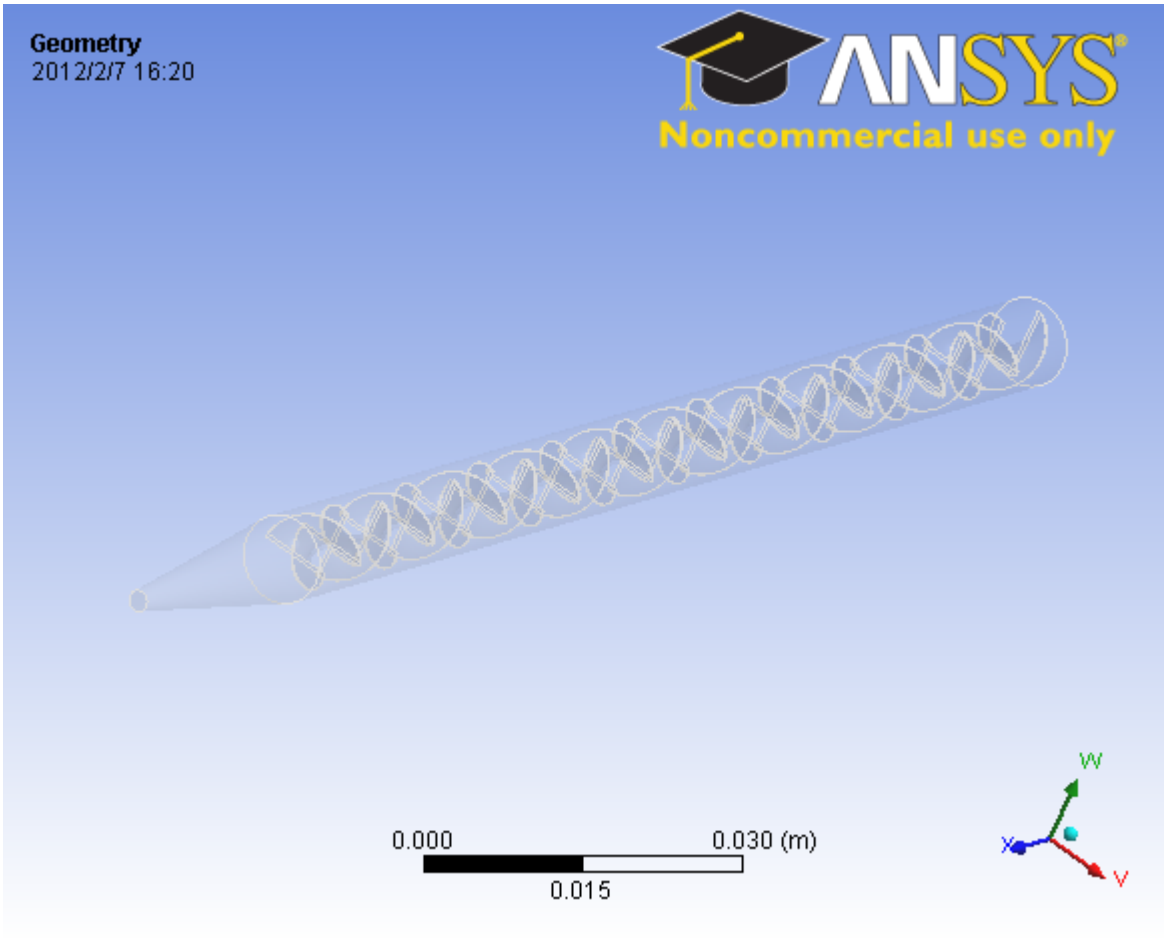

Figure 4.2: Mixer's Model in Fluent

important factor to be discussed, thus calculations will performed to determine whether cells can be successfully labeled and travel through the mixer without sedimentation.

The model for simulation is set up in Ansys^{TM} ICEM CFD program (Figure 4.2).

The shape of baffles is designed for delivering two streams of fluids into the static mixer. As the streams move through the mixer, the baffles can continuously blend the fluids. The helical shape is a widely used design for fluid division. At each new baffle, the fluid will be divided into 2 layers. The result is an exponential increase in fluid's stratification, and fig 4.3 shows the division of flow. The number of striations produced is 2^n where 'n' is the number of baffles in the mixer. The particle inside the fluid is considered performing a Brownian motion and the time it needed to cross the striation is considered to be the diffusion time.

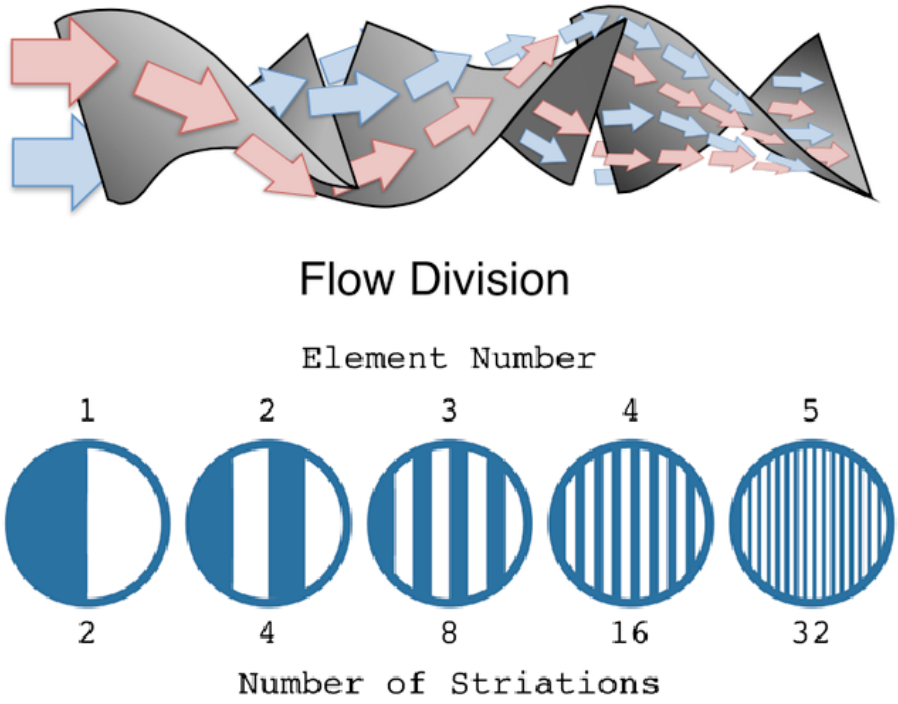

Figure 4.3: Flow Division Inside the Mixer[105]

The more stages we have, the thinner the layer of fluid is, and it'll take less time for particles to diffuse.

Two types of fluid were induced into the mixer, one is 25ml blood sample consisting red blood cells, white blood cells and tumor cells, the other is 5ml reagent consisting magnetic beads and quantum dots. The mixture will flow through the tube in 30 minutes at a flow rate of 1ml/min. The table 4.1 lists properties of particles contained in samples.

It's easy to find out that compare with the red blood cells and white blood cells, the concentration of tumor cells is rather low. The existence of RBC and WBC will interfere with the labeling process thus it's rather difficult to detect the tumor cell. A solution is to increase the concentration of magnetic beads and quantum dots, which will increase the probability for collision between particles, thus tumor cells will more likely be labeled, and the amount of blood sample will increase to provide enough CTCs for labeling and detection.

cell type	diameter (μm)	density (g/cm^3)	concentration (ml^{-1})	sticks to
red blood cell	8.0	1.09	10^9	nothing
white blood cell	10.0	1.07	10^6	nothing
tumor cell	10.0	1.07	100	mag bead and Qdots
magnetic bead	2.8	1.6	10^6	tumor cell
quantum dots	0.02	2.0	10^7	tumor cell

Table 4.1: Properties of Particles Contained in the Mixing Samples

4.3.2 Diffusion of particles within system

To determine the static mixer's performance on cell labeling, it's necessary to set up a model of diffusion first. Our static mixer is considered as an Interfacial Surface Generator (ISG). ISG means the mixer has no-moving parts. It is generally used on applications that involve the mixing of higher viscosity fluids. It's found out that such device is effective in increasing diffusion rate (Vuorema et al, 2010). [88]

The inlet fluid of blood and reagent is considered as two phases. The buffers inside the mixer will divide fluid into multiple layers. Then particles will diffuse between phases, and to have the fluid well mixed, the particle is needed to travel across the distance W between interfaces, which will be:

$$W = R/2^n$$

Here R is the radius of the mixer interior and n is the number of mixer stages. Then it's possible to estimate the time for micro beads to diffuse by Brownian motion across the interfacial distance W. This diffusion time then must be applied to the remainder of the total operation time. By comparing the time needed for a particle to cross layer distance W and the time it stays inside the mixer, it's possible to determine whether two phases can get well mixed.

To calculate the time for diffusion, we'll use Stokes-Einstein equation:

$$W = \sqrt{2Dt}$$

W is interfacial distance, and t is diffusion time and D is diffusion coefficient.

And the coefficient D is defined as:

$$D = \frac{kT}{6\pi\eta r}$$

Where k is Boltzmann's constant, T for temperature, η for fluid's viscosity and r is the radius of the spherical particle.

In our case, the Boltzmann constant $k = 1.38 * 10^{-23} m^2 kg s^{-2} K^{-1}$

And consider T=300K(27℃), here we assume fluid viscosity is the average value of blood and reagent, so the viscosity is 3.5 cP=$0.0035 kg m^{-1} s^{-1}$ [106] and the radius for particle is around 10^{-5}m.

It may be assumed that the dissociation constant for the bead-cell reaction is zero. Thus the magnetic particles and quantum dots will instantly attach upon the cell when they contacts. So in a well-mixed system the tumor cells can be successfully labeled by magnetic particles and quantum dots.

4.3.3 The effect of sedimentation

During the separation process, gravity will affect the motion of particles. At a low flow rate, blood cells and labeled CTCs will sediment inside the mixer and be left undetected. Also, the great number of blood cells affect the interaction between particles would also hinder the target particles' movement, so it's necessary to discuss the sedimentation factor inside the system.

Assume the environment has no other disturbance and the particle is only affected by gravity. According to the Stokes' equation, the particle is affected by the fluids' drag force

F, with the formula:

$$F = 6\pi\eta\nu r$$

Here F is the viscous drag force, η is viscosity of fluid, ν is particle's velocity relative to fluid and a is radius of particle.

In a state of balance, the drag force applied to the particle is equal to the resistant force inside the fluid, thus we may obtain the formula:

$$6\pi\eta\nu a = \frac{4\pi r^3}{3}(\rho_s - \rho)g$$

Here ρ_s is density of particle and is density of fluid, g is acceleration of gravity. Reorganize the formula we have the velocity of a single particle's sedimentation is:

$$\nu = \frac{2(\rho - \rho_0)gr^2}{9\eta}$$

Here v is the sedimentation velocity, a is radius of particle, ρ and ρ_0 are density of particle and fluid, g is acceleration of gravity and η is viscosity of fluid.

The Re number of single particle is:

$$Re = \frac{2r\nu\rho}{\eta}$$

And consider the existence of other particles during sedimentation process, the resistance force inside fluid also depends on the presence of other particles since they'll affect the flow pattern. So it's necessary to discuss the relationship between single particle sedimentation (v) and sedimentation velocity with other particle involved (v_c).

The resistance force received by particle is determined by viscosity of fluid (μ) and density of particle (ρ), radius of particle (a) and the initial velocity of particle inside fluids. Then there's a function describing the relationship between the resistance force and particles'

properties. It can be written as:

$$R = f_1(\eta, \rho, r, \nu)$$

The existence of other particle will affect the resistance force as well. With a higher volume fraction of particle, the flow between particles will have steeper velocity gradients and increase the shearing stresses. The equation can be rewritten as:

$$R = f_2(\eta, \rho, r, \nu, \phi)$$

Here ϕ is the ratio of particles among the mixer, and then the ratio of particle diameter to tube diameter is included:

$$R = f_3(\eta, \rho, r, \nu, \phi, \frac{d}{D})$$

Also, the variables can be rearranged as:

$$\nu = f_4(\eta, \rho, r, R, \phi, \frac{d}{D})$$

To simplify the calculation, next step is to reorganize the variables to get a dimensionless combination.

The unit for viscosity η is kg/(m*s), for density ρ is $\frac{kg}{m^3}$, for radius r the unit is m and for resistant force R, the unit is $\frac{kg*m}{s^2}$

So the dimensionless form is:

$$\frac{R\rho}{\eta^2}$$

Thus we have the result formula:

$$\nu = f_5(\frac{R\rho}{\eta^2}, \phi, \frac{d}{D})$$

And for particle in a system without hinder, the sedimentation velocity $\nu_0$is:

$$\nu_0 = f_6(\frac{R\rho}{\eta^2}, \frac{d}{D})$$

Divide them we have a ratio equation:

$$\frac{\nu}{\nu_0} = f_7(\frac{R\rho}{\eta^2}, \phi, \frac{d}{D})$$

For the dimensionless value:

$$\frac{R\rho}{\eta^2}$$

Since we have:

$$Re = \frac{2r\nu\rho}{\eta}$$

So the dimensionless value can be rewritten as:

$$\frac{R\rho}{\eta^2} = Re^2 * \frac{R}{(2r\nu\rho)^2}$$

Here$\frac{R}{4\rho\nu^2}$ is a resistance coefficient, which is a constant value for a given particle. Then we have a relationship between ν_c and ν:

$$\frac{\nu_c}{\nu} = f(Re, \phi, \frac{d}{D})$$

The relationship between sedimentation rate and volume fraction can be defined from experiments. It's proved that there's a linear relationship between $log\nu_c$ and $log(1-\phi)$.

So the velocity of sedimentation should be adjusted as:

$$\nu_c = \nu(1-\phi)^n$$

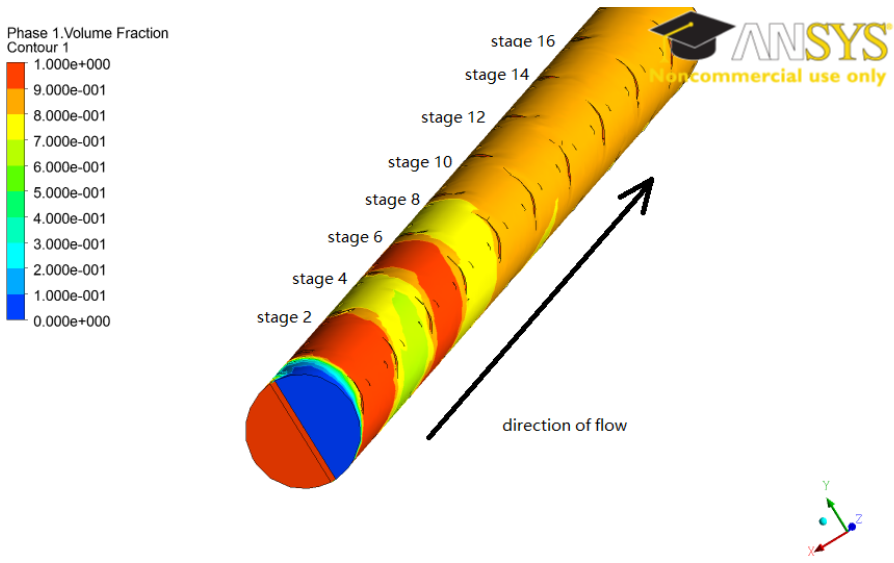

Figure 4.4: Volume Fraction of Fluid Mixing (front sight, blood phase)

Where ν_c is the adjusted sedimentation velocity of particles in the mixing system, ν is the sedimentation velocity of individual particles, and ϕ is volume fraction of particles, and n is the function of shape and Re number.

4.4 Results and discussion

4.4.1 result of static mixer's simulation

With the help of Ansys^{tm} fluent system, we've worked out a simulation of the two phases' mixing. The simulation result indicates that two phases will get well mixed at the center of the mixer. It's showed in Fig 4-4 to Fig 4-7, Phase 1 is blood sample (red) and phase 2 is reagent (blue). from 4-4 we may find after 11∼12 stages of mixing, the volume fraction of mixture will reach a balance point with 80% of blood sample and 20% of reagent. Fig 4-5 shows the center of mixing fluids, the change of volume fraction indicates the diffusion process. Fig 4-6 shows at the outlet of mixer, blood and reagent are well mixed. Fig 4-7 shows the phase of reagent inside the mixer.

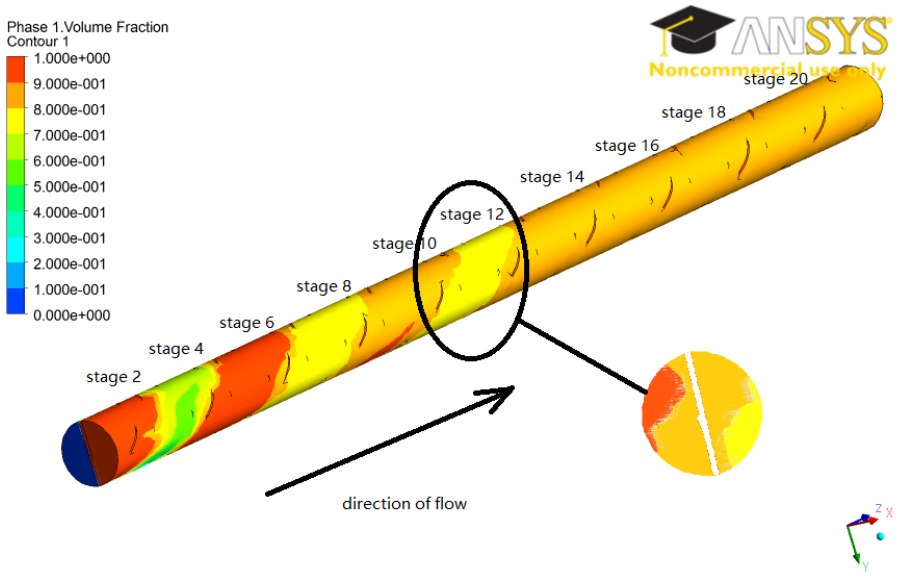

Figure 4.5: Volume Fraction of Fluid Mixing (side sight, center cuts, blood phase)

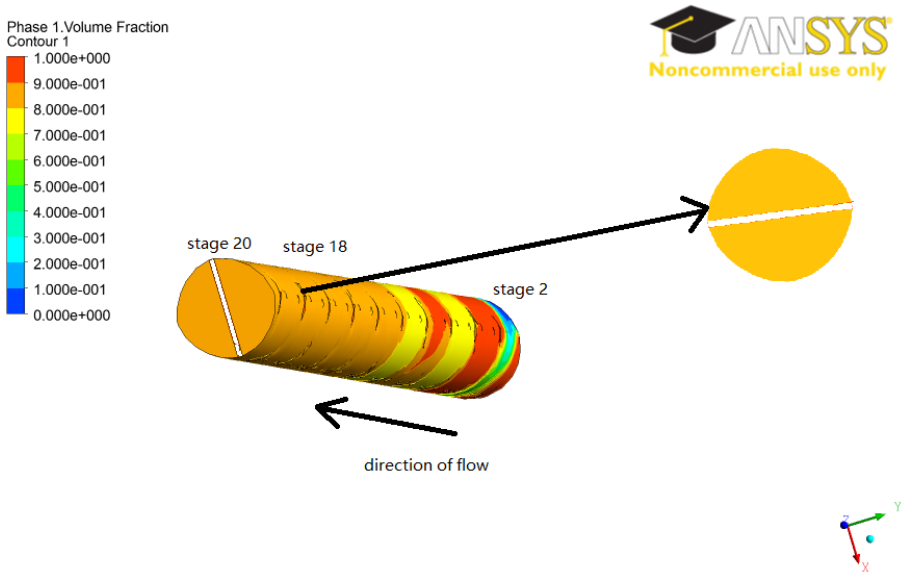

Figure 4.6: Volume Fraction of Fluid Mixing (outlet side, blood phase)

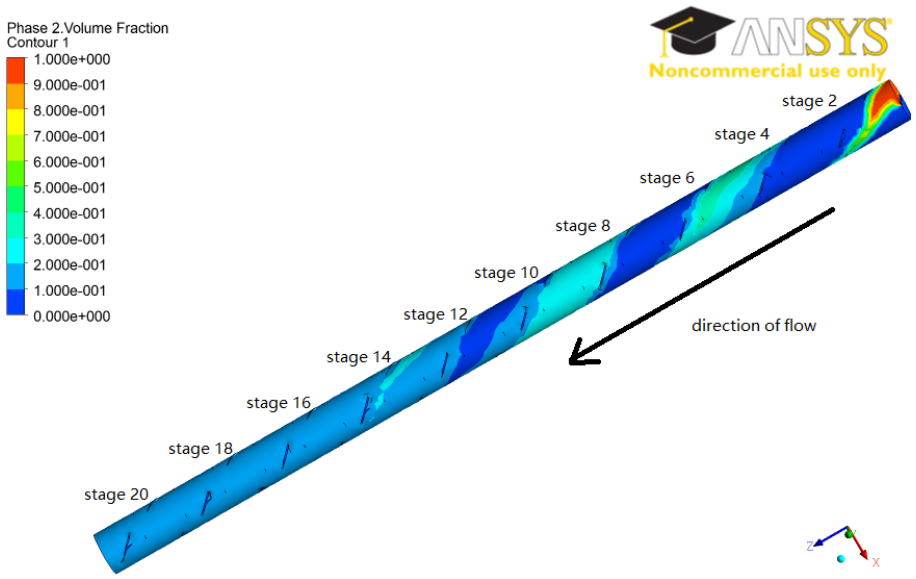

Figure 4.7: Volume Fraction of Fluid Mixing (side view, reagent phase)

Another set of simulations shows the streamline of particle velocity in the mixer, from the picture it is shown that there is a difference of velocity at the inlet of mixer, and the speed of velocity unified at the middle of the mixer. Fig 4-8 and 4-9 showed the velocity profile in the form of stream lines. From the result it is easy to see, the difference of speed was eliminated after 2∼3 stages of mixing. Another group of pictures showed the stream lines of particle velocity in the mixer, from the picture it is observed that there is a difference of velocity at the inlet of mixer, and the speed of velocity unified at the middle of the mixer.

4.4.2 discussion of particle's diffusion

The calculation results in table 4.2 showed for a 20-staged mixer, the quantum dots' diffusion time is around 0.5 minute, and the result showsed the quantum dots are easier to cross the layer more easily while magnetic particles' labeling efficiency is lower. The volume of the mixer is 12cm^3, so the time for the mixture travel through the flow is around 20 minutes. In conclusion the static mixer provides enough time for particles get well mixed. The flow rate of blood sample is 0.83 ml/min and the rate of reagent flow is 0.16 ml/min,

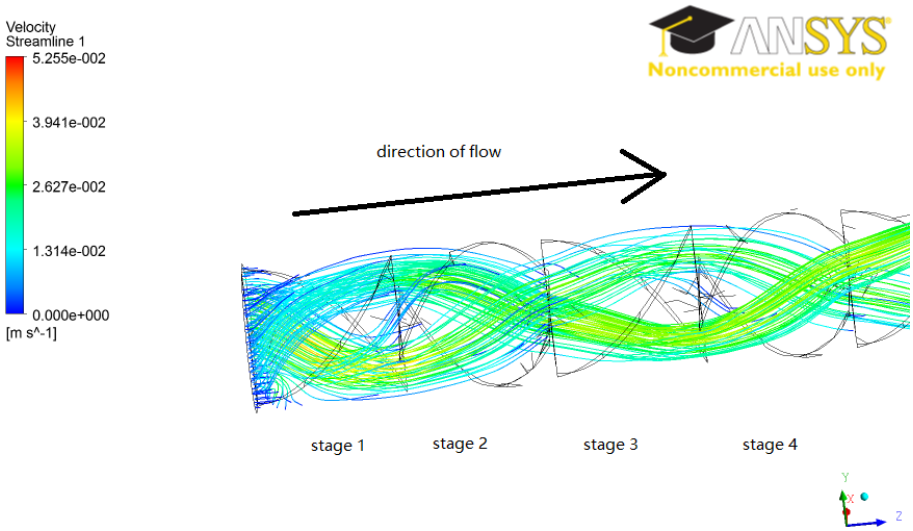

Figure 4.8: Stream Lines in the mixer (partial)

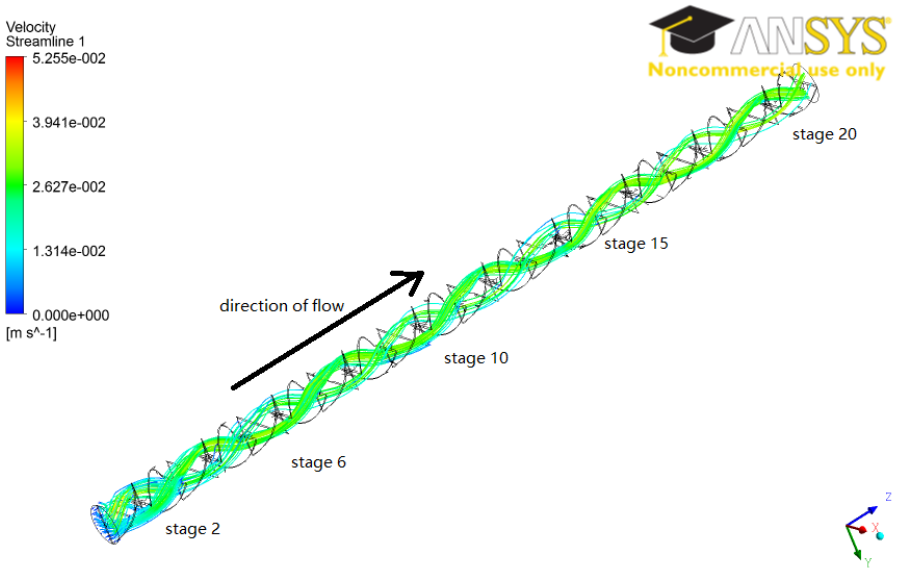

Figure 4.9: Stream Lines in mixer (overview)

n(stages)	W(mm)	t(Qdots) (s)	t(mag beads) (s)
1	2.5	$4.98*10^{5}$	$6.98*10^{7}$
2	1.25	$1.24*10^{5}$	$1.74*10^{7}$
3	0.625	$3.11*10^{4}$	$4.36*10^{6}$
4	0.3125	$7.78*10^{3}$	$1.09*10^{6}$
5	0.1263	$1.94*10^{3}$	$2.72*10^{5}$
6	0.0781	$4.86*10^{2}$	$6.81*10^{4}$
7	0.0391	$1.21*10^{2}$	$1.70*10^{4}$
8	0.0195	30.4	$4.26*10^{3}$
9	$9.77*10^{-3}$	7.59	$1.06*10^{3}$
10	$4.88*10^{-3}$	1.90	*266
16	$7.63*10^{-5}$	$4.63*10^{-4}$	$6.5*10^{-2}$
17	$3.81*10^{-5}$	$1.16*10^{-4}$	$1.62*10^{-2}$
18	$1.91*10^{-5}$	$2.90*10^{-5}$	$4.06*10^{-3}$
19	$9.54*10^{-6}$	$7.24*10^{-6}$	$1.02*10^{-3}$
20	$4.77*10^{-6}$	$1.81*10^{-6}$	$2.54*10^{-4}$

Table 4.2: Capture Counts for Low Cell Concentration

cell type	diameter(μm)	density(g/cm^3)	concentration(ml^{-1})
tumor cell	10	1.07	100
magnetic bead	2.8	1.6	10^6

Table 4.3: Properties of Tumor Cell and Beads

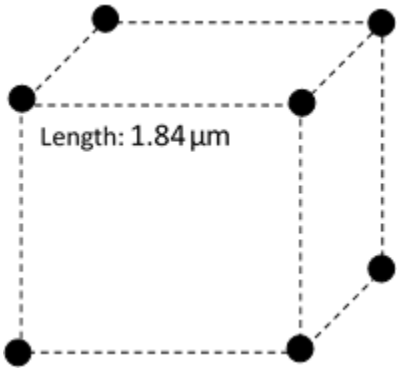

Figure 4.10: Cubic Model of Bead Distribution

considering information of cell types shown in table 4.3, we can perform further analysis. For tumor cells the concentration is about 0.83*100=83(cells/ml)

For magnetic beads the concentration is about $10^6 * 0.16 = 1.6 * 10^5$ (beads/ml), which means in average a magnetic bead will occupy $1/(1.6 * 10^5) = 6.25 * 10^{-6}$(ml/per bead),or $6.25 * 10^6 \mu m^3$ per bead.

Here we made an assumption: the shape of occupied space is cubic, the size of the cube is 184*184*184(μm), and consider tumor cell as a mass point at the center of cube, magnet beads form corners of cube.

To simplify the calculation, here we consider reagents and samples are well-mixed, and magnetic beads have a uniform distribution. As Fig 4-10 showed, the length of cube is much larger than tumor cell, which means it's unlikely for tumor cells labeled by magnetic beads in a still state.

In the laboratory, the solution is to use shake bed move the fluid, thus increase cells and magnetic bead's collision ratio. For static mixer, the divided layer W is getting thinner with increasing stages. From the data in table 4.2, when n>5, the layer thickness W will less than the average distance between magnetic beads, this means between 2 beads in Fig 4-6, there'll be more magnetic particles in this area. When n>9, the layer thickness W will less than tumor cell's diameter, which will further increase the collision ratio between magnetic beads and tumor cells. The simulation result proves our conclusion as well, after 4∼5 stages, the difference between blood phase and reagents become smaller, and the mixture reach balance state after 10 stages.

Two more factors increase the probability of collision: magnetic beads are sort of spheres than mass points, and the concentration of beads are usually higher than 106 beads/ml; and the existence of RBCs and WBCs reduce the space for magnetic beads. Thus the occupied area per beads is smaller and further ensures that they can touch CTCs in the mixer.

In conclusion, the calculation proves that magnetic beads will have a throughout collision with tumor cells. When consider the labeling process as a zero-order reaction, it's able for us to consider the cells are successfully labeled.

4.4.3 calculation result of sedimentation

In the mixing fluid the WBC, tumor cells, magnetic particles and quantum dots are all simplified as spherical particles, while the RBC is a cylinder with a height of around $1.5\mu m$.

Considering the particle attached to the cells, the diameter of a CTC is around $10\mu m$ and for magnetic particles and quantum dots, the diameter is 2.8 and $0.02\mu m$, respectively. Taking the relative size into account and ignoring the antibody arrangement on surfaces, the surface area of a tumor cell is around $100\pi\mu m^2$, each magnetic particle will cover an area of $1.96\pi\mu m^2$. So we can simplify the model by assuming 10 magnetic particles and 100 quantum dots attached on one tumor cell. From the data given on tables, it's easy to find

the size of labeled tumor's overall Volume is $6.385 * 10^{-7} mm^3$ and the particle's overall mass is $7.44156 * 10^{-10}$ g, and particle's average density is 1.165 (g/cm^3)

Assuming the labeled cell's shape is spherical; the average radius is $5.34195 * 10^{-3}$ mm. And the particle's mass flow rate is$2.0671 * 10^{-13}$ kg/s. The viscosity of fluid is close to blood thus it's considered as no higher than 0.035g/cm/s. From the equation given:

$$\nu = \frac{2r^{2(\rho-\rho_0)g}}{9\eta}$$

It's easy to get the sediment velocity of an individual cell as 0.00103 mm/s.

$$Re = \frac{2r\nu\rho}{\eta}$$

For The Re number of single particle is 0.0008, and then it's possible to discuss the sedimentation velocity:

$$\nu_c = \nu(1-\phi)^n$$

From researchers' experimental data (Richard et al. 1954) [103], when Re<0.2, corresponding to conditions under which inertial forces can be neglected, the results are correlated by a single line with equation:

$$n = 4.65 + 19.5\frac{d}{D}$$

Here d is diameter of particle and D is diameter of the static mixer.

So for the labelled cells the ratio d/D is close to 0, so the result can be simplified to n=4.65. The particle occupied in the mixture is around $319 mm^3$, thus the volume fraction ϕ is 0.319.

Taking those values into the volume fraction, we have sedimentation velocity $\nu = 0.00103 * (1 - 0.319)4.65 = 3.3 * 10^{-4} mm/s$. For a 5 mm*4 mm channel, a particle at the middle of the channel, it will take around 6000s (100 min) to reach the bottom of the trap.

In this system the flow rate in the channel is 1 ml/min, take the channel size into calculation, we have the average speed of flow is 0.69 mm/s, to flow through the channel (around 12 cm in length), it'll take around 280 s, compare the sediment speed, it's easy to get the conclusion that during the separation process, the sediment wont be a major factor on the particle motion.

4.5 Conclusion

The static mixer is able to divide the incoming fluid into multiple layers. The particle's diffusion inside the device enables cells' successful labeling.

The size of particles is an important factor in diffusion, for quantum dots (d=0.02 μm), it will take about 10^{-6} s to be successfully uniform, and for magnetic particles (d=0.28 μm), the time it will take for fully mixed is around 10^{-4} s, so at this flow rate, the magnetic particles and quantum dots can be completely uniform. The results of simulations and particle calculations both showed at a flow rate of 1ml/min, the static mixer is able to make the blood and reagents well mixed within 12$\sim$15 stages of mixing.

The shape of baffles can successfully divide fluids into multiple layers, the thinner the layer is, the shorter time particles required for crossing the layer. For a 20-stage mixer, it will take 10^{-4} s for magnetic particle to cross the layer, which is shorter than the time it needed to travel across the mixer (around 5 min). And the sedimentation time for labelled cells is around 6000s, which means labelled cells travel through the mixer long before ittheythem sediment into the bottom of mixer.

The result of simulation and particle calculation both showed the static mixer is able to make the blood and reagents well mixed within 12$\sim$15 stages of mixing, and the sediment time is longer than time particles stay inside the mixer. Thus the flow mixer is a proper design for the requirement of point-of-care device.

4.6 Acknowledges

The model of circulating tumor cell detector including the static mixer is provided by Techshot inc. Also, the sample of blood and reagent are both provided by Techsot as well.

Chapter 5

Experiments on Cell Labeling and Separation

5.1 Abstract

To test the point-of-care detector's efficiency, experiments on cell labeling and separation were performed. The tests check particle diameters and magnetophoretic mobility, so we are able to determine the magnetic trap's capture ability as well as the static mixer's cell labeling efficiency. The whole blood is used to test how the red blood cells will affect the detection. During the test, first hemacytometer is used to test the capture ratio of the magnetic trap. After the cell labeling and separation tests were performed, Hyperflux^{tm} system is used to detect particle motion and magnetophoretic mobility distribution. A statistical analysis of data is obtained during the test and a better understanding of cell labeling is gained.

The results of hemacytometer counts indicated the magnetic particle was able to perform the cell separation task with good capture efficiency. The static mixer proves to have a similar cell labeling efficiency to that of the traditional way using shake-bed labeling. The Hyperflux^{tm} plotting data showed cells are successfully labeled by magnetic beads by static mixer, and the magnetic trap is able to capture particles for detection. The whole blood has hindered cell detection, and it's necessary to process the blood sample and ensure unlabeled cells are washed away properly.

Keywords: cell labeling, magnetic particles, magnetic separation, Hyperflux^{tm} analysis

5.2 Introduction

To test the performance of the circulating tumor detector, to complement the results of simulations performed in previous chapters, a series of tests was undertaken to analyze

the device's ability in separation and mixing. The magnetic trap should be able to separate labeled cells from unlabeled cells, while the static mixer is designed to have all targeted cells labeled.

The cell labeling is an essential part in circulating tumor cell detection. In this design, cell labeling is based on antibody-antigen interaction to attach magnetic beads to cells. Considering the low concentration of tumor cells expected in blood samples, the mixing time should be adequate to ensure at least a number of detectable tumor cells can be labeled.

In the laboratory, to mix 1ml of cell sample with reagent, the procedure requires at least 30 minutes for cells to get labeled. For the static mixer, at the current designed flow rate, the mixing time is around 10∼15 minutes. The simulation result accomplished in chapter 4 was based on an assumption that the labeling process is a zero-order reaction, and cells will get labeled instantly after becoming mixed with the reagent. The desired result is all target cells in a mixture can successfully be labeled. If some cells escape during the test, the escape ratio should be low enough to avoid a false-negative result.

The magnetic separator determines how successful the detection is. When a cell mixture flows through the device, the majority of blood cells will flow through the system, thus target cells and free-moving magnetic beads will stay inside the trap. Hemacytometer counting is applied to compare the capture ratio before and after the magnetic separation; however, hemacytometer counts are reliable only when over 100 target cells are accounted. At a low cell concentration, the result of hemacytometer counting is always less than 20 in the whole counting area, so at a low concentration like in patient blood samples, it's only able to determine whether the tumor cells are able to be detected or not. To determine the magnetic trap's performance can only be determined accurately at a high concentration, with around 104∼105 tumor cells per sample.

To check the result of separation and mixing, the Hyperflux^{tm} velocimeter system is applied to analyze magnetophoretic mobility. There are differences in mobility among magnetic beads, labeled cells, and escaped cells. By comparing the mobility histograms and

particle tracks, we obtain information about the efficiency and selectivity of the cell capture process.

5.3 Material and devices

5.3.1 Cells and Culture Media

The tumor cell line used in all tests is CRL-211, DT40; the cell's type is Bursa Lymphoma of Chicken (Gallus gallus), and the cell is produced in Manassas, VA by ATCC.

The antibody used is Mouse monoclonal M-1 Anti-Chicken IgM mu chain (Biotin), the antibody is produced in Cambridge, MA by Abcam^{tm}, and product id is ab99719.

The components of cell culture media are listed below:

69% Dulbecco's modified eagle's medium (DMEM), produced in Milwaukee and producer is SIGMA^{tm}. Its product id is D6429.

10% of tryptose phosphate broth solution, produced in Milwaukee and producer is SIGMAtm. Its product id is T8159.

10% of fetal bovine serum (FBS), produced in Manassas, VA, produced by ATCC^{tm}. Its produce id is ATCC 30-2020.

5% of chicken serum, produced in St. Louis. Producer is SIGMA^{tm}. Its product id is C5405.

1% of ABAM (Antibiotic-Antimycotic mixture, producer is SIGMA^{tm} and the product is from St. Louis, the product id is A5955) is also added into the media.

The blood sample used is 500ml bovine whole blood provided by Animal Tech, TX.

5.3.2 Magnetic Beads

Magnetic beads used in the testing are Dynabeads^{tm} Biotin Binder (InVitrogen/Dynal), the producer is InVitrogentm in Oslo, Norway, and the catalog number is 11047. The magnetic bead's magnetophoretic mobility range is between $1.3\sim2.0*10^{-11}m^3$/TAS and the concentration of beads is $4*10^8$ beads/mL in the original product.

The simulations in Chapter 3 used the magnetophoretic mobility μ_m as $8*10^{-11}$ m^3/TAs. A lower mobility is expected to reduce the magnet trap's capture ability.

5.3.3 Static Mixer and Magnet Trap

The version of the trap used in these studies was designed with three pairs of curved trapping stations and three pairs of magnets with pole-face field strengths of 430, 470 and 520 mT. The length of the trap is about 15 cm (Figure 3-10). At each station the north pole of the magnet was adjacent to the channel. Thus magnets of each pair, though at some distance from one another, were matched in north-to-north configuration to maintain maximum field divergence. The width of the channel is 4 mm, and the height is 5mm. Distance between magnet and channel is 1 mm. The magnet is attached with bolts and can be installed and removed easily. Additional details are given in Chapter 3, especially Figures 3-1 and 3-7.

The static mixer is made up of a tube 1 cm in diameter and 15 cm in length. The mixer's inside structure consists of 20 helical baffles which divide each of the two fluids mixture into multiple alternating layers. A mesh file is set up and a model is used to simulate flow development. Based on the model used in Chapter 4, a laminar flow pattern is deduced for calculation. In the simulations of Chapter 4, two types of fluid were induced into the mixer, first was 25ml blood sample consisting of red blood cells, white blood cells and tumor cells, the other is 5ml reagent consisting of magnetic beads and quantum dots. The mixture will flow through the tube in 30 minutes at a flow rate of 1ml/min. And the flow is achieved using one or two digitally controlled syringe pumps. In our test, the pump is produced by Cole-Parmertm and the product type is ew-74900-15. However, the syringe we use in the test is different from the product default setting, and the pump setting is shown in Chapter 4.

5.3.4 Hyperflux^{tm} Velocimeter System for Determining Magnetophoretic Mobility

The Hyperflux^{tm} Velocimeter system is a particle analyzer and velocimeter that is used to measure the speed of movement of cells based on magnetophoretic mobility. It is driven by a calibrated magnetic field within the device. In addition to measured speed, the Hyperflux^{tm} also measures and generates 22 other characteristics about each identified particle including: size, sedimentation rate, shape, intensity etc. The image sets created by the high-definition video camera are stored in memory and can be used for processing and data evaluation. These image sets were captured using the IKOVision program with specifically selected particles and operation conditions.

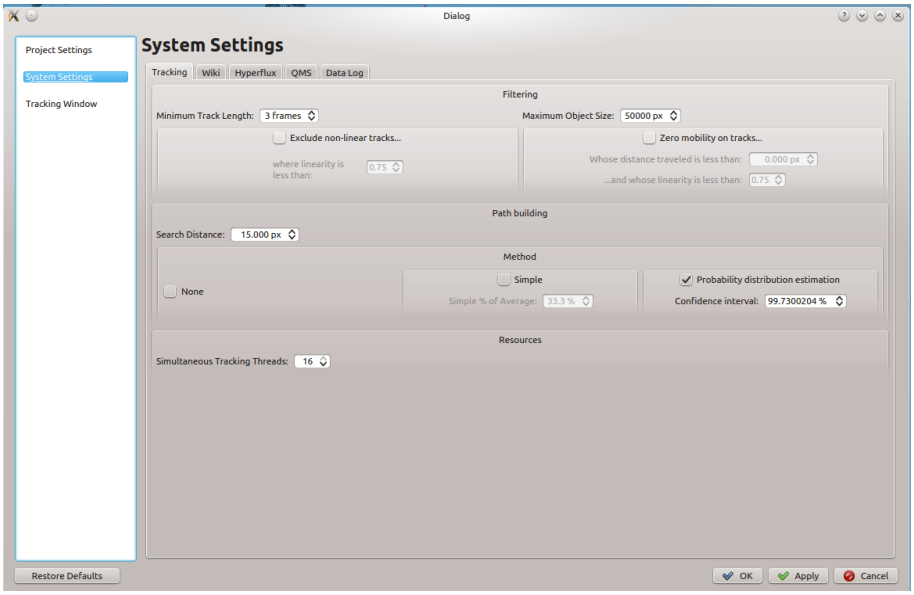

Figure 5.1: "Project Settings" Setup Interface for Hyperflux^{tm}

The figure 5.1 above shows the setup of the tracking system. The unit used here is pixel. With fluids flowing through the channel, the system can capture the particles flowing through it and record its track and mobility. Before running particle tracking, the first thing to do is to adjust the search distance. It determines the search area for particles, a large search distance is necessary when target particles have a large size, or the moving speed is too fast

to be captured. However, the larger the search distance, the more undesired particles will be detected and affect the tracking result. When the system is set at a high concentration, a large search distance will reduce the accuracy of particle tracking. The default value (15 pixel) is suitable for most cases of cell detection. Figure 5-2 shows the manual fluids setup

Figure 5.2: Interface for Manual Fluid Operations

interface, before running the particle analysis it's necessary to run the vacuum pump and create a pressure drop inside system. After clean up of the channel with buffer and filling the detection area with sample, it's ready to run particle tracking.

After tracking is finished, next is to analyze the results. To get the desired result, it's necessary to adjust the threshold and size rage of the particles accepted. The adjustment of threshold performs as a filter and will increase or decrease number of cells be accounted. A high threshold will reduce undesired particles, but the number of available samples is reduced

as well. In our test, as the concentration of particle is rather high, a higher threshold is necessary to improve the tracking

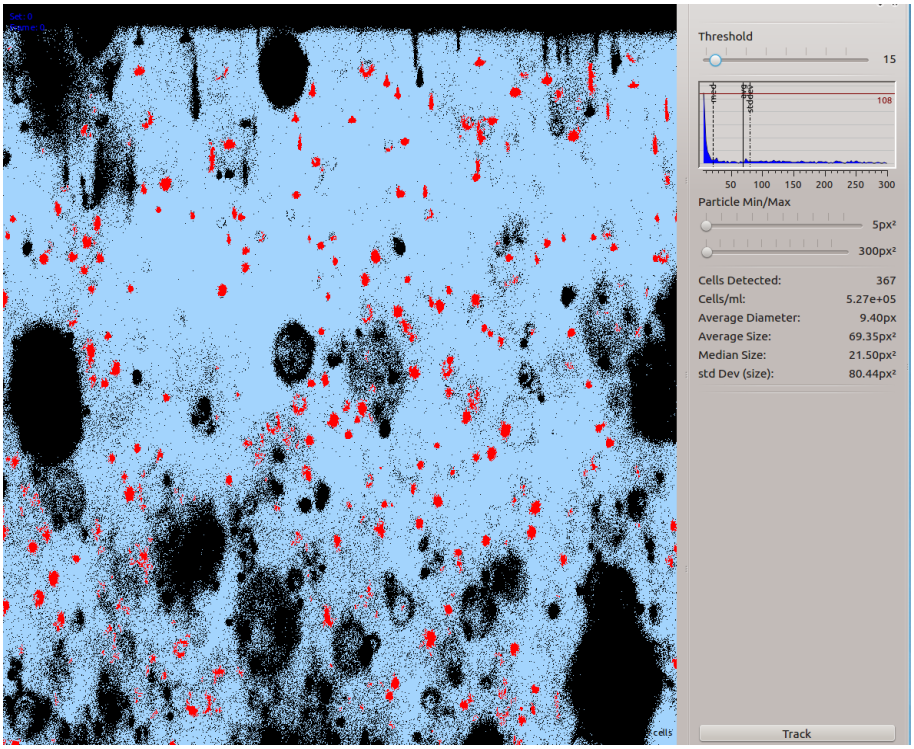

Figure 5.3: Figures of Particle with Low Threshold

Figure 5-3 shows an image display with default intensity threshold. A lot of undesired particles are in the area, this will slow down the simulation speed and take many wrong tracks into account.

With a higher threshold, as in figure 5-4 the number of beads has been reduced to a value able to be tracked with a correct value. And after tracking, the result can be seen directly in software. Figure 5-5 showed the magnetic beads' track inside the system. Hyperflux^{tm} captured and recorded motions of particles inside the channel. Beads affected by the magnetic force and traveling from left to right.

After tracking, a histogram is created and the sample's mobility distribution is shown in the histogram (Figure 5-6). It is possible to obtain the particle's peak mobility value.

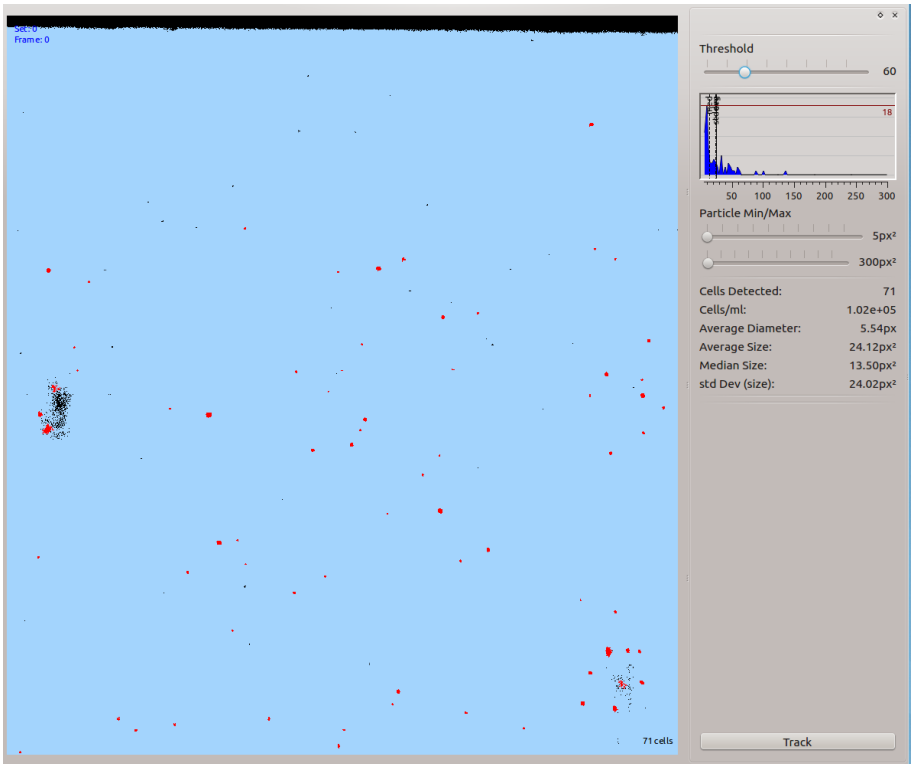

Figure 5.4: Figures of Particle with High Threshold

By comparing peak mobility and mobility distributions before and after magnetic separation, it's possible to tell whether the cells are successfully labeled and the magnetic separator is able to separate labeled cells from unlabeled cells.

5.4 Test Plan and Procedures

First the device's magnetic separation ability was tested using known labeled target cells. The magnetic beads and cells were mixed in 15 mL centrifuge tubes on a shaking bed for 20 minutes at 23 ℃. Thus all target cells are considered as labeled.

First we used a high concentration cell sample that will provide an indication of the magnetic trap's performance. It's expected that the device is able to keep a relatively high and steady capture efficiency at a high tumor cell concentration. Then we dilute the suspended cells to the lowest practical concentration and checked the separation patterns using hemacytometer counts and with the help of the Hyperflux^{tm} analyzer. The system

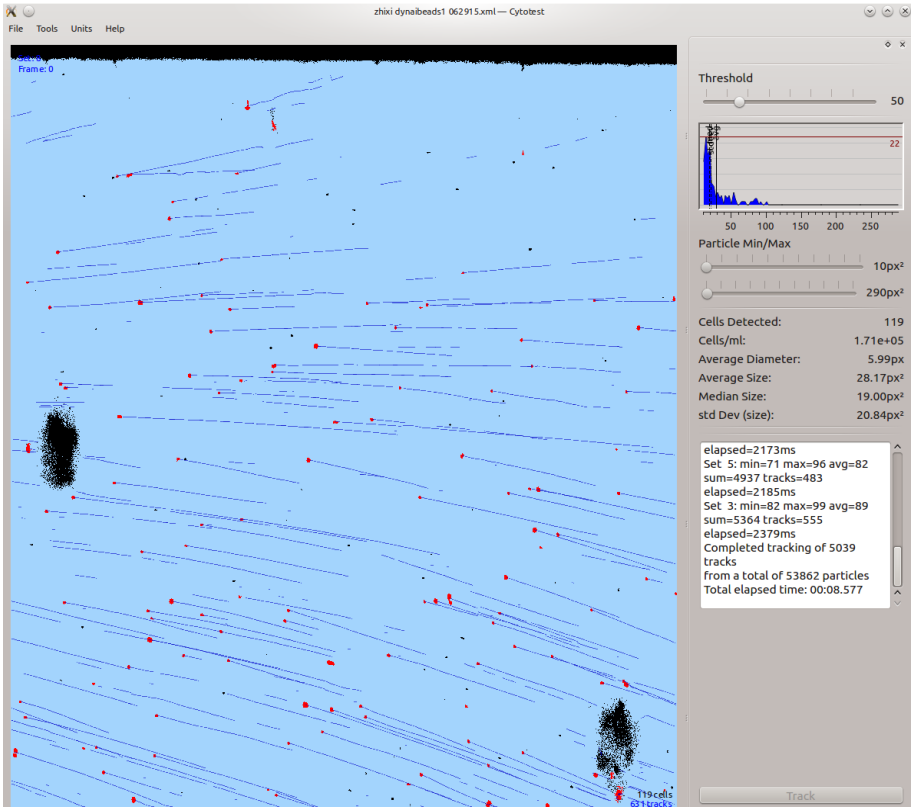

Figure 5.5: Result of Particle Tracking

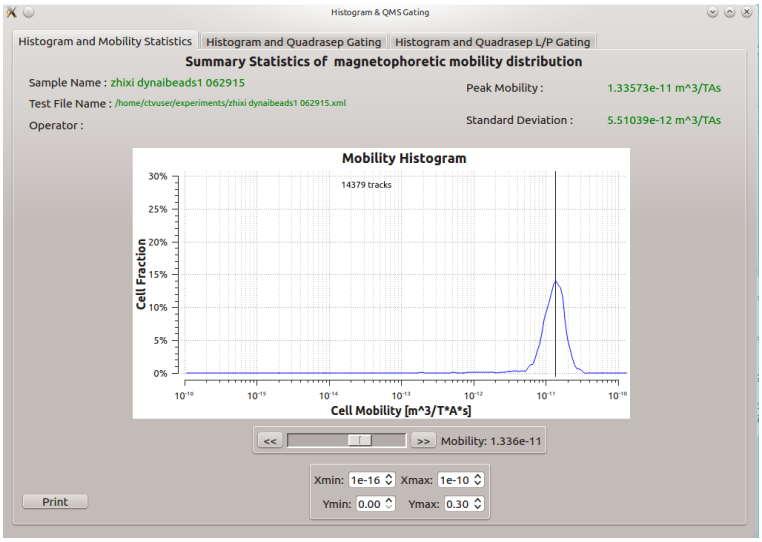

Figure 5.6: Histogram of Magnet Beads

can check the diameter and mobility of particles, thus the difference between magnetically labeled cells and unlabeled cells can be understood.

Then we attach the static mixer upstream of the magnetic trap to test whether the system can successfully perform a test from labeling cells to separating tumor cells. After proving performance, whole blood is used in the final test, thus leading to a conclusion concerning potential clinical performance.

5.4.1 Cell culturing

During the test period, the tumor cell line was cultured in the laboratory. Each time 50 ml of media is used and put into 4 tissue culture flasks separately, after defrosting, cells are added into flask with media, the flask is put into a 37℃incubator in a 5% CO2 water-saturated atmosphere. The culture flask is produced by Nunclontm and its size is 40ml.

The medium is changed every 2∼3 days and the cultured cells are considered as original media. First the cells with media is pipetted out into a 15 ml centrifuge tube with a 10-ml serological pipet. And media then is centrifuge at 200g for 6 minutes. After centrifuging, the cells stay at the bottom of the centrifuge tube and the supernatant can be discarded. New media then will be put into centrifuge tube and mixed with cells, the mixture will be pipetted back into flasks and ready for incubation again.

5.4.2 Cell Capture Test at High Concentration

The focus of high concentration testing is to obtain accurate values of the cell capture ratio by cell counting by hemacytometer and evaluation by Hyperflux$^{\text{tm}}$ velocimetry. The procedure for cell labeling and capture is shown in appendix 1.

The magnetic beads are coated by antibody M-1 Anti-Chicken IgM, the mixture is put on a shake bed for 30 minutes at 15 cycles per minute to have it completely labeled.

The Dynal beads' original concentration is $4*10^8$ beads/ml, and 25 μl contains exactly 10^7 beads, so according to Dynal instructions shown in Figure 5-7, we may use:

Table 2: Volumes for direct cell isolation.

Step	Step description	Volumes per 1×10^7 MNC	Volumes per 2×10^8 MNC
	Recommended tube size	5–7 mL	50 mL
	Recommended magnet	DynaMag™-5	DynaMag™-50
1**	Dynabeads® magnetic beads	25 µL	500 µL
2**	Primary biotinylated antibody	~1 ug	~20 ug
4*	Isolation Buffer	1 mL	20 mL
5–6	Wash magnetic beads (Isolation Buffer)	2 x ~2 mL	2 x ~40 mL
8***	Cell volume	1 mL	20 mL
10*	*Optional:* Increase volume (Isolation Buffer)	~1 mL	~8 mL
13-14*	**For positive isolation only:** Wash the cells (Isolation Buffer)	3 × ~1 mL	3× 20 mL

* Adjust the Buffer volumes to fit to the tube you are using.
** If the target cell population is high (e.g. > 2.5×10^6 target cells/mL), increase/double the amount of Dynabeads® magnetic beads and antibody.
*** When incubating, tilt and rotate so the cells and beads are kept in the bottom of the tube. Do not perform end-over-end mixing if the volume is small relative to the tube size.

Figure 5.7: volumes of components used for cell isolation

Then 1ml of original cell sample is taken and mixed with magnetic beads, the mixture is put on the shake bed for labeling. The labeling time is 20 minutes, which is adequate for cell labeling.

A sample is taken from the mixture and counted under the hemacytometer, the cells' and magnetic bead's concentrations are recorded. The sample then is put into a piston pump and caused to flow through the magnetic trap at a flow rate about 0.5ml/min. Then the collected fluid and waste volume is recorded, and the concentration of cells and magnetic beads is checked. After that, we will compare the material balance and then check the magnetic trap's capture efficiency.

5.4.3 Cell capture test at low concentration

The test on low tumor cell concentration is closer to actual conditions, as the concentration of tumor cells is too low to get a static reliable result in hemacytometer (less than 100

cells are able to be counted), so Hyperflux^{tm} will be used in sample analysis to determine the result of magnetic separation.

The low-concentration test procedure is mainly the same as at that for high concentration, the difference is at low concentration (10^3∼10^4 cells/ml), the result from cytometer becomes not so reliable. And the test's focus turns to Hyperflux^{tm} mobility analysis.

During the process of labeling, at least 1ml of labeled cells of the original sample is kept, after the magnetic separation, 1ml from both the collected sample and waste fluid will be taken to analyze.

5.4.4 Test on cell mixing and capture

The static mixer is an important part in device's design. The device is designed to have magnet beads labeled on tumor cells with accuracy and efficiency. In laboratory test, it will take 20∼30 minutes to ensure all cells be labeled successfully, however, the time mixing fluid stay inside the mixer is 10∼15 minutes. The simulation test indicates the mixer is adequate in cell mixing. So we'll verify the result in the test. With the help of Hyperflux^{tm}, before checking the separation ability of magnetic trap, we will check the mixing efficiency to compare the result with shake bed and make sure CTCs are successfully labeled.

The test is based on 5.3.2, the difference is a static mixer takes the place of shake bed for cell labeling, and flow rate is 1ml/min which is the same as designed speed. The test procedure is shown in appendix 2.

5.4.5 Test with whole blood

In practical detection, the large number of blood cell is a factor can't be neglected. Whether these inert cells will affect the result of cell labeling and separation is still to be determined. The procedure should be adjusted to ensure all blood cells will not cause cells unable to be labeled by magnetic beads or cause error counts in cell detection.

The bovine blood (500ml whole blood, provided by Animal Tech, Tyler, TX) is premixed with tumor sample, the magnet beads is coated by antibody in advance. Then reagents and cells are flowed through the static mixer, then blood cells will flow through the magnet trap and labeled tumor cell and free-moving magnet beads will stay inside. The test procedure is same as appendix 2, while the tumor cells is mixed with whole blood instead of buffers.

5.5 Results and Discussion

As mentioned in the previous section a systematic approach to testing the point-of-care separator prototype was used. First, the ability to trap a high concentration of tumor cells labeled by conventional (shake table) method was demonstrated, then the ability to trap lower cell concentrations was demonstrated. Next, the application of the Hyperflux^{tm} magnetic velocimeter to analyze reagent beads, unlabeled cells and labeled tumor cells was demonstrated and used to confirm the validity of cell labeling with the static mixer by comparison with shake-table labeling. Once successful labeling was demonstrated, successful trapping of labeled cells was demonstrated by analyzing input, trapped and non-trapped ("waste") samples. Finally, tumor cells were mixed with blood and magnetically labeled in the static mixer and trapped in the magnetic trap successfully as shown by analysis using the Hyperflux^{tm} magnetic velocimeter, thus achieving the goal of the experimental study.

5.5.1 Result of Cell Separation at High Cell Concentration

The results of magnetic separation of cells labeled using shake table and separated at high concentration in buffer and analyzed by hemacytometer are shown in the following tables. Table 5-2 lists the starting cells and bead concentrations and numbers for four experiments. Table 5-2 lists the material balances for cells captured and in the waste fraction for the same four experiments. Table 5-3 lists the corresponding material balances and calculated capture ratios.

sample	vol(ml)	cell conc (cells/ml)	Mag bead conc	cell counts	mag counts
sample (July7)	1	$1.68*10^6$	$8.85*10^6$	$1.68*10^6$	$8.85*10^6$
sample (July9)	1	$2.06*10^6$	$6.72*10^6$	$2.06*10^6$	$6.72*10^6$
sample1 (July10)	1	$8.7*10^5$	$6.65*10^6$	$8.7*10^5$	$6.65*10^6$
sample2 (July10)	1	$3.7*10^5$	$6.45*10^6$	$3.7*10^5$	$6.45*10^6$

Table 5.1: Starting Cell and Bead Concentrations for Four Experiments.

sample	volume(ml)	cell concentration (ml^{-1})	cell captured
collected (July 7)	5	$2.02*10^5$	$1.01*10^6$
waste (July 7)	6.5	$3.8*10^4$	$2.5*10^5$
collected (July 9)	6	$1.4*10^5$	$8.4*10^5$
waste (July 9)	4	$5.4*10^4$	$2.16*10^5$
collected 1 (July 10)	6	$9.4*10^4$	$5.64*10^5$
waste 1 (July 10)	4	$4*10^3$	$1.6*10^4$
collected 2 (July 10)	5.5	$5.8*10^4$	$3.2*10^5$
waste 2 (July 10)	4.2	10^4	$4.2*10^4$

Table 5.2: Collected Cell Concentration and Counting

sample	origin counted cells	captured cells	escaped cells	capture ratio (%)
sample (Jul7)	$1.68*10^6$	$1.01*10^6$	$2.5*10^5$	66.25
sample (Jul9)	$2.06*10^6$	$8.4*10^5$	$2.16*10^5$	40.78
sample 1 (Jul10)	$8.7*10^5$	$5.64*10^5$	$1.6*10^4$	64.83
sample 2 (Jul10)	$3.7*10^5$	$3.2*10^5$	$4.2*10^4$	86.49

Table 5.3: Capture Ratio of Samples

The ratio between magnetic beads and cells is an important factor affecting capture efficiency. With a low ratio like July 9's sample, cells vs beads has a ratio of 1:3, the capture ratio is only 40%. The highest capture ratio observed reaches 86%, when the cells vs beads has a ratio over 1:10. The result indicates the device's capture ability meets the requirement for cell detection, also, the high number of magnetic beads will increase the capture ratio as well.

5.5.2 Cell Separation at Low Cell Concentration with Hyperflux^{tm} Analysis

Two samples were used for labeling and capturing tests: Sample 1: 1ml original cell culture suspension+2ml isolation buffer Sample 2: 0.5ml origin cell culture suspension +2.5ml isolation buffer. After labeling, 1ml of sample was kept for Hyperflux^{tm} analysis and 2 ml for separation testing. The hemacytometer counts were as follows:

sample	volume(ml)	cell concentration (ml^{-1})	cell counts
sample 1	2	1.98*10^5	3.96*10^5
sample 2	2	1.3*10^5	2.6*10^5
collect 1	5.5	4*10^4	2.2*10^5
collect 2	4.5	3.6*10^4	1.62*10^5
waste 1	6	6*10^3	3.6*10^4
waste 2	6	8*10^3	4.8*10^4

Table 5.4: Capture Counts for Low Cell Concentration

sample	origin counted cells	captured cells	escaped cells	capture ratio (%)
sample 1	3.96*10^5	2.2*10^5	3.6*10^4	55.6
sample 2	2.6*10^5	1.62*10^5	4.8*10^4	62.3

Table 5.5: Table 5-5 Capture Ratio for Low Cell Concentration

The capture ratio showed in table 5-5 is not a high value. However, the capture ratio is not accurate enough as there're only 20 cells counted under cytometer.

At low cell concentration, the capture ratio cannot have a precise value owing to the low number of cells available in the hemacytometer, which was the rationale for the research at high cell counts described in the previous section. The starting and separated samples from these tests were subjected to detailed mobility analysis using the Hyperflux^{tm} Velocimeter.

First, the Hyperflux velocimeter was evaluated for data collection on unlabeled cells, reagent beads and mixed reagents and cells.

Analysis of unlabeled cells and magnetic beads

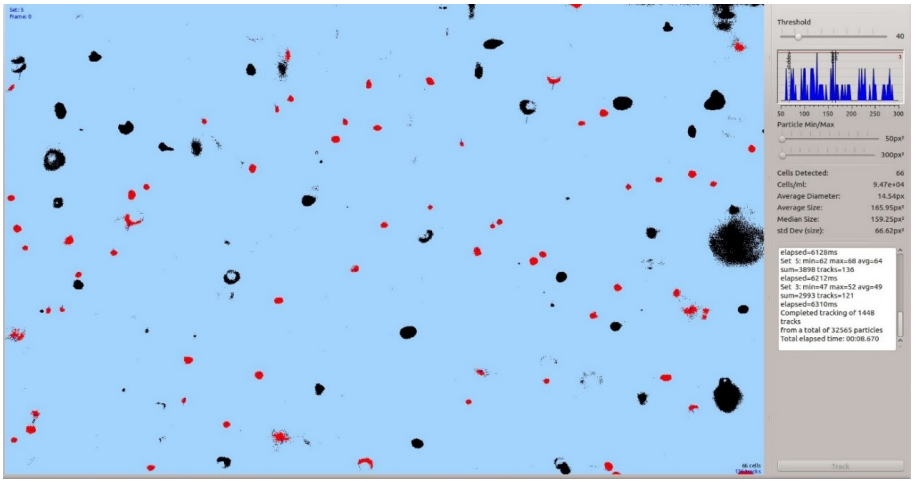

Figure 5.8: Track Screenshot for Unlabeled Cell

Figure 5-8 is the track screenshot for cells unlabeled. With a proper set up, and it's able to check particles with desired size. The red dots are cells being counted and analyzed, black dots are undesired particles as waste or background dirt.

Figure 5-9 shows the reagent bead's tracks. Compared with unlabeled cells, these detected beads have a long blue track, indicating the particles have a detectable motion in the magnetic field. The analyzer forms a histogram file showing the sample's mobility distribution; thus, it's easy to distinguish unlabeled cells from reagent.

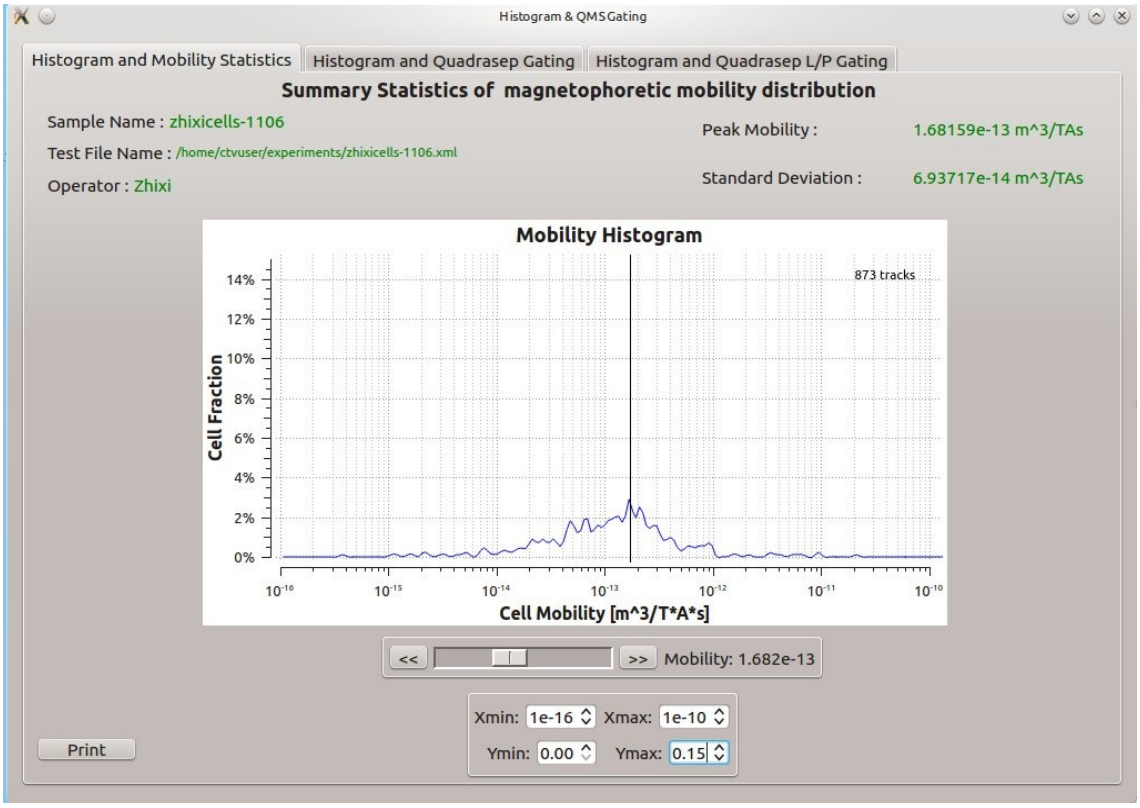

Figure 5.9: Track Screenshots for Reagents

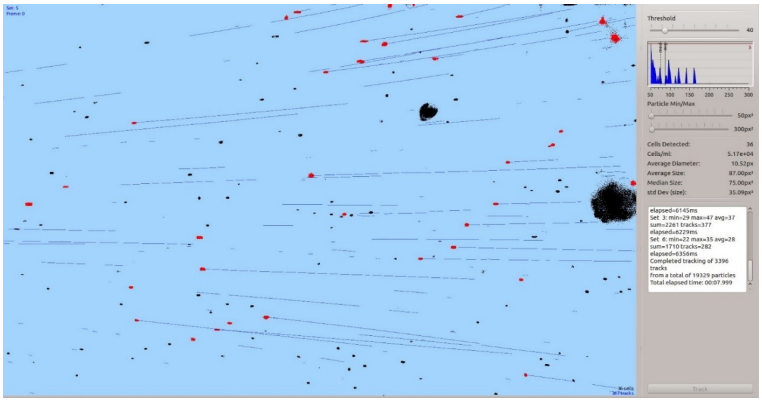

Figure 5.10: Mobility Histogram of Unlabeled Cells

Fig 5-10 showed the histogram of unlabeled cells. The magnetic mobility for beads is around 10^{-11} m^3/TAs, while for cells, they have a much lower peak and a mobility around 10^{-13}, indicated it's merely a background particle.

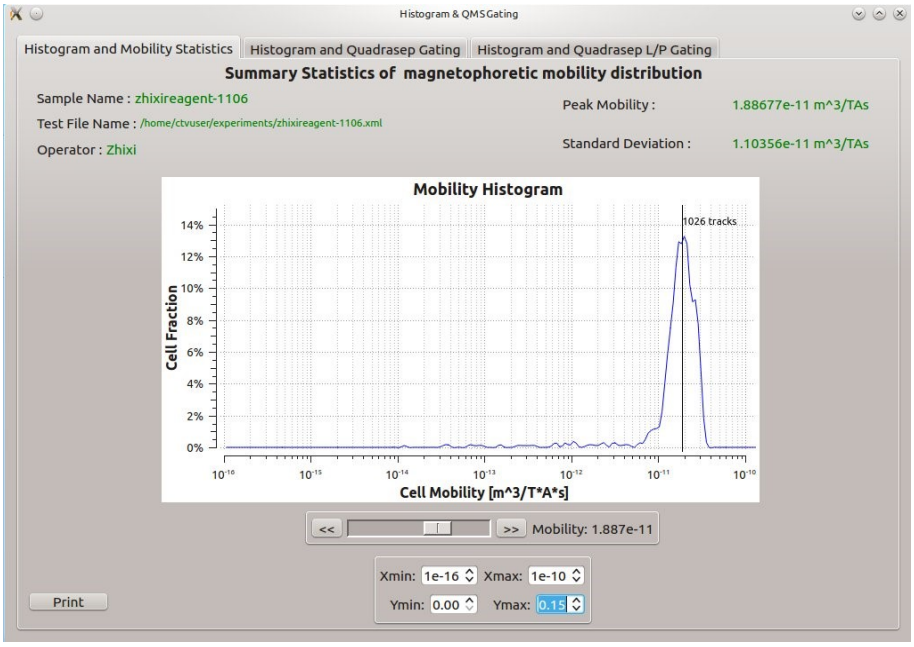

Figure 5.11: Mobility Histogram of Reagent

Compared with the unlabeled cells, the peak of magnetophoretic mobility is much higher, indicating a high concentration of magnetic beads. Also, the mobility peak detected is close to the magnetic beads used in the test.

Fig 5-12 shows the underflow ratio of unlabeled cells, here underflow ratio indicates the particles showed no magnetic mobility inside the system. The ratio is determined both by cell properties as well as sample's concentration. As the system contains a constant background particles, a sample with low concentration will more likely have a high underflow ratio.

For unlabeled cells, the underflow ratio is 52%, indicating a lot of cells with no magnetophoretic mobility is detected.

Figure 5-13 shows the reagent's underflow ratio. The reagents underflow ratio is less than 5%. Compare with unlabeled cells in Figure 5-12, it's easy to find out a pattern difference between particles with different magnetophoretic mobility. Fig 5-14 is a xy-plot of

Figure 5.12: Underflow Ratio for Unlabeled Cells

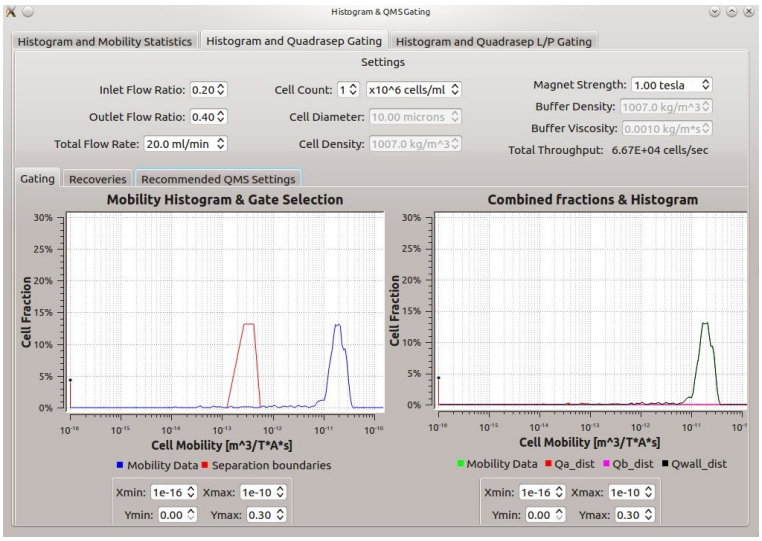

Figure 5.13: Underflow Ratio for Reagent

diameter (pixel)	counts
7.5∼10	421
10∼12.5	234
12.5∼15	174
15∼17.5	158
17.5∼20	461

Table 5.6: Counts of Unlabeled Cells vs. Size

unlabeled cell, the results showed the particles detected are mainly gathering at y-axis, with varied diameter and a mobility close to 0. Figure 5-15 is a xy-plot for reagents, compare with unlabeled cells, magnetic beads has a wide distribution of magnet mobility, and the size of reagents are mainly between 7.5∼10.

The statistical result of particle size and its distribution is shown below, which gives a clearer comparison between cells and magnetic beads.

Table 5-6 and Figure 5-16 show the number of unlabeled cells counted with different size. From the data of table and figure, we find the cells have a varied size distribution. Considering the difference in cell's initial size, and the cell tends stick with each other, there'll be a large number of particles with diameter over 17.5 pixel.

Table 5-7 and figure 5-17 showed the number of unlabeled cells counted with different mobility. It can be considered the unlabeled cell has no magnet inside the unlabeled cells.

The result of reagent's distribution on size is shown in table 5-8 and figure 5-18. For the reagents, most of beads have a diameter smaller than 12.5px. Which is a smaller value than unlabeled cells.

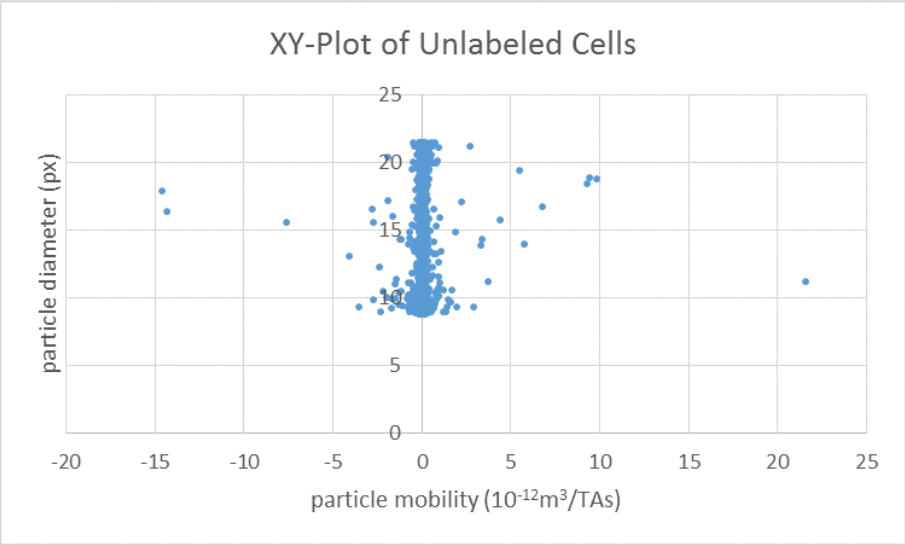

Figure 5.14: xy-plot for Unlabeled Cells

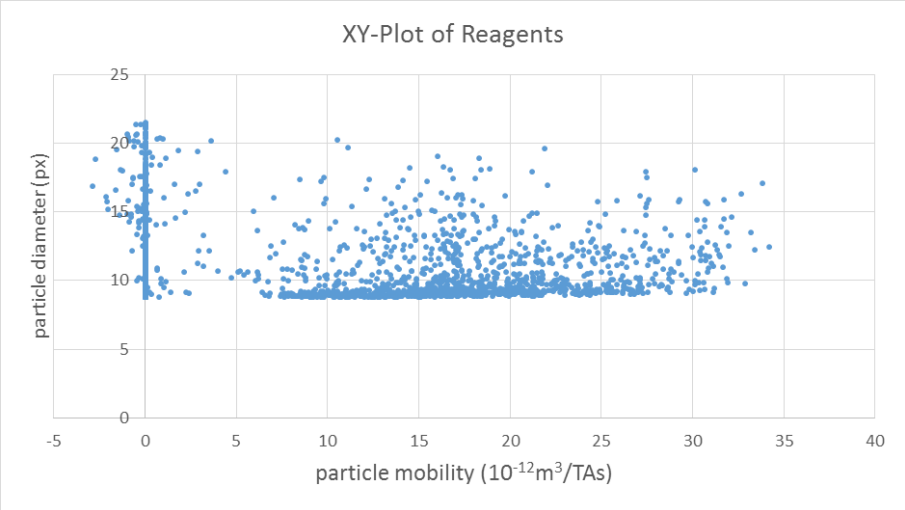

Figure 5.15: xy-plot for Reagents

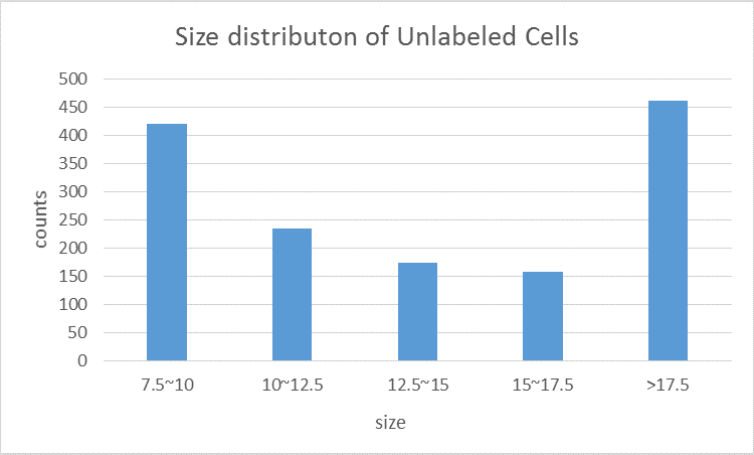

Figure 5.16: Counts on Unlabeled Cells and Size Distribution

Mobility (m^3/TAs)	counts
<0.005	1441
0.005∼0.01	7
0.01∼0.015	0
0.015∼0.02	0
0.02∼0.025	1
>0.025	0

Table 5.7: Counts of Unlabeled Cells vs. Mobility

diameter (pixel)	counts
7.5∼10	1417
10∼12.5	1004
12.5∼15	588
15∼17.5	261
17.5∼20	126

Table 5.8: Counts of Reagents vs Size Distribution

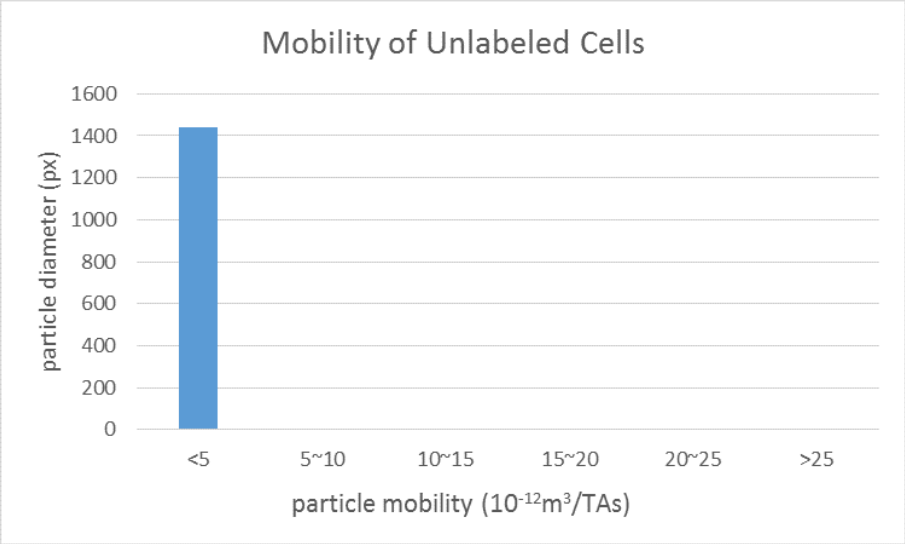

Figure 5.17: Mobility Counts of Unlabeled Cells

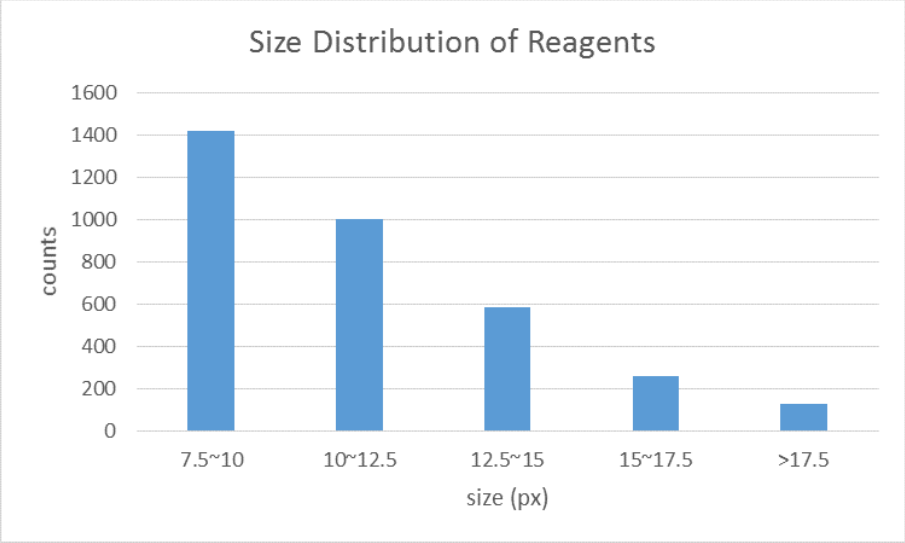

Figure 5.18: Size distribution of Reagents

Mobility (m^3/TAs)	counts
<0.005	2184
0.005∼0.01	122
0.01∼0.015	299
0.015∼0.02	391
0.02∼0.025	226
>0.025	174

Table 5.9: Counts of Reagents Mobility vs Distribution

The difference on magnetophoretic mobility is clearer: In table 5-9 and Figure 5-19, theres a peak of magnetophoretic mobility at around $15*10^{-12}m^3$/TAs. This is the detected magnetic particles.

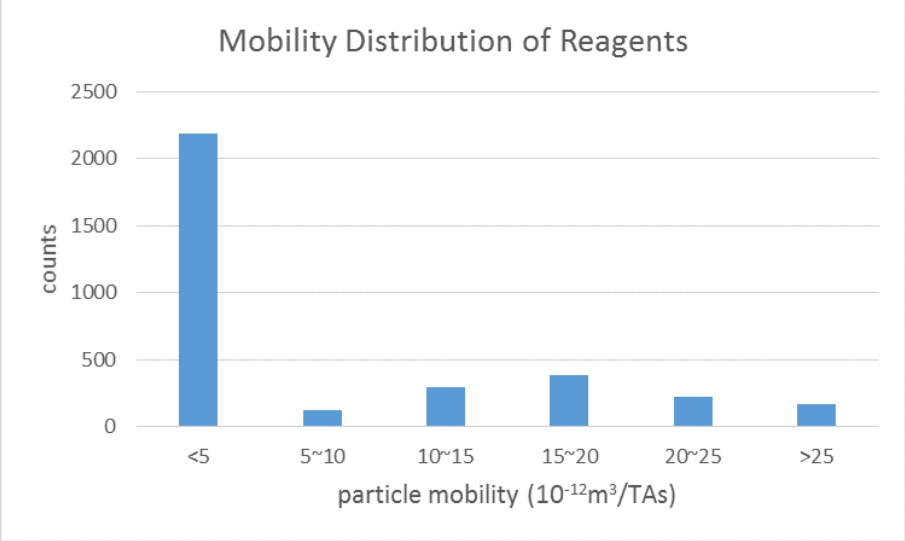

Figure 5.19: Mobility Distribution of Reagents

The result indicates there's a lot of particles with low size and mobility inside the system, when exclude the background particles, we find out theres a peak of mobility for magnetic beads between 0.015 to 0.02 m^3/TAs.

Analysis of mixed reagents and cells

After mixing, cells are labeled with reagents, then inside the sample, we have the following: labeled cells, free moving magnetic beads and inactive particles consists in system. The tracks of mixture is shown in Figure 5-20, particles with and without magnetophoretic mobility are both detected in device:

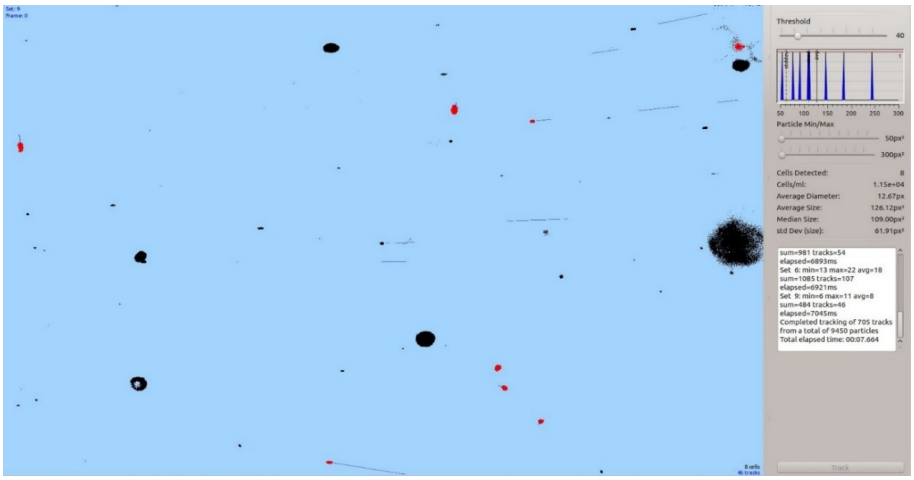

Figure 5.20: Track screenshot for Premixed Sample

The histogram of premixed sample is shown in Figure 5-21. Two peaks are detected, one is high and narrow, which comes from labeled cells and magnetic beads, and the other is low and wide, which comes from inactive particles. The underflow ratio of mixed sample is shown in figure 5-22, the ratio is 32%, between the value of unlabeled cells (50%) and reagents (5%). The xy-plot of mixed sample is displayed in Figure 5-23, including low mobility particles gathered at y-axis and high mobility particles around diameter = 10 pixel, it can be considered as a combination of Figure 5-14 and Figure 5-15. The size distribution of mixed sample is shown in table 5-10 and figure 5-24. Also, both particles with a diameter less than 12.5 and larger than 20 have a high counting.

The mobility distribution of premixed cells are shown in figure 5-25 and table 5-11. The particle with high mobility is still detectable.

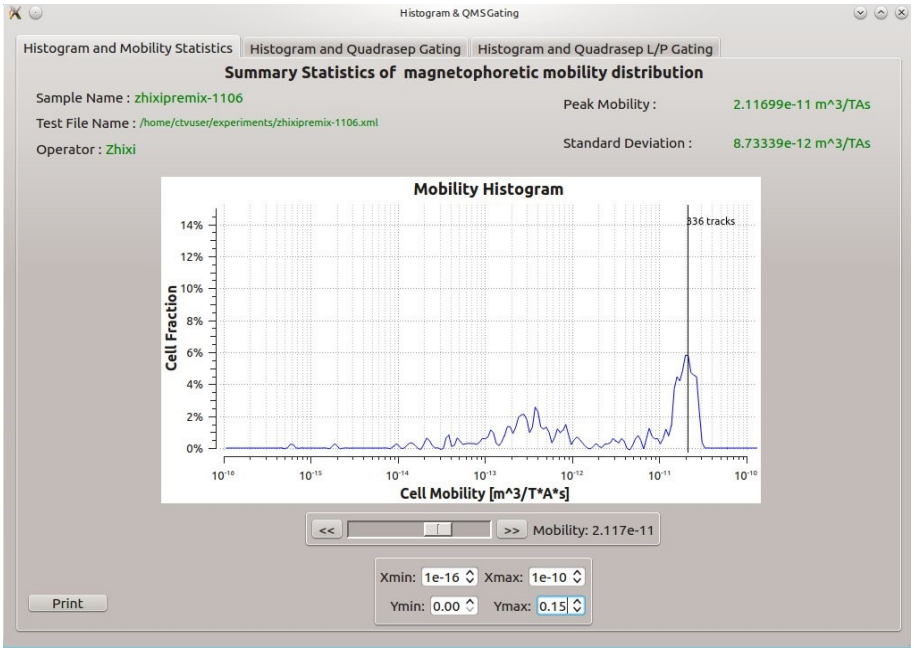

Figure 5.21: Mobility Histogram for Mixed Sample

Figure 5.22: Underflow Ratio of Mixed Sample

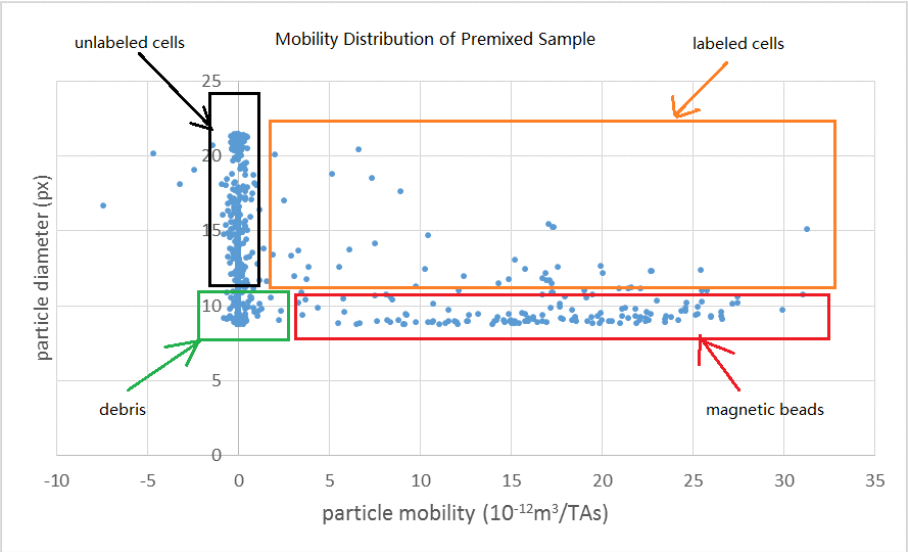

Figure 5.23: XY Plot of Mixed Sample with Areas Defined for the Components of Suspension.

diameter (pixel)	counts
7.5∼10	302
10∼12.5	151
12.5∼15	71
15∼17.5	79
17.5∼20	102

Table 5.10: Counts of Mixed Sample vs Size

Mobility (m^3/TAs)	counts
<0.005	545
0.005∼0.01	27
0.01∼0.015	29
0.015∼0.02	52
0.02∼0.025	34
>0.025	18

Table 5.11: Counts of Premixed Sample vs Mobility

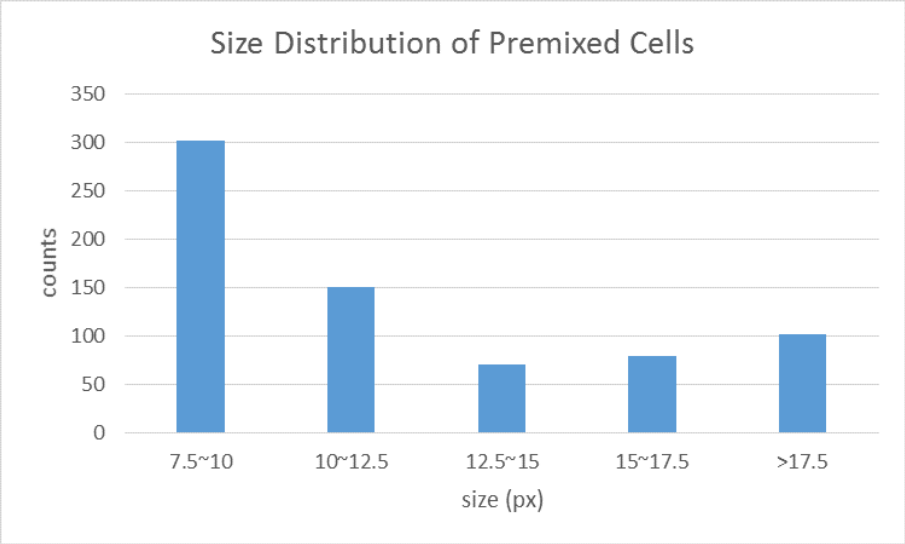

Figure 5.24: Size Distribution of Premixed Cells

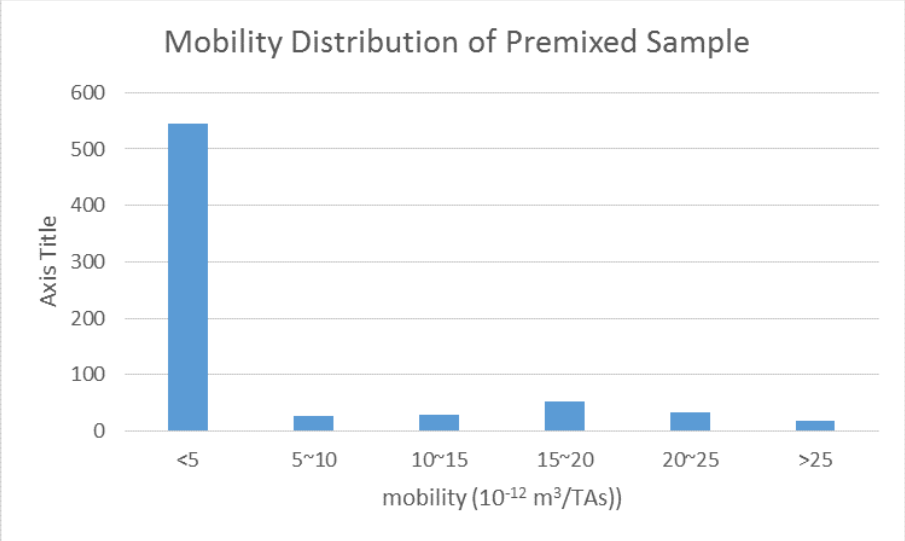

Figure 5.25: Mobility Distribution of Premixed Sample

5.5.3 Separation of cells using the magnetic trap

After separation, we have sample collected and waste fluids for analysis, the capture sample's tracking is shown in Figure 5-26, looks like reagent, particles with high mobility is detected. As Figure 5-27 shows, the concentration of waste fluid is rather low, and particles detected are with little or no mobility. The histogram of mobility shows the difference

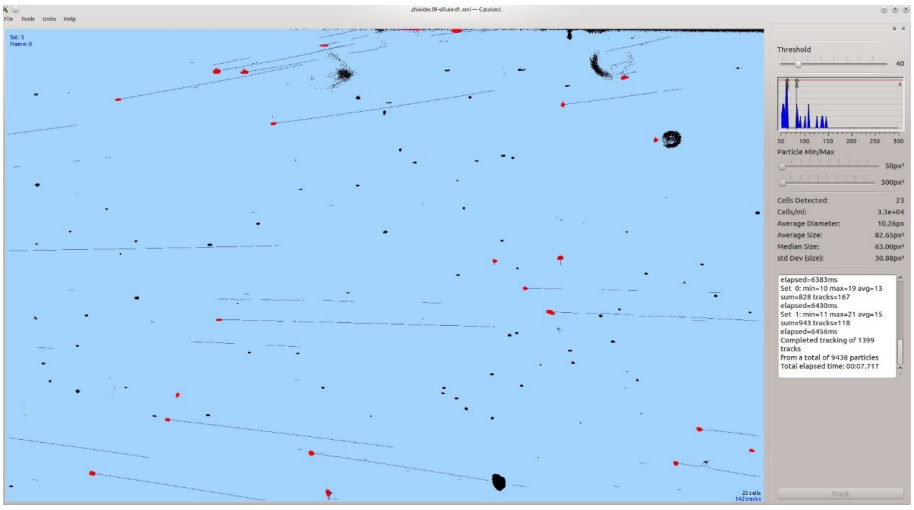

Figure 5.26: Tracks of Collected Sample

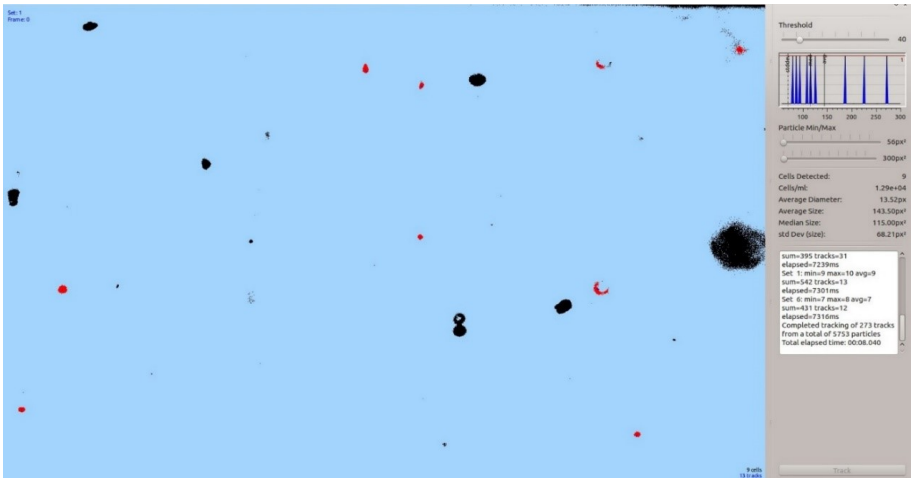

Figure 5.27: Tracks of Waste Fluid

between collected sample and waste as well.

Figure 5-28 shows the mobility distribution of captured cells, and it looks like the pattern of labeled cells (Figure 5-21) but with unlabeled cells missing. Figure 5-29 is the mobility distribution of waste, like unlabeled cells, it doesn't have a particular mobility peak.

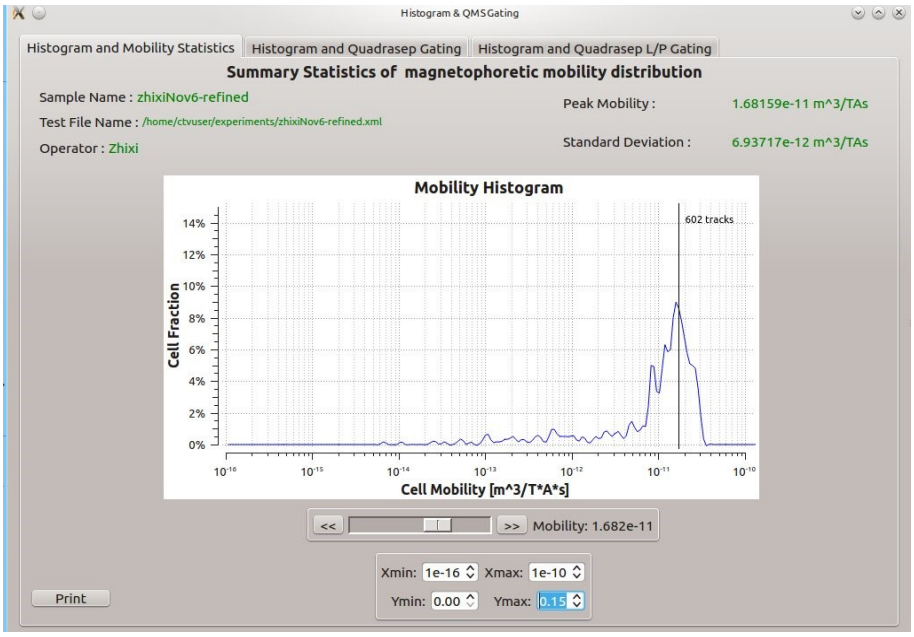

Figure 5.28: Mobility Histogram of Collected Sample

Figure 5-30 and 5-31 show underflow ratio of captured sample and waste, the underflow ratio for collected cells is 10%, higher than reagent (5%) but lower than premixed sample (30%), the underflow ratio for waste is as high as 42%, which is close to that of unlabeled cells (50%)

The xy-plot for collected sample and waste is shown in Figure 5-32 and 5-33. For collected sample, compared with reagents' xy plot, particles with high diameter as well as high mobility are detected, indicating the existence of labeled cells. For escaped cells, the pattern looks like the unlabeled cells, while the diluted sample has a lower concentration. The size distribution of collected cells and escaped sample is shown below, table 5-12 and table 5-13 shown the distribution of collected cells and escaped particles. Compare with reagents, the particle size of collected sample is generally larger. The escaped particles number is rather low, while the distribution of size is rather balanced.

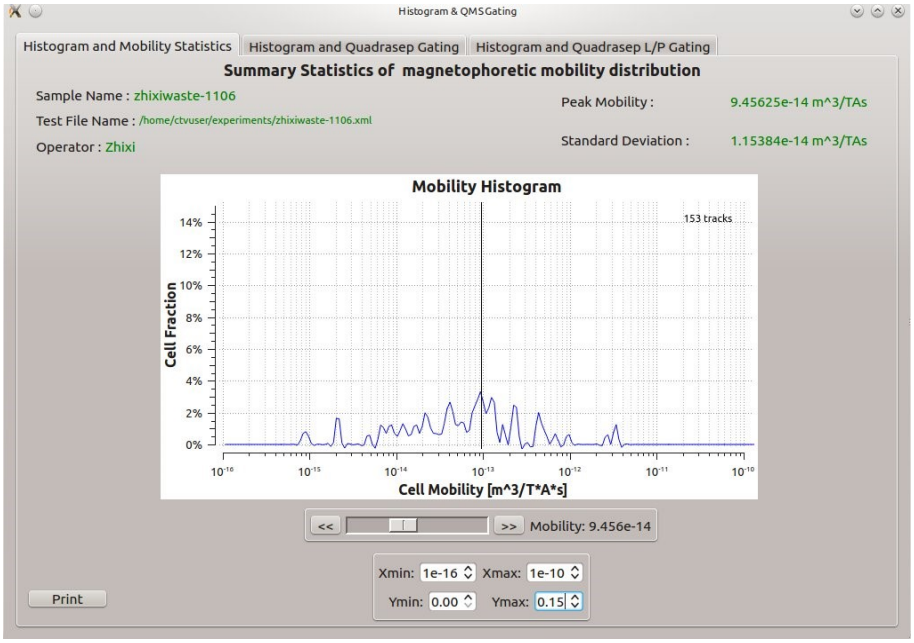

Figure 5.29: Mobility Histogram of Waste

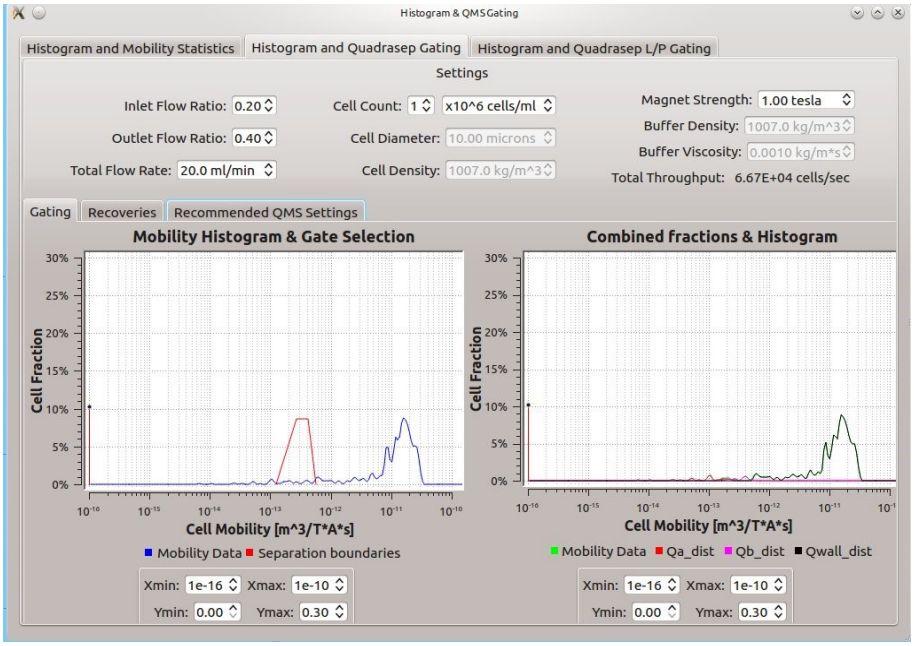

Figure 5.30: Underflow Ratio of Collected Sample

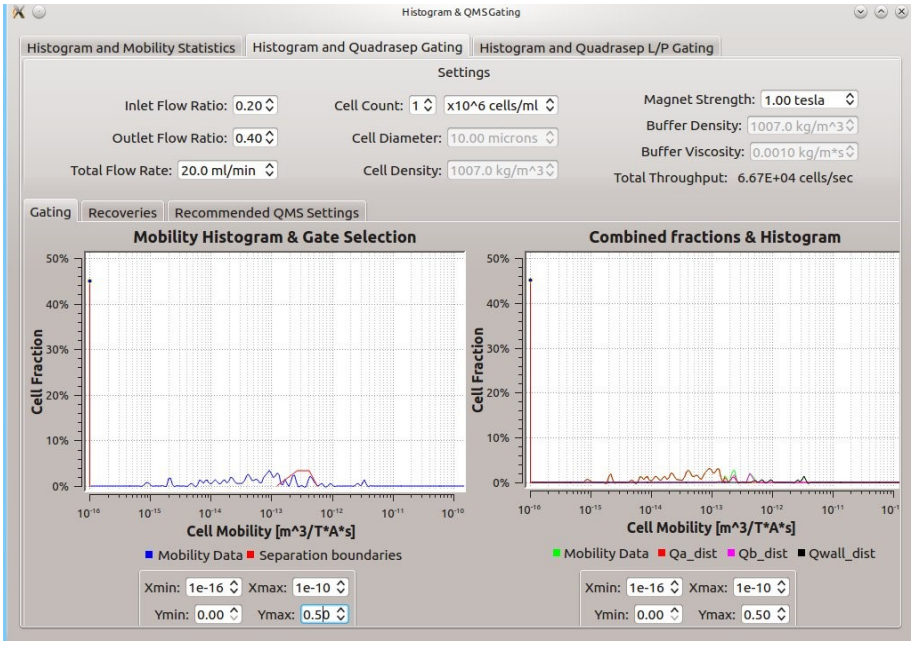

Figure 5.31: Underflow Ratio of Waste

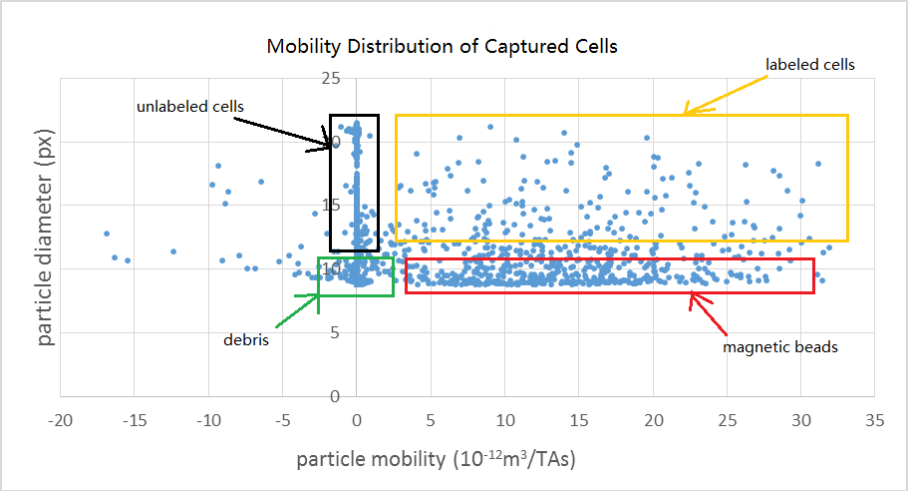

Figure 5.32: Mobility Distribution for Collected Sample

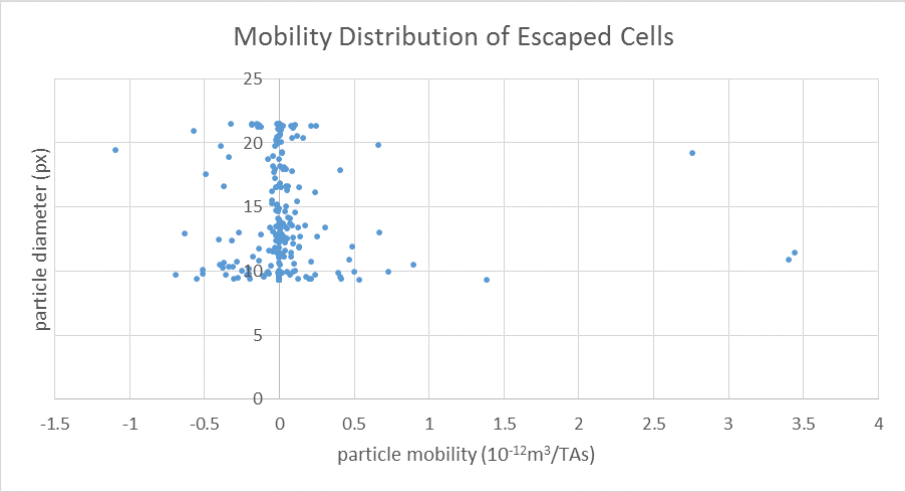

Figure 5.33: Mobility Distribution for Escaped Cells

diameter (pixel)	counts
7.5∼10	652
10∼12.5	394
12.5∼15	169
15∼17.5	90
17.5∼20	93

Table 5.12: Size Distribution of Collected Cells

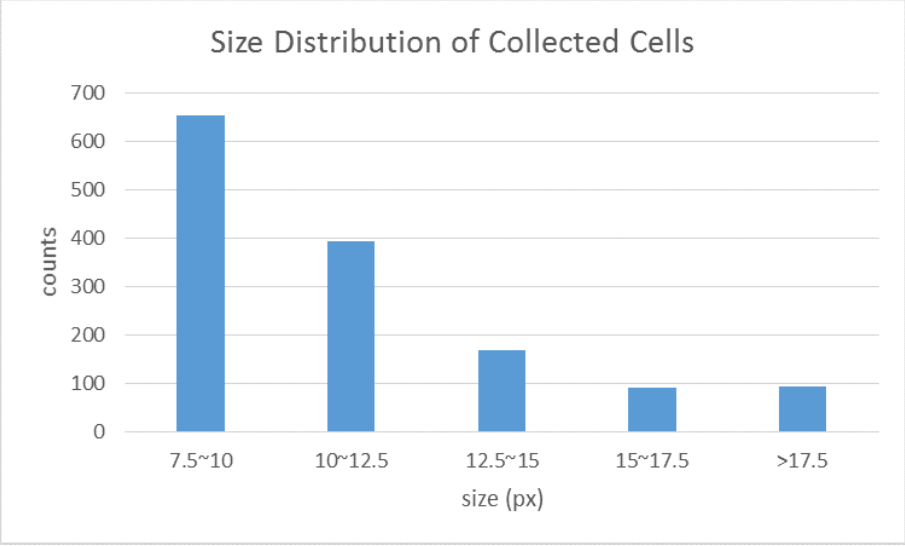

Figure 5.34: Size Distribution of Collected Cell

diameter (pixel)	counts
7.5∼10	79
10∼12.5	54
12.5∼15	47
15∼17.5	19
17.5∼20	75

Table 5.13: Counts of Collected Cells vs Size.

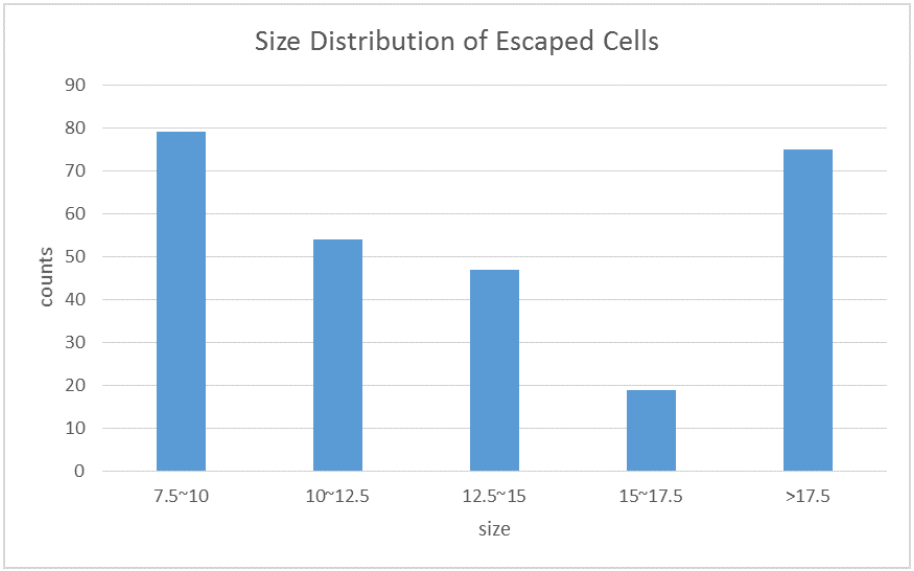

Figure 5.35: Size Distribution of Escaped Particle

Mobility (m^3/TAs)	counts
<0.005	842
0.005∼0.01	146
0.01∼0.015	163
0.015∼0.02	138
0.02∼0.025	65
>0.025	45

Table 5.14: Counts of Escaped Cells vs Size

For the particle's magnetic distribution, the collected cell has a higher ratio of beads with mobility over 0.015, which is higher than reagents, while for the escaped cell, there's no mobility detected.

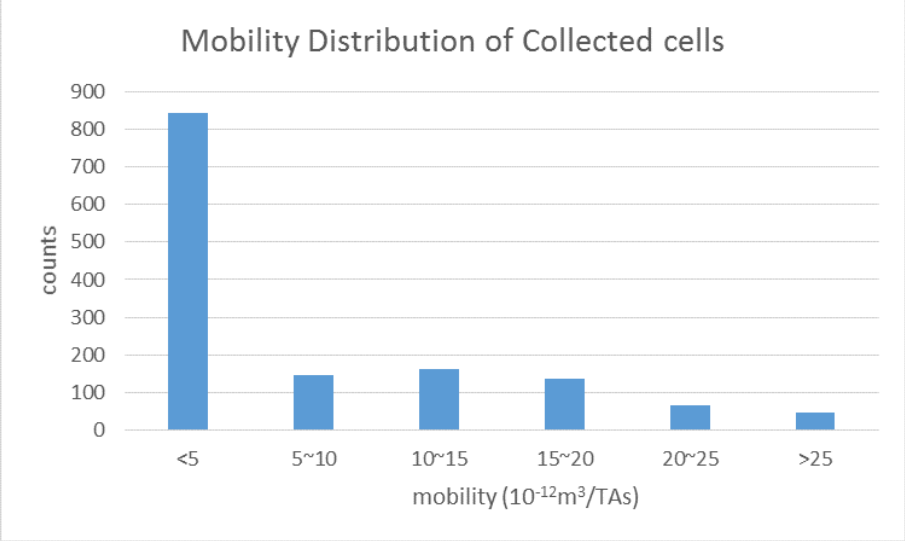

Figure 5.36: Magnetic Distribution of Collected Cell

Mobility (m^3/TAs)	counts
<0.005	274
0.005∼0.01	0
0.01∼0.015	0
0.015∼0.02	0
0.02∼0.025	0
>0.025	0

Table 5.15: Counts of Collected Cells vs Mobility

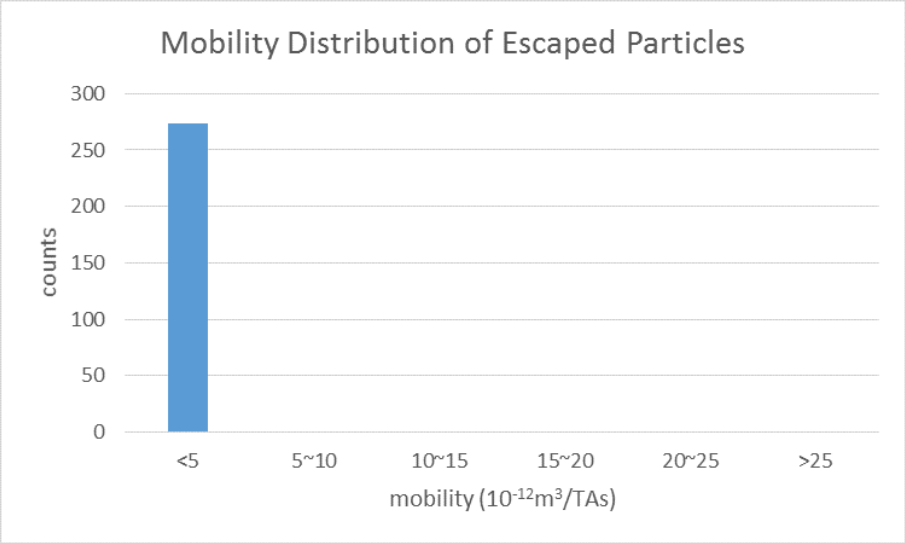

Figure 5.37: Magnetic Distribution of Escaped Cell

In these graphs, four different types of particles are spotted:

First type of particle has a very low mobility, which is around 0, the diameter of the particles are varied. These are major components of underflow particles, which are mainly unlabeled cells that making a Brownian motion inside the detector. And the particles spotted in the waste collector is mainly this type of beads.

Second type of particle has a modest mobility and low diameter. These beads are more likely to be free-moving magnet beads. It will likely to appear in the collected sample.

The third type of particle has a low mobility and low diameter. It exists in both unlabeled cells and reagent beads, it looks like debris inside the system or some particles inside the reagent.

The fourth type of particle has the highest mobility and a rather scattered diameter distribution, this is more likely to be the labeled cell considering the varied size of the cell, and the higher mobility also indicates multiple magnet beads are attached to the labeled cell.

The result of Hyperflux^{tm} tracking showed the magnet bead's mobility is between 1.3$\sim$2.0*10$^{-11}m^3$/TAs, which is a lower value than in chapter 3, so the simulation result is different as well:

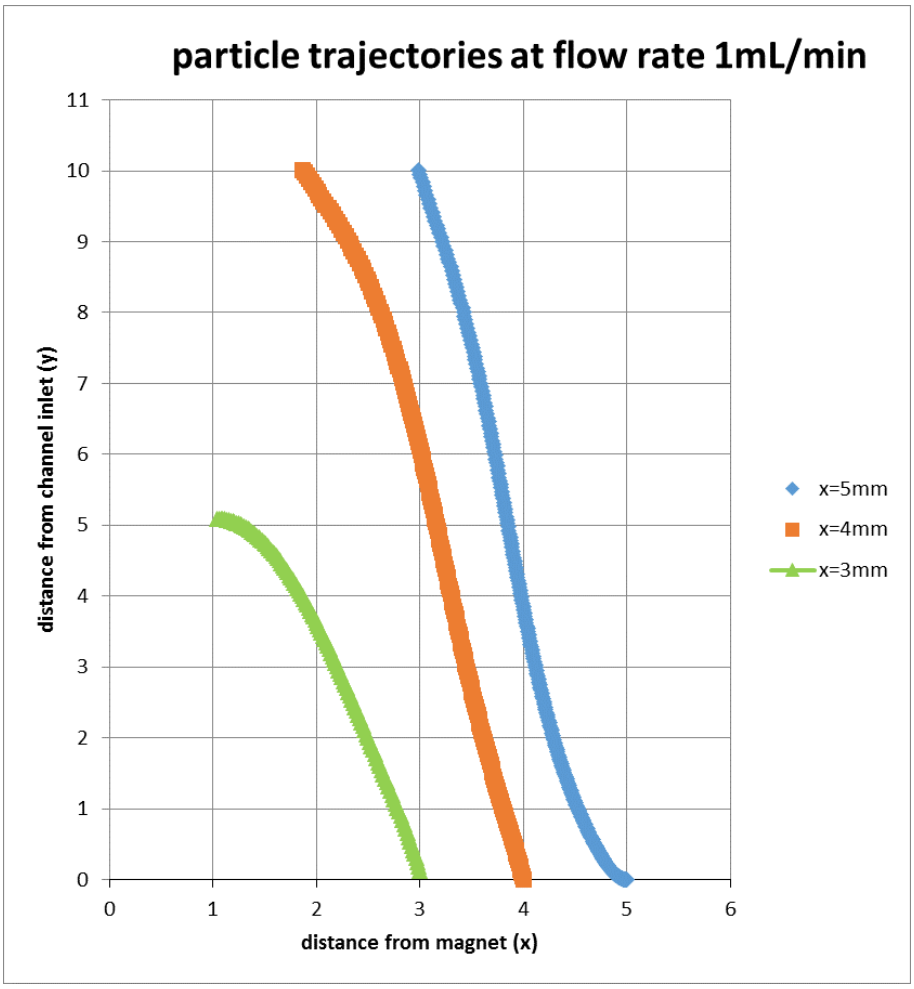

Figure 5.38: Simulation Result of Magnet Beads' Track at 1st Stage of Magnet Trap

The first stage of magnets can't capture all beads inside the trap; however, the beads which have a distance from magnet less than 2mm can be captured. After 1-stage magnetic capture, those beads at x=5mm will have moved to position of x=3mm, which will be able to be captured by the second-stage magnets. So the 3-stage magnet ensures the capture ability, just as the above data have shown.

5.5.4 Result of cell mixing and separation

A comparison test was made between static mixer and traditional shake bed, the test's result indicated the static mixer can satisfy the need to perform the task for cell labeling.

The data below all come from collected samples, the source and amount of sample used are all the same, while the only difference is in cell labeling method. From Figure 5-39 and 5-40, we can see there's no clear difference between the tracks of samples from the static mixer and the shake bed.

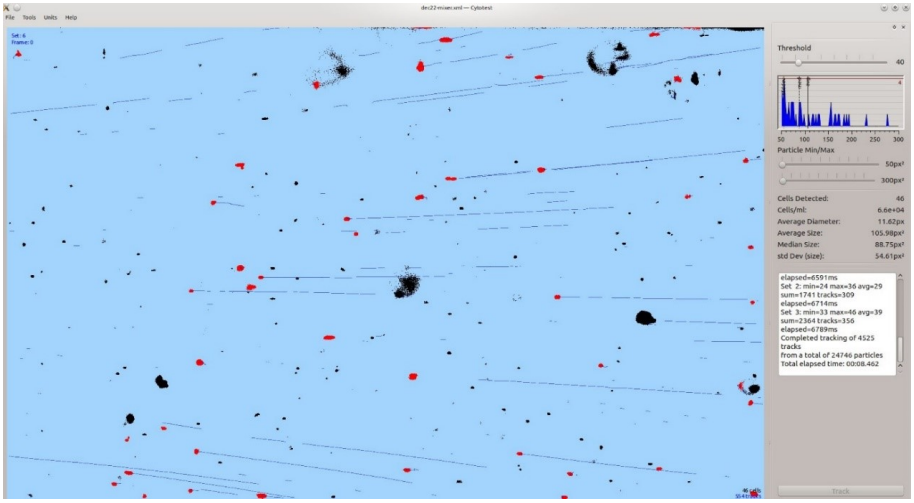

Figure 5.39: Tracks for suspension from the Static Mixer

From the histogram of mobility displayed in Figure 5-41 and Figure 5-42, the static mixer proves to be able to show a clear peak of mobility as well as shaker table. The xy plot distribution shown in Figure 5-43 and Figure 5-44 indicated the static mixer has a same size distribution as in the shaker table, while a higher number of inactive particles are

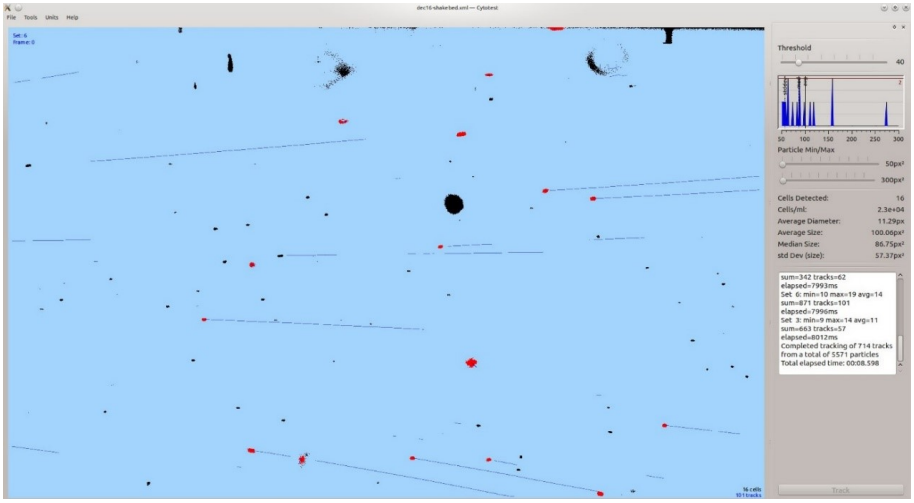

Figure 5.40: Tracks for suspension from the Shaker Table

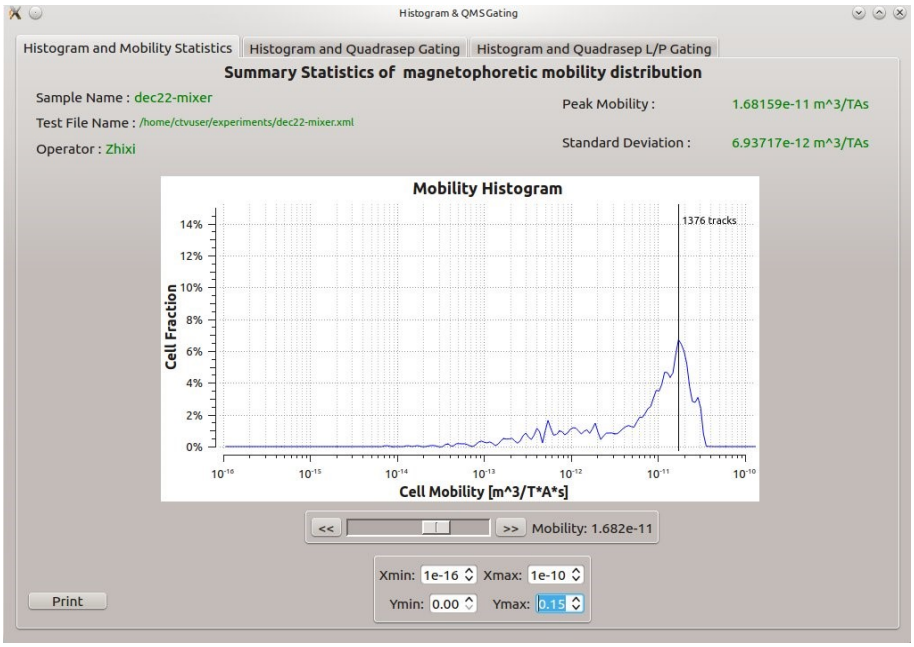

Figure 5.41: Histogram of Mobility for Suspension from the Static Mixer

diameter (pixel)	counts
7.5∼10	1357
10∼12.5	950
12.5∼15	886
15∼17.5	676
17.5∼20	656

Table 5.16: Counts of Static Mixer vs Size

diameter (pixel)	counts
7.5∼10	478
10∼12.5	262
12.5∼15	275
15∼17.5	361
17.5∼20	434

Table 5.17: Counts for Shaker Table vs Size

observed. The size distribution of static mixer and shake bed is shown in figure 5-45 and 5-46 as well as table below, we can see the mixer has a good performance to capture labeled cells.

In conclusion, the static mixer proves to be as effective as traditional shake bed, which makes the device a proper cell separator.

5.5.5 Results for cells mixed with whole blood

When the whole blood is used in the test, the huge number of blood cells is a factor that can't be ignored, and the test shows a proper treatment is still necessary.

Fig 5-47 shows the track profile of the sample of cells collected in the magnetic trap using tumor cells mixed with whole blood: a lot of inactive particles are detected, which are red blood cells. And in fig 5-48, the histogram of mobility proves the red blood cells affects

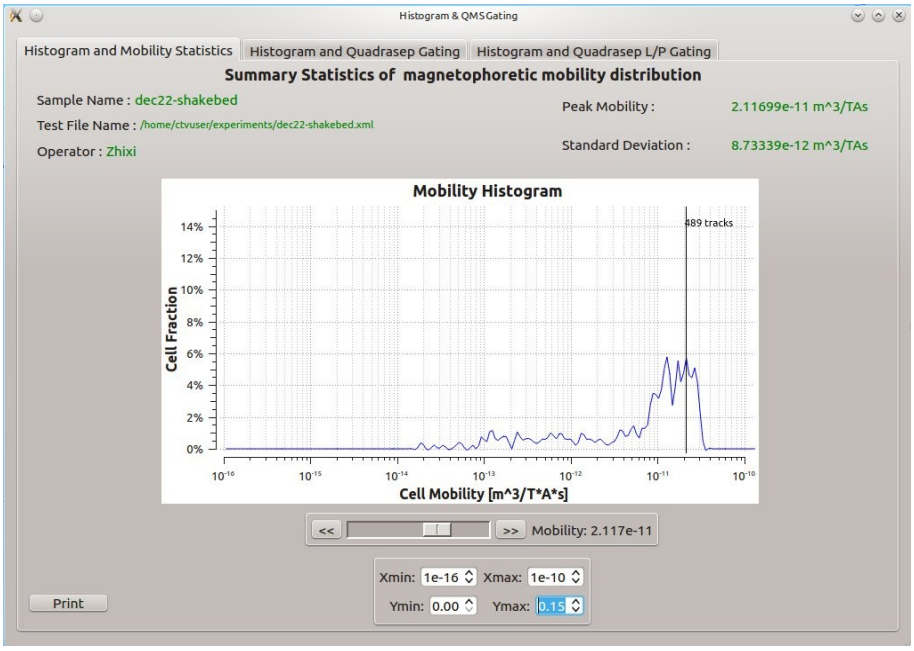

Figure 5.42: Histogram of Mobility for suspension from the Shaker Table

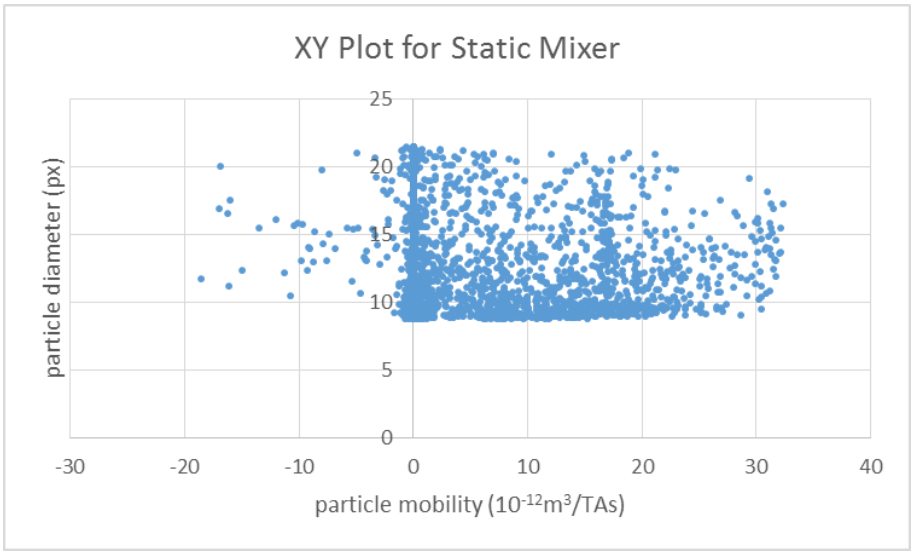

Figure 5.43: XY-Plot for Static Mixer sample

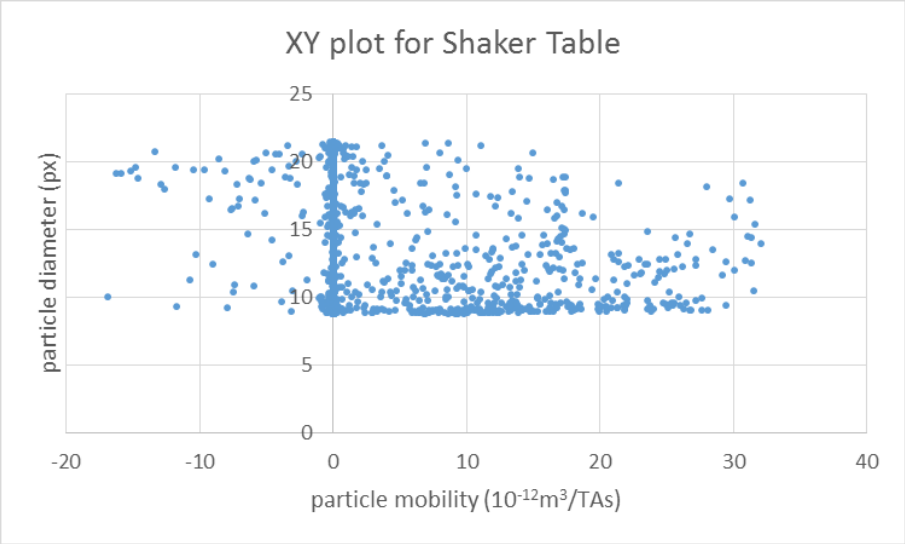

Figure 5.44: XY Plot for Shaker Table Sample

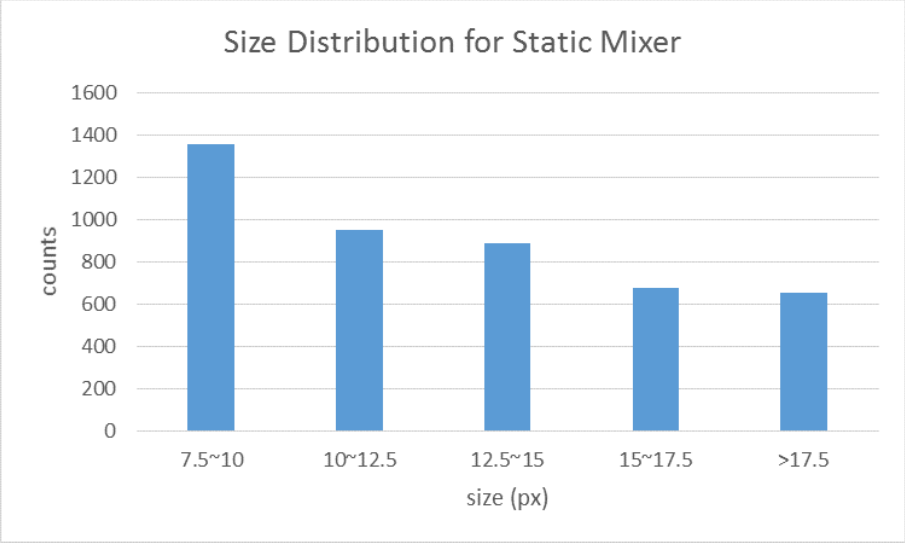

Figure 5.45: Size Distribution of Static Mixer

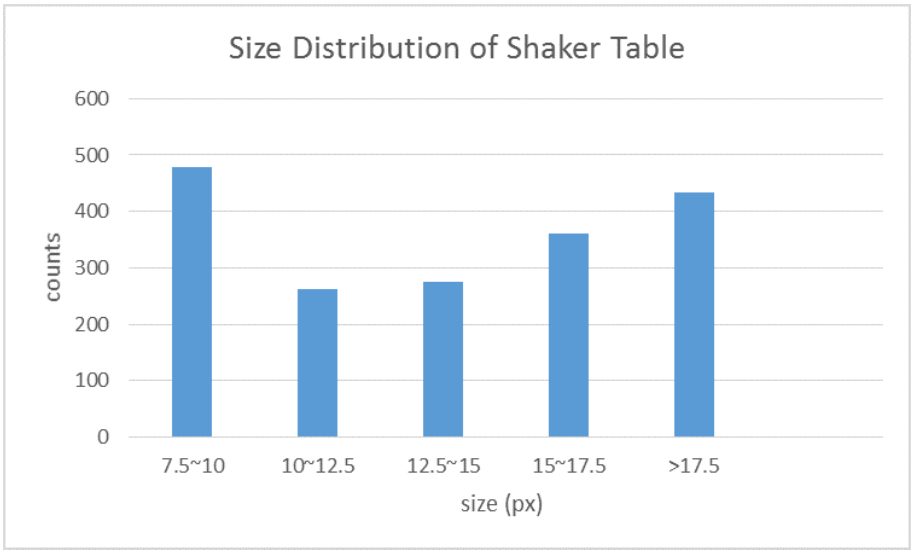

Figure 5.46: Size Distribution of Shaker Table Sample

the detection of mobility. The existence of red blood cells overlaps the magnetic particle's mobility distribution.

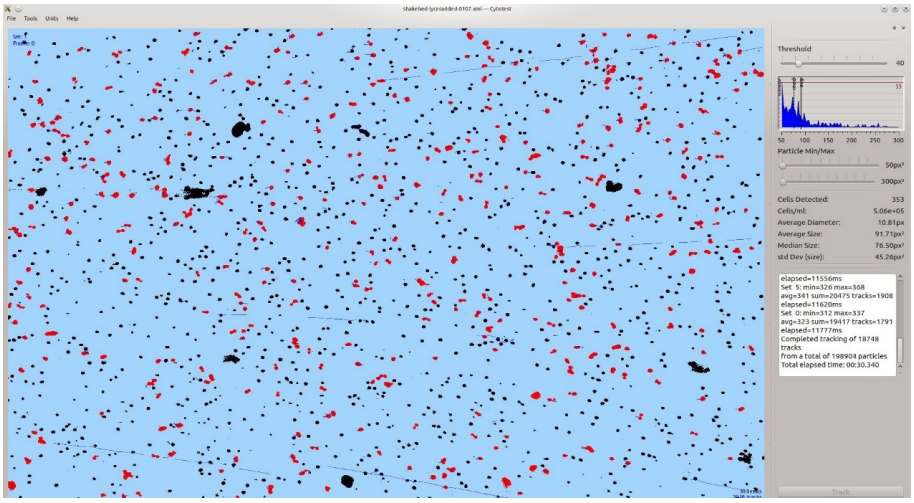

Figure 5.47: Track Profile of Collected Sample with Whole Blood

In the xy plot data, the result is clearer that whole blood's existence have a strong effect on cell detection.

From figure 5-50, the collected sample with whole blood looks like unlabeled cells, a large number of particles less than 12.5 existed, and the distribution of mobility shown in

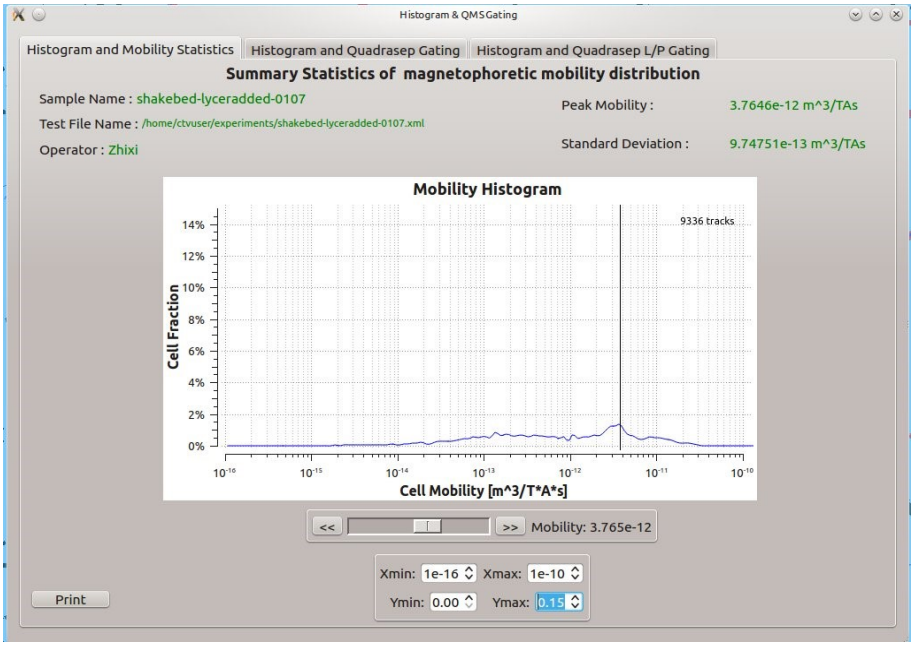

Figure 5.48: Mobility Histogram of Collected Sample with Whole Blood

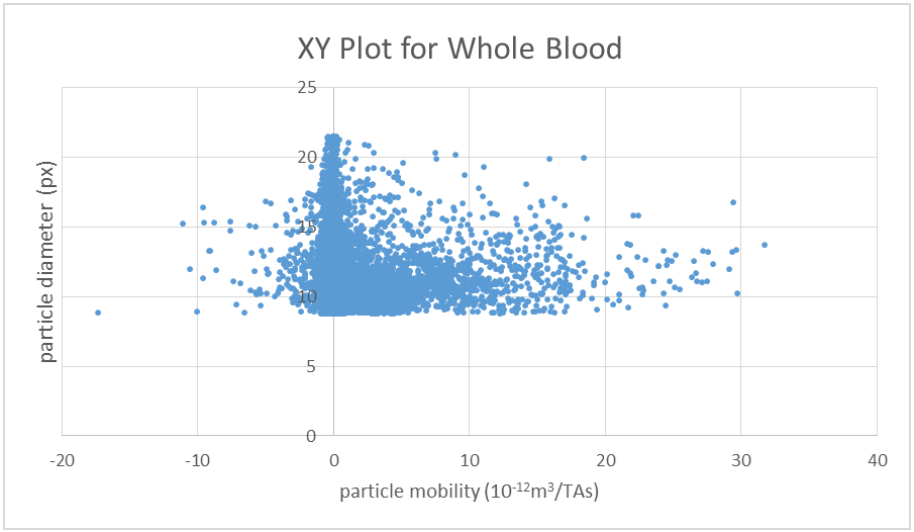

Figure 5.49: XY plot of magnetically separated Sample with Whole Blood

diameter (pixel)	counts
7.5∼10	10605
10∼12.5	5619
12.5∼15	1524
15∼17.5	618
17.5∼20	382

Table 5.18: Counts of Blood Sample vs Size

table 5-18 and figure 5-51 indicates its difficult to check the sample's mobility as it's affected by red blood cells.

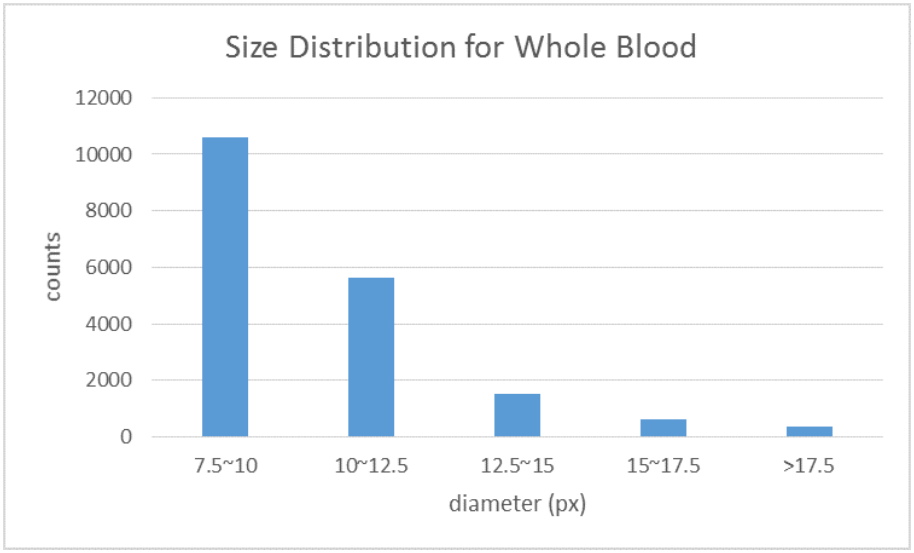

Figure 5.50: Size Distribution of Sample with Whole Blood

So to make a successful detection, a blood cell lyser has been added. The result looks better with cell lyser added, and the system is able to detect the cells successfully. From figure 5-52 we may see that a lot of tracks have been screened out, and the lysing is an important process in sample treatment.

From the histogram result in figure 5-53, also it's able to detect the mobility peak. Still, large number of blood cells make the peak not clear.

Mobility (m^3/TAs)	counts
<0.005	17857
0.005∼0.01	518
0.01∼0.015	224
0.015∼0.02	101
0.02∼0.025	30
>0.025	18

Table 5.19: Counts of Blood Sample vs Size

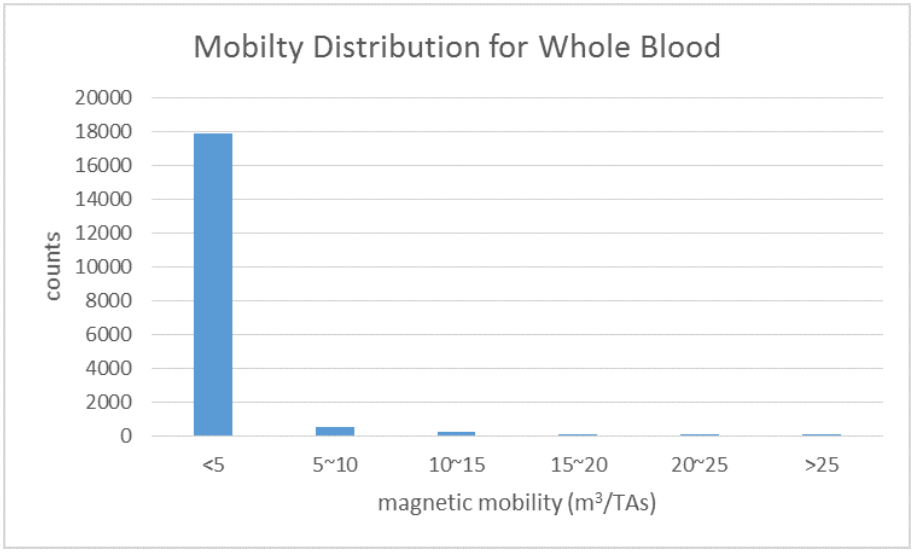

Figure 5.51: Magnetophoretic mobility Distribution of Sample with Whole Blood

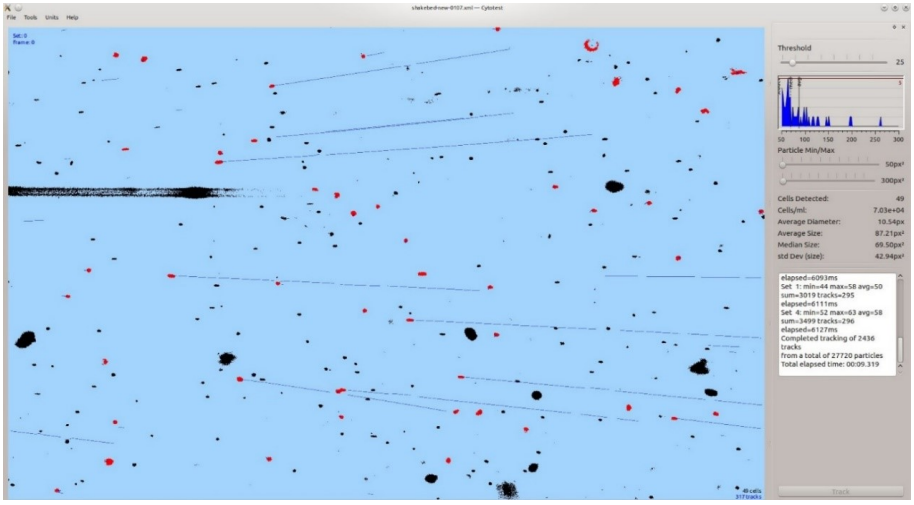

Figure 5.52: Particle Tracks for Sample Lysed

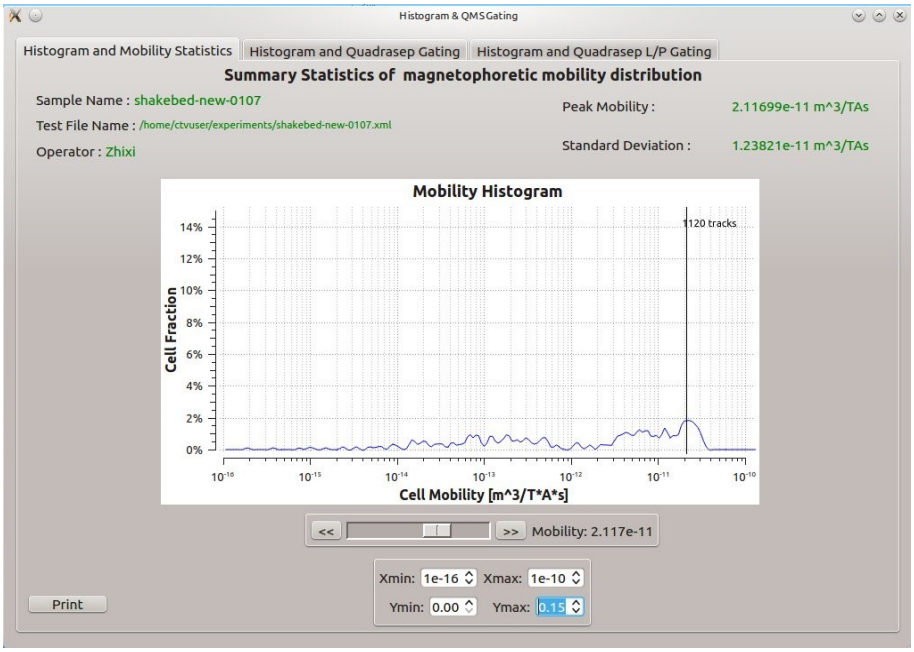

Figure 5.53: Histogram of Mobility for Sample Lysed

diameter (pixel)	counts
7.5∼10	1530
10∼12.5	514
12.5∼15	231
15∼17.5	48
17.5∼20	113

Table 5.20: Counts of Lysed Sample vs Size

The xy plot in figure 5-54 showed the improvement as well. The number of inactive particles is reduced after lysing. The size distribution of lysed sample showed the lysing

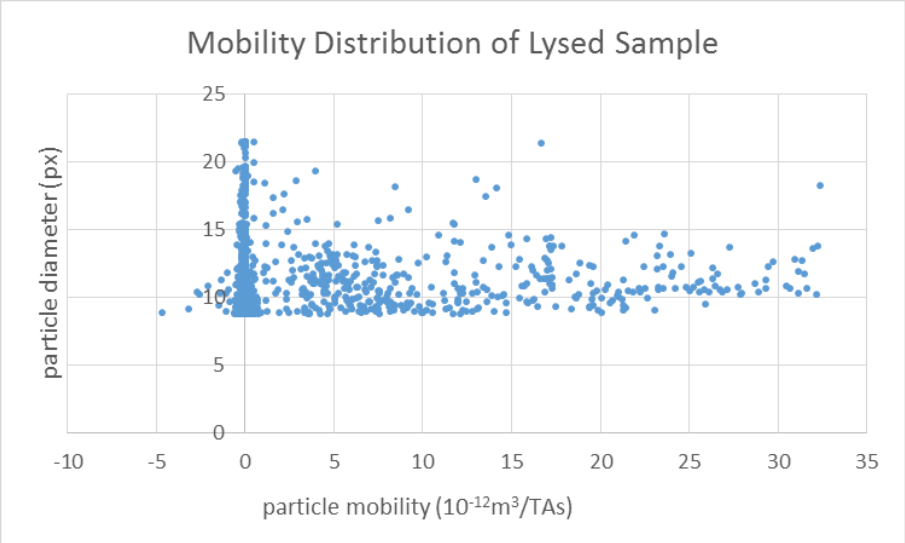

Figure 5.54: xy Plots for Sample Lysed

process reduced the number of RBCs, and make the detection for labeled cell possible.

5.6 Conclusions

The result of high concentration capture shows the device's ability in handling large amount of tumor cells. In blood sample, the tumor cell's concentration is less than 1000 cells/ml, so the test condition with $10^6 \sim 10^7$ cells/ml is greatly exceeding the upper limit

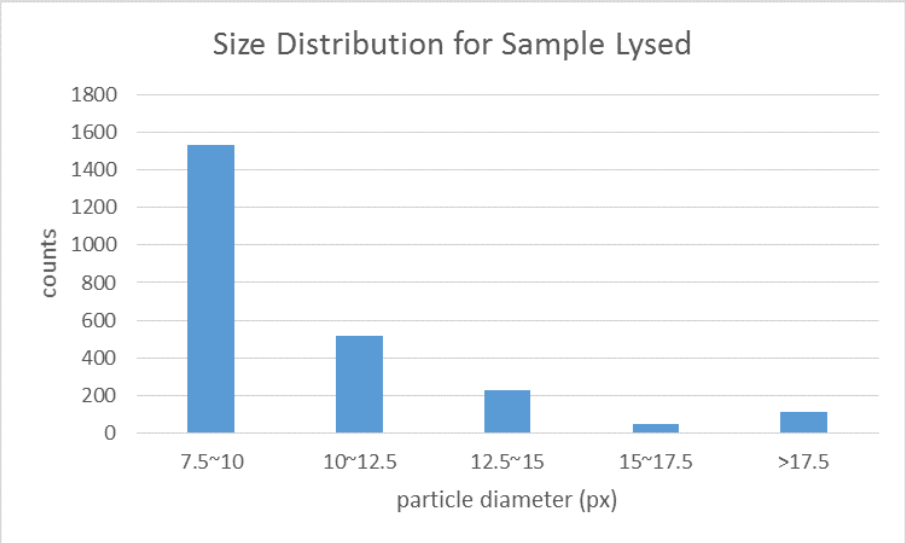

Figure 5.55: Size Distribution for Sample Lysed

Mobility (m^3/TAs)	counts
<0.005	2127
0.005∼0.01	121
0.01∼0.015	56
0.015∼0.02	56
0.02∼0.025	38
>0.025	38

Table 5.21: Counts of Lysed Sample vs Mobility

of the magnetic trap. Still, the device can stably capture over 60% of labeled tumor cells. This proves the number of labeled cells the device can capture is over 10^6 cells, which is greatly larger than the amount of tumor cells actually in a patient's blood sample. And this shows the system is adequate in performing the task of cell separation. It's discovered that the concentration of magnet beads and cells at a ratio over 10:1, the capture ratio will reach a capture ratio over 80%. As in practical use, the ratio is much higher than 10:1, so the separation is proved to be a successful method.

The analysis result from the Hyperflux$^{\text{tm}}$ showed difference particles and their properties in the mixer. Unlabeled cells are varied in size and have a mobility around 0, free-moving magnetic beads have a small size and high mobility, and labeled cells have a larger size than free-moving magnetic beads and the highest mobility. In the analyzer report of magnetic beads, we may see the original sample contains all three types of particles.

After separation. Most particles with low mobility is flowing through the separator and into the waste flow, the captured cells and free-moving magnetic beads stay inside the device. The Hyperflux$^{\text{tm}}$ result proves the device can separate the labeled cells from unlabeled ones with a good selectivity.

From the data we have via Hyperflux$^{\text{tm}}$, we may have a better understanding of cell labeling and separation. The result of magnetic beads track shows particles with higher mobility can display a long track in the system, while particles with little or no mobility won't display a track. The histogram of mobility shows peaks of particles detected. The magnetic beads in reagent have a sharp and tall peak of mobility around $1.5*10^{-11}m^3$/TAs, while the labeled cell has a magnetophoretic mobility higher than this value. For inactive particles, the mobility is usually around $10^{-13}m^3$/TAs. The significant difference makes labeled cells easy to detect.

The xy-plots of particle distributions show a lot of particles have both a low magnetophoretic mobility as well as a small diameter. These inactive particles are probably beads without magnetophoretic mobility, the dirt inside the solution or just exists in detector.

With a change of system setting, its possible to screen out these undesired particles. The magnetic beads have a relatively small diameter (7.5∼10 px) and moderate mobility, while labeled cells have a larger diameter as well as higher mobility. The size distribution and mobility counting shows the pattern of labeled cells as well as magnetic beads.

The multistage design proves necessary in supporting a wider range of magnet bead's choice. In this test, the labeled cells are collected within the first two sets of magnetic poles, indicating labeled cells labeled with lower magnet mobility can still be captured by the magnetic trap.

The result of cell mixing shows that at low cell concentration, the cell can be successfully both labeled and trapped at a flow rate around 1ml/min. The plotting pattern of cells labeled in the static mixer from Hyperflux^{tm} is the same as labeled samples using shake bed. This proves the effect of static mixer is same as traditional methods. Thus cells can be considered as successfully labeled.

The result with whole blood also proves the device's ability. With adequate treatments, the large number of unlabeled cell won't affect the result of detection and separation. Although some cells tends to be left inside the magnetic trap, the device proved effective in separating tumor cells from blood.

Still there's work to be done, first is the purity of magnetic beads, which will affect the particle detection. The existence of particles with low mobility and diameter makes it difficult to determine different types particles, so a method to remove the particles from background will be necessary. The quantum dots is used in CTC's detection, however, further tests are still in need to test the labeling process and efficiency. The microfluidic cytometer also needs further tests as well.

5.7 Acknowledges

This research was supported by U. S. Department of Health and Human Services, National Institutes of Health, National Cancer Institute Small Business Innovation Research

(SBIR) contract HHSN261201000067C to Techshot, Inc. and by Auburn University. We thank Ikotech for providing Hyperflux system, and Dr Boland in Techshot, Inc provides support for laboratory work.

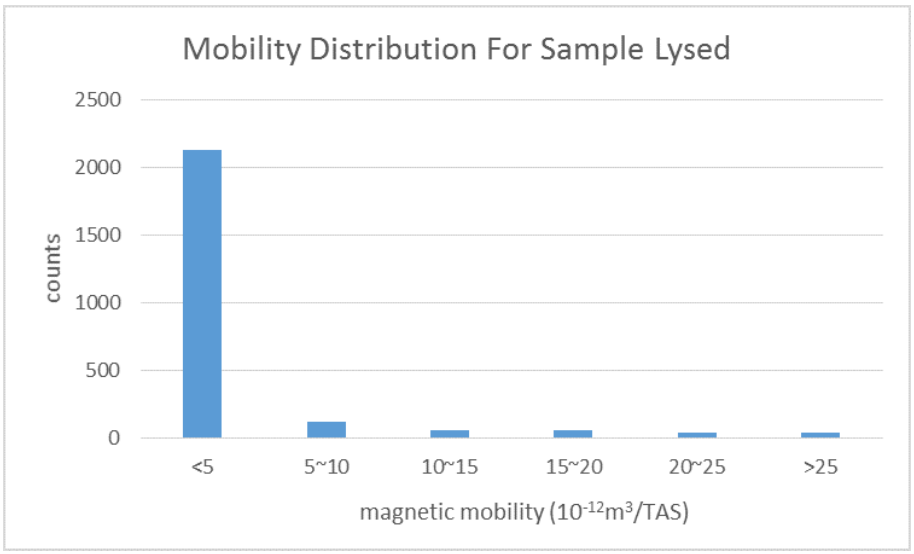

Figure 5.56: Magnet Mobility Distribution for Sample Lysed

Bibliography

[1] Etzioni, R., N. Urban, S. Ramsey, Mcintosh M., Schwartz S., Reid B., Radich J. Anderson G. and Hartwell L. 2003. "The case for early detection", Nature Reviews (Cancer), 3, 1-10.

[2] Wulfkuhle, J. D., L. A. Liotta and E. F. Petricoin, 2003. "Proteomic applications for the early detection of cancer", Nature Reviews (Cancer), 3, 267-275

[3] America Cancer Society: American Cancer Society. Cancer Facts & Figures 2015. Atlanta: American Cancer Society; 2015

[4] Gallagher, D. J., M. I. Milowsky, N. Ishill, A. Trout, M. G. Boyle, J. Riches, M. Fleisher and D. F. Bajorin, 2009. "Detection of circulating tumor cells in patients with urothelial cancer"; Annals of Oncology, 20(2), 305308.

[5] Cohen, S. J., C. J. Punt, N. Iannotti, B. H. Saidman , K. D. Sabbath, N. Y. Gabrail, J. Picus, M. Morse, E. Mitchell, M. C. Miller, G. V. Doyle, H. Tissing and L. W. Terstappen, 2008. "Relationship of circulating tumor cells to tumor response, progression-free survival, and overall survival in patients with metastatic colorectal cancer". J. Clin. Oncol., 26(19), 3213-3221..

[6] Fan, T., Q. Zhao, J. J. Chen, W-T. Chen and M. L. Pearl, 2009. "Clinical significance of circulating tumor cells detected by an invasion assay in peripheral blood of patients with ovarian cancer", Gynecologic Oncology, 112, 185-191.

[7] Allard, W. J., J. Matera, M. C. Miller, M. Repollet, M. C. Connelly, C. Rao, A. G. J. Tibbe, J. W. Uhr and L. W. M. M. Tersappen, 2004. "Tumor cells circulate in the peripheral blood of all major carcinomas but not in healthy subjects or patients with nonmalignant diseases", Clin. Cancer Res., 10, 6897-6904.

[8] Pachmann K., Dengler R., Lobodasch K., Frhlich F, Kroll, T., Rengsberger M., Schubert R., Pachmann U., 2008; An increase in cell number at completion of therapy may develop as an indicator of early relapse QuantiWcation of circulating epithelial tumor cells (CETC) for monitoring of adjuvant therapy in breast cancer; J Cancer (2008) 134:59 Res Clin Oncol 65

[9] Lustberg M , Jatana KR , Zborowski M , Chalmers JJ; Emerging technologies for CTC detection based on depletion of normal cells. Recent Results in Cancer Research. Fortschritte der Krebsforschung. Progres Dans les Recherches sur le Cancer [2012, 195:97-110]

[10] Yukako S.; Junko K.; Takahito A.; Rie T. Shogo N; Miwa Y.; Kimihito F; Miwa A.; Tsuneo I.; Takashi F.; Katsumasa K; Clinical significance of circulating tumor cells (CTCs) with respect to optimal cut-off value and tumor markers in advanced/ metastatic breast cancer; Breast Cancer (2016) 23:120127

[11] Baker M., W. E Gillanders, K. Mikhitarian, M. Mitas and D. J. Cole, 2003. "The molecular detection of micrometastatic breast cancer", Amer. J. Surg., 186(4), 351-358..

[12] Wang, N., Lan, S., Li H., Hu Y., Du W., Liu W, Zheng J., Huang S., Qu, X.; "Detection of circulating tumor cells and tumor stem cells in patients with breast cancer by using flow cytometry"; Tumor Biol. (2012) 33:561569.

[13] Bossolasco,P., Ricci, C., Farina,G., Soligo,D., Pedretti, D., Scanni,A., Deliliers,G., "Detection of micrometastatic cells in breast cancer by RT-PCR for the mammaglobin gene", Cancer Detection and Prevention 26 (2002) 6063.

[14] Cristofanilli, M., Thomas B., Ellis, M., Stopeck, A, Matera, J., Miller, C., Reuben, J, Doyle, G., Allard J., Terstappen, L and Hayes, D. "Circulating Tumor Cells, Disease Progression, and Survival in Metastatic Breast Cancer"; N Engl J Med 2004;351:781-91.

[15] Long F., Gao C., Shi H.C., He M., Zhu A.N., Klibanov A.M., Gu A.Z., 2011; "Reusable evanescent wave DNA biosensor for rapid, highly sensitive, and selective detection of mercury ions". Biosensors and Bioelectronics 26 (2011) 40184023

[16] Tong X, Yang L, Lang JC, et al. Application of immunomagnetic cell enrichment in combination with RT-PCR for the detection of rare circulating head and neck tumor cells in human peripheral blood. Cytometry B Clin Cytom. 2007;72:310323.

[17] Qian X.; Peng X.H., Ansari, D. O., Goen, Q., Chen, G. Z., Shin D. M. , Yang L., Young A. N., Wang M.D. 2008; Nie S.; "In vivo tumor targeting and spectroscopic detection with surface-enhanced Raman nanoparticle tags"; NATURE BIOTECHNOLOGY VOLUME 26 NUMBER 1 JANUARY 2008

[18] Wu,Y.; Clayton,J D,; Brandon,L;,Priya B.; Lustberg,M.,B; Zborowski,M.; Chalmers,J,J, 2013, "Isolation and analysis of rare cells in the blood of cancer patients using a negative depletion methodology." METHODS 64, no. 2, 169 - 182.

[19] Subramaniam D. R.; Gee D. King, M. R.; 2013; "Deformablecellcellandcellsubstrateinteractionsin semi-infinitedomain"; Journal ofBiomechanics46(2013)10671074

[20] Ruan, G., Vieira, G., Henighan, T., Chen, A., Thakur, D.; Sooryakumar, R., Winter, J.; 2010; "Simultaneous Magnetic Manipulation and Fluorescent Tracking of Multiple Individual Hybrid Nanostructures"; Nano Letters. 2010, vol10, 22202224

[21] Molloy, T. J., L. A. Devriese, H. H. Helgason, A. J. Bosma, M. Hauptmann, E. E. Voest, J. H. Schellens and L. J. van't Veer, 2011. "A multimarker QPCR-based platform for the detection of circulating tumour cells in patients with early-stage breast cancer", Br. J. Cancer, 104(12), 1913-1919.

[22] Rosenbach, A. E., P. Koria, J. Goverman, K. T. Kotz, A. Gupta, M. Yu, S. P. Fagan, D. Irimia and R. G. Tompkins, 2011. "Microfluidics for T- lymphocyte cell separation and inflammation monitoring in burn patients", Clin. & Trans. Sci., 4(1), 6368.

[23] Farlow E., Patel K., Basu S.; 2010; "Development of a Multiplexed Tumor-Associated Autoantibody-Based Blood Test for the Detection of Non -Small Cell Lung Cancer"; Clin Cancer Res 2010;16:3452-3462

[24] Punnoose, E. A., S. K. Atwal, J. M. Spoerke, H. Savage, A. Pandita, R-F. Yeh, A. Pirzkall, B. M. Fine, L. C. Amler, D. S. Chen and M. R. Lackner, 2010. "Molecular biomarker analyses using circulating tumor cells", PLOS ONE, 5(9).

[25] Stott, S. L., C. H. Hsu, D. I. Tsukrov, M. Yu, D. T. Miyamoto, B. A. Waltman, S. M. Rothenberg, A. M. Shah, M. E. Smas, G. K. Korir, F. P. Floyd Jr., A. J. Gilman, J. B. Lord, D. Winokur, S. Springer, D. Irimia, S. Nagrath, L. V. Sequist, R. J. Lee, K. J. Isselbacher, S. Maheswaran, D. A. Haber and M. Toner, 2010. "Isolation of circulating tumor cells using a microvortex-generating herringbone-chip", Proc Natl Acad Sci U S A., 107(43), 18392-18397.

[26] Shan Z., Zhou Z., Chen H., Zhang Z., Zhou Y., Wen A., Oakes K. D., Servos M. R., 2012; "PCR-ready human DNA extraction from urine samples using magnetic nanoparticles"; Journal of Chromatography B, 881 882 (2012) 63 68

[27] Khleif S. N., Doroshow J. H., Hait W. H.,2010; AACR-FDA-NCI Cancer Biomarkers Collaborative Consensus Report: Advancing the Use of Biomarkers in Cancer Drug Development; Clin Cancer Res 2010;16:3299-3318

[28] Cho M., Xiao Y., Nie J., Stewart R., Csordas A., Oh S. S., Thomson J., Soh H., 2010; "Quantitative selection of DNA aptamers through microfluidic selection and high-throughput sequencing"; PNAS August 31, 2010 vol. 107 no. 35 1537315378

[29] Haun, J. B., T-J. Yoon, H. Lee and R. Weissleder, 2010. "Magnetic nanoparticle biosensors, Nanomedicine and Nanobiotechnology", 2, 291-304.

[30] Kildew, B. "Magnetic Micropar ticles Used in Molecular and Cellular Isolations"; BUSINESS BR IEFING : MEDICAL DEVICE MANUFACTURING & TECHNOLOGY 2002

[31] Issadore, D., H. Shao, J. Chung, A. Newton, M. Pittet, R. Weissleder and H. Lee, 2011. "Self-assembled magnetic filter for highly efficient immunomagnetic separation", Lab Chip, 11, 147151.

[32] Afshar, R., Moser Y., Lehnert T. and Gijs M. A., 2011. "Magnetic particle dosing and size separation in a microfluidic channel"; Sensors and Actuators B 154 (2011) 7380

[33] Chung, Y-K., J. Reboud, K. C. Lee, H. M. Lim, P. Y. Lim, K. Y. Wang, K. C. Tang, H. M. Ji and Y. Chen. (2011). An electrical biosensor for the detection of circulating tumor cells, Biosensors and Bioelectronics, 26(5), 2520-2526.

[34] Zheng S, H. Lin, J. Q. Liu, M. Balic, R. Datar, R. J. Cote and Y. C. Tai, 2007. Membrane microfilter device for selective capture, electrolysis and genomic analysis of human circulating tumor cells, J Chromatogr A., 1162(2), 154-161.

[35] Xu, W., L. Cao, L. Chen, J. Li, X. F. Zhang, H. H. Qian, X. Y. Kang, Y. Zhang, J. Liao, L. H. Shi, Y. F. Yang, M. C. Wu and Z. F. Yin, 2011. Isolation of circulating tumor cells in patients with hepatocellular carcinoma using a novel cell separation strategy, Clin Cancer Res., 17(11), 3783-3793.

[36] Choi J.W. Liakopoulos, T., Ahn, C.; "An on-chip magnetic bead separator using spiral electromagnets with semi-encapsulated permalloy"; Biosensors & Bioelectronics 16 (2001) 409416

[37] Jarrige, V., J. H. Nieuwenhuis, J. P. H. F. van Son, M. F. W. C. Martens, and J. L. M. Vissers, 2010. A fast intraoperative PTH point-of-care assay on the Philips handheld magnotech system, Langenbecks Arch Surg., 396(3), 337343.

[38] Li W. W., Shen G. P., Liu X.W., Shen G. P., Liu X. W., Cai P. J., Sun M., Xiao X., Wang Y. K., Tong Z. H., Dong F. Yu H. Q., 2011; Impact of a static magnetic field on the electricity production of Shewanella-inoculated microbial fuel cells; Biosensors and Bioelectronics 26 (2011) 39873992

[39] Haverkort J. W., Kenjeres, S., Kleijin C. R., Computational Simulations of Magnetic Particle Capture in Arterial Flows; Annals of Biomedical Engineering, Sept 16 2009 Published online.

[40] Wiwatanapataphee B., Chayantrakom C., Wu Y. H., 2007; Mathematical Modelling and Numerical Simulation of Fluid-Magnetic Particle Flow in a Small Vessel; INTERNATIONAL JOURNAL OF MATHEMATICAL MODELS AND METHODS IN APPLIED SCIENCES; Issue 3, Volume 1, 2007

[41] Habibi, M. R., and M. Ghasemi, 2011. Numerical study of magnetic nanoparticles concentration in biofluid (blood) under influence of high gradient magnetic field, J. Magnetism & Magnetic Matl., 323(1) 32-38

[42] Moore, L.R., Nehl F., Dorn J., Chalmers, J. J., Zborowski, M.; Open Gradient Magnetic Red Blood Cell Sorter Evaluation on Model Cell Mixtures; IEEE TRANSACTIONS ON MAGNETICS, VOL. 49, NO. 1, JANUARY 2013

[43] Lianidou E.S., Markou A, Circulating Tumor Cells in Breast Cancer: Detection Systems, Molecular Characterization, and Future Challenges, Clinical Chemistry 57:9 12421255 (2011)

[44] Balic M, Rapp N, Stanzer S, Lin H, Strutz J, Szkandera J, et al. Novel immunofluorescence protocol for multimarker assessment of putative disseminating breast cancer stem cells. Appl Immunohistochem Mol Morphol 2011;19:33 40.

[45] Markou A, Strati A, Malamos N, Georgoulias V, Lianidou ES. Molecular characterization of circulating tumor cells in breast cancer by a liquid bead array hybridization assay. Clin Chem 2011; 57:42130

[46] Hsieh, H. B., D. Marrinucci, K. Bethel, D. N. Curry, M. Humphrey, R. T. Krivacic, J. Kroener, L. Kroener, A. Ladanyi, N, Lazarus, P. Kuhn, R. H. Bruce and J. Nieva, 2006. High speed detection of circulating tumor cells, Biosensors and Bioelectronics, 21(10), 18931899.

[47] Pachmann, K., Camara O., Kavallaris A., Krauspe, S., Malarski, N., Gajda, M., Kroll, T., Jrke, Hammer U., Altendorf-Hofmann A., Rabenstein C., Pachmann U.,Runnebaum I. and Hffken K., 2008. Monitoring the response of circulating epithelial tumor cells to adjuvant chemotherapy in breast cancer allows detection of patients at risk of early relapse, Clin. Oncol., 26(8), 1208-15

[48] Sieuwerts, A. M., B. Mostert, J. Bolt-de Vries, D. J. E. Peeters, F. de Jongh, J. Stouthard, A. van Galen, L. Y. Dirix, P. A. van Dam, V. de Weerd, J. Kraan, P. van der Spoel, R. Ramirez-Moreno, C. van Deurzen, M. Smid, J. Yu1, J. Jiang, Y. Wang, J. Gratama, S. Sleijfer, J. A. Foekens and J. W Martens, 2011. mRNA and microRNA expression profiles in circulating tumor cells and primary tumors of metastatic breast cancer patients, Clin. Cancer Res., 17, 3600-3618.

[49] Zheng, S., H. K. Lin, B. Lu, A. Williams, R. Datar, R. J. Cote and Y-C. Tai, 2011. 3D microfilter device for viable circulating tumor cell (CTC) enrichment from blood, Biomed. Microdevices, 13, 203-213.

[50] Hsieh, Y. H., L. J. Lai, S. J. Liu and K. S. Liang, 2011. Rapid and sensitive detection of cancer cells by coupling with quantum dots and immunomagnetic separation at low concentrations, Biosens. Bioelectron., 26(10), 4249-4252.

[51] Nagrath, S., L. V. Sequist, S. Maheswaran, D. W. Bell, D. Irimia, L. Ulkus, M. R. Smith, E. L. Kwak, S. Digumarthy, A. Muzikansky, P. Ryan, U. J. Balis, R. G. Tompkins, D. A. Haber and M. Toner, 2007. Isolation of rare circulating tumour cells in cancer patients by microchip technology, Nature, 450, 1235-1240.

[52] Zhao C., Chen X., 2011; Microfluidic separation of viruses from blood cells based on intrinsic transport processes; BIOMICROFLUIDICS 5, 032004 (2011)

[53] Seo, H-K., Y-H. Kim, H-O. Kim and Y-J. Kim, 2010. Hybrid cell sorters for on-chip cell separation by hydrodynamics and magnetophoresis, J. Micromech. Microeng., 20(9), 095019.

[54] Han, K-H., Han A.and Frazier B., 2006. Microsystems for isolation and electrophysiological analysis of breast cancer cells from blood, Biosensors and Bioelectronics, 21(10), 1907-1914.

[55] Cui S., Liu Y, Wang W., Sun Y., Fan Y., 2011; A microfluidic chip for highly efficient cell capturing and pairing; BIOMICROFLUIDICS 5, 032003

[56] Warkiani, ME; Khoo, BL ; Wu, LD; Tay, AKP; Bhagat, AAS; Han, J; Lim, CT; Ultra-fast, label-free isolation of circulating tumor cells from blood using spiral microfluidics; Nature Protocols 11, 134148 (2016)

[57] Kuczenski R. S., Chang, H.C., Revzin, A., 2011; Dielectrophoretic microfluidic device for the continuous sorting of Escherichia coli from blood cells; BIOMICROFLUIDICS 5, 032005

[58] Jerant A. F., Johnson J. T., Sheridan, C. D., Caffrey T. J., 2000; Early Detection and Treatment of Skin Cancer; Am Fam Physician. 2000 Jul 15;62(2):357-368.

[59] Lucas R., McMichael T., Smith W., Armstrong B., 2006; Solar Ultraviolet Radiation: Global burden of disease from solar ultraviolet radiation; World Health Organization Public Health and the Environment Geneva 2006, Environmental Burden of Disease Series, No. 13

[60] Braam, K. I., Overbeek A., Kaspers, G. J. L., Ronckers, C. M., Schouten-van Meeteren A.Y.N., Van D. Broeder E. and Veening M. A., 2012; Malignant Melanoma as Second Malignant Neoplasm in Long-Term Childhood Cancer Survivors: A Systematic Review; Pediatr Blood Cancer 2012;58:665674

[61] Nezos, A., P. Msaouel, N. Pissimissis, P. Lembessis, A. Sourla, A. Armakolas, H. Gogas, A. J. Stratigos, A. D. Katsambas and M. Koutsilieris, 2011. Methods of detection of circulating melanoma cells: a comparative overview; Cancer Treatment Review, 37(4), 284290.

[62] Ma J., Lin J. Y., Alloo A., Wilson B. J., Schatton T., Zhan Q., Murphy G. F., Hodi S., Frank N.Y., Frank, M. H., 2010; Isolation of tumorigenic circulating melanoma cells; Biochemical and Biophysical Research Communications 402 (2010) 711717

[63] Giorgi V. D., Pinzani P., Salvianti F., Panelos J., Paglierani M., Janowska A.,Grazzini M., Wechsler J., Orlando C., Santucci M., Lotti T., Pazzagli M. and Massi D.,2010; Application of a Filtration- and Isolation-by-Size Technique for the Detection of Circulating Tumor Cells in Cutaneous Melanoma; Journal of Investigative Dermatology (2010) 130, 24402447

[64] Georgieva, J; Milling, A; Orfanos, CE; Geilen, CC, Magnetic bead RT-PCR: establishment of a new method for detecting circulating melanoma cells; MELANOMA RESEARCH Volume: 12 Issue: 4 Pages: 309-317

[65] Steen, S ; Kuhn, JA; Senzer, N; Maples, P; Nemunaitis, J; Genomic and proteomic analysis of high risk cancer patients; ANNALS OF SURGICAL ONCOLOGY Volume: 15 Pages: 71-72 Supplement: 2

[66] Han S. I., Han K.H., Frazer. B, Ferrance J.P., Landers, J. P. 2009; An automated micro-solid phase extraction device involving integrated high-pressure microvalves for genetic sample preparation; Biomed Microdevices (2009) 11:935942

[67] Soper, S. A., K. Brown, A. Ellington, B. Frazier, G. Garcia-Manero, V. Gau, S. I. Gutman, D. F. Hayes, B. Korte, J. L. Landers, D. Larson, F. Ligler, A. Majumdar, M. Mascini, D. Nolte, Z. Rosenzweig, J. Wang and D. Wilson, 2006. Point-of-care biosensor systems for cancer diagnostics/prognostics, Biosensors and Bioelectronics, 21(10), 19321942

[68] Kotz, K.T., Xiao W., Graziano C., Qian W. J.; Russon A., Warner E, Moldawer L., De A., Benkey P., Rosenbach A., Goverman J. Fagan S., Brownstein B. Toner M, Fagan. S etc al.2010; Clinical microfluidics for neutrophil genomics and proteomics; nature medicine VOLUME 16, NUMBER 9, 1042-1048 SEPTEMBER 2010

[69] Tierling S., Sers C., Lehmann A, Walter, J., A fast, cost-efficient and sensitive approach for KRAS mutation detection using multiplexed primer extension with IP/RP-HPLC separation, Int. J. Cancer: 130, 567574 (2012)

[70] Maetzel D., Denzel S., Mack B., Cansis M., Went P., Benk M., Kieu C., Papior P., Baeuerle P., Munz M., Gires O.,2009; Nuclear signalling by tumour-associated antigen EpCAM; Nature Cell Biology 11, 162 - 171 (2009)

[71] Schweitzer M., Generalizations of the Finite Element Method, Cent. Eur. J. Math. 10(1) 2012 3-24

[72] Charles W. M., Vandenberg E., Lin H.X., Heemink A. W., Verlaan M., 2007; Parallel and distributed simulation of sediment dynamics in shallow water using particle decomposition approach; J. Parallel Distrib. Comput. 68 (2008) 717728

[73] Mohanty, S., T. Baier and F. Schnfeld, 2010. Three-dimensional CFD modelling of a continuous immunomagnetophoretic cell capture in BioMEMs, Biochem. Engr, J., 51(3), 110-116.

[74] Marchetta J. G., Roos K., 2008; Simulating magnetic positive positioning of cryogenic propellants in a transient acceleration field; Computers & Fluids 38 (2009) 843850

[75] Tang X. W., Sun Z. F., Chen G.C., 2012; Simulation of the relationship between porosity and tortuosity in porous media with cubic particles; Chin. Phys. B Vol. 21, No. 10 (2012) 100201

[76] Ramamurthy A. S., F.ASCE; Han S. S. and Biron P. M. 2013; Three-Dimensional Simulation Parameters for 90 Open Channel Bend Flows; J. Comput. Civ. Eng. 2013.27:282-291.

[77] Hamidipour M., Chen J. Larachi F.2012, CFD study on hydrodynamics in three-phase fluidized bedsApplication of turbulence models and experimental validation; ChemicalEngineeringScience78(2012)167180

[78] Toljic N., Adamiak K., Peter Castle G. S., Kuo H. H., Fan H. T., 2012; 3D numerical model of the electrostatic coating process with moving objects using a moving mesh; Journal of Electrostatics 70 (2012) 499e504

[79] Xin,SH; Le Quere, P; Stability of two-dimensional (2D) natural convection flows in air-filled differentially heated cavities: 2D/3D disturbances; FLUID DYNAMICS RESEARCH Volume: 44 Issue: 3

[80] Xu J. , Mahajan K. , Xue W., Winter J. , Zborowski M , Chalmers J J.; Simultaneous, single particle, magnetization and size measurements of micron sized, magnetic particles; J Magn Magn Mater. 2012 Dec 1;324(24):4189-4199.

[81] Plouffe, B. D. Lewis L. H. and Murthy S. K., 2011. Computational design optimization for microfluidic magnetophoresis , Biomicrofluidics, 5, 013413.

[82] Cichocki B., Felderhof B. U., 1990; Diffusion of Brownian particles with hydrodynamic interaction and hard core repulsion; J. Chern. Phys. 94 (1),1 January 1991

[83] Sieuwerts A.M, Kraan J, Bolt J, van der Spoel P, Elstrodt F, Schutte M, et al. Anti-epithelial cell adhesion molecule antibodies and the detection of circulating normal-like breast tumor cells. J Natl Cancer Inst 2009;101:61 6.

[84] Afshar, R., Moser Y., Lehnert T. and Gijs M. A., 2011. Magnetic particle dosing and size separation in a microfluidic channel; Sensors and Actuators B 154 (2011) 7380

[85] Mostert, B., S. Sleijfe, J. A. Foekens and J. W. Gratam, 2009. Circulating tumor cells (CTCs): detection methods and their clinical relevance in breast cancer, Cancer Treatment Reviews, 35, 463-474.

[86] Knigsberg, R., M. Gneist, D. Jahn-Kuch, G. Pfeiler, G. Hager, M. Hudec, C. Dittrich and R. Zeillinger, 2010. Circulating tumor cells in metastatic colorectal cancer: efficacy and feasibility of different enrichment methods, Cancer Letters, 293, 117123.

[87] Paul, Edward L. (2004). Handbook of Industrial Mixing-Science and Practice. Hoboken NJ: John Wiley & Sons. pp. 399 section 73.1.4.

[88] Vuorema, A.; Meadows, H; Ibrahim N. B.; Cambo, J.D.; Puig M. C.; Vagin, M. Y.; Karyakin, A. A.; Sillanpaa, M.; Marken, F.; Ion Transport Across Liquid j Liquid Interfacial Boundaries Monitored at Generator-Collector Electrodes; Electroanalysis 2010, 22, No. 24, 2889 2896

[89] Zeliadt N., Capturing Cancer Cells on the Move, http://www.the-scientist.com/?articles.view/articleNo/39503/title/Capturing-Cancer-Cells-on-the-Move/#articleComments

[90] Lin C.T; Hou, H W; Warkiani,M. E.; Khoo, B L; Li, Z R; Soo, R. A.; Tan D. SW, Lim W.T, Han J., Asgar A., Bhagat S., Isolation and retrieval of circulating tumor cells using centrifugal forces; Scientific Reports 3, Article number: 1259, Published 12 February 2013

[91] Gascoyne PR, Shim S. Isolation of Circulating Tumor Cells by Dielectrophoresis, Cancers 2014, 6(1), 545-579;

[92] Toner M, Ozkumur E, Shah A. M.; Emmink B. L., Chen P.; Morgan, B. L.; Barber T. A.; Smith K. etc al.; Inertial Focusing for Tumor AntigenDependent and Independent Sorting of Rare Circulating Tumor Cells; Sci Transl Med 3 April 2013: Vol. 5, Issue 179, p. 179ra47

[93] Kuhn P.; Marrinucci D., Bethel K., Kolatkar A, Luttgen M., Malchiodi1 M., Baehring F. , Voigt K., Lazar D., Nelson D. etc al; Fluid Biopsy in Patients with Metastatic Prostate, Pancreatic and Breast Cancers; Phys Biol. 2012 February ; 9(1): 016003.

[94] Gossett D, Weaver W, Mach A, Hur S, Tse W, Lee W, Amini H and Carlo D.;Label-free cell separation and sorting in microfluidic systems; Anal. bioanal chem 2010, 397, 3249-3267

[95] Choesmel, V; Anract, P; Hoifodt, H; Thiery, JP; Blin, N; A relevant Immunomagnetic assay to detect and characterize epithelial cell adhesion molecule-positive cells in bone marrow from patients with breast carcinoma - Immunomagnetic purification of micrometastases; CANCER Volume: 101 Issue: 4 Pages: 693-703

[96] Zhou J, Pang H, Garcia L, Iborra E, Clement M, Miguel R, Jin H, Luo J K, Smith S., Dong S R, Wang D M., Fu Y Q; Discrete microfluidics based on aluminum nitride surface acoustic wave devices; Microfluid Nanofluid (2015) 18:537548

[97] Hou H. W., Warkiani M. E., Khoo B. L., Li Z. R.; Soo R. A.; Tan D. S. W.; Lim W. K.; Han J., Bhagat A. S., Lim C. T; Isolation and retrieval of circulating tumor cells using centrifugal forces, SCIENTIFIC REPORTS 3 : 1259; published in Feb,12, 2013 DOI: 10.1038/srep01259

[98] Chen P., Huang Y.Y., Hoshino K., Zhang X. J.; Multiscale immunomagnetic enrichment of circulating tumor cells: from tubes to microchips; Lab Chip 2014. 14. 446-458

[99] Marrinucci D., Bethel K, Kolatkar A, Luttgen M, Malchiodi, M, Barhring F, Voigt, K,; Lazar D, Nieva J, Bazenova, L, Ko A. H., Coward M.; Yang X., Metzner T., Lamy R., Honnatti M., Yoshioka C., Kunken J., Petrova Y, Sok D., Nelson D., Kuhn P.; Fluid Biopsy in Patients with Metastatic Prostate, Pancreatic and Breast Cancers; Phys Biol. 2012 February ; 9(1): 016003. doi:10.1088/1478-3975/9/1/016003.

[100] Khashan S. A., Elnajjar E., Haik Y., 2011 CFD simulation of the magnetophoretic separation in a microchannel; Journal of Magnetism and Magnetic Materials 323 (2011) 29602967

[101] Liu M; Age distribution and the degree of mixing in continuous flow stirred tank reactors; Chemical Engineering Science 69 (2012) 382393

[102] Liu M.; A method for computing the degree of mixing insteady continuous flow systems; Chemical Engineering Science 66(2011) 30453048

[103] Richardson J.K.; Zaki W.N.; Sedimentation and fluidization: part 1; Trans Instn Chem Engrs, vol 32 1954

[104] Garcia P. D., Rubio M.A., 2013; Single and multi-particle passive microrheology of low-density fluids using sedimented microspheres; APPLIED PHYSICS LETTERS 102, 074101 (2013)

[105] $htttps://en.wikipedia.org/wiki/static_mixer$, figure created by Alastair Bor in Mar 2009

[106] $physic.info/viscosity$Elert. G,viscosity, the physics hypertextbook

Appendix A

operation procedure for cell capture test at high concentration

1.1 Prepare immunomagnet beads

For cell labeling process, the concentration of cells is less than 10^7 cells/ml, and according to the Dynabeads' manual, when working with lower volumes than $1*10^7$ cells or 1 mL blood, use the same volumes as for $1*10^7$ cells or 1 mL blood.

1.2 For the isolation buffer, we use PBS with 1% HSA as the solution.

1.3 The amount of antibody required is 1 microgram/10^7 cells, and considering the activity loss during the frost-defrost cycle, the amount of antibody should be increased. The original concentration of antibody is 0.5mg/ml, so 3 microliter of original antibodies is required for each sample.

In our test, 3 microliter of original antibody is diluted with PBS solution into 1ml of isolation buffer as antibody source.

Step 2: Attach magnet beads with antibodies

2.1. Re-suspend the magnetic beads in the vial, here we use a vortex mixer (Cole-Palmer, item number UX-04726-01) and run for 30 seconds.

2.2. Add 1ml Isolation Buffer to a tube.

2.3. Transfer 50 μL of magnetic beads (from original sample) into the tube, and re-suspend on the vortex mixer for 30s.

2.4. Take a magnet and hold it against the conical part of the tube, keep for 2$\sim$3 min and discard the supernatant. Check the supernatant under the microscope to see if it contains microbeads.

2.5. Remove the tube from the magnet.

Step 3. Label cells with magnetic particles

3.1. Add antibody from the dilute solution (around 1ml) into magnetic beads

3.2 Incubate for 30 minutes at room temperature with a shaker-table; the rocking rate is 15 rpm.

3.3. Place the tube in a magnet for 2 min and discard the supernatant. Carefully watch the tube during this step to avoid accidental discard of beds.

3.4. Remove the tube from the magnet and add 1 mL Isolation Buffer.

3.5. Repeat steps 3.3 and 3.4 once to remove excess of antibodies.

3.6. Place the tube in the magnet for 2 min and remove the supernatant to sample B. (Sample B will be checked later for containing magnet beads)

3.7. Take 0.5ml of cell suspension from each original culture flask. Collect $20\mu L$ into a pipette and put under hemacytometer and count cells in the central area.

3.9. Add the 1 ml cell suspension to the magnetic beads and re-suspend. Transfer it to the tube.

3.10. Incubate for 20 min at room temperature with the shaker-table, also at 15 rpm.

Step 4. Capture the labeled cells in the magnetic trap

4.1 Take a spare syringe (10ml) filled with 4$\sim$5ml of isolation buffer. Connect the syringe with the tubing of the magnetic trap

4.2 Hold the magnetic trap up vertically, inject the buffer into the system slowly, making sure all bubbles are removed during the process; stop when the magnetic trap is filled with buffer. Use a stopper to seal the outlet of the magnetic trap.

4.3 Remove the syringe with buffer, and connect the trap to a syringe containing the labeled cells. Fix syringes on piston pump.

4.4 Put a centrifuge tube at the outlet of the magnetic trap as waste receptacle. Remove the stopper.

4.5 Start the pump. For a 1 ml sample, set the scale at $80\mu L$, flow velocity at $6\mu L$/min and wait for pumping. The scale exceeds the volume of the cell sample, so keep watching the pump. Here the collected sample at the outlet of the trap is called Waste A.

4.6. Put a stopper onto the trap outlet, remove syringes from the pumping device, and connect the 5 mL syringe with buffer to the trap, insert the buffer syringe into the pump; remove the stopper.

4.7 Use the piston pump to put 5ml of buffer into the system slowly using the same pump speed as was used for the cell sample. The outlet fluid is collected into the Waste A tube as well.

4.8. Put a stopper on the outlet of the magnetic trap, remove the plastic magnetic trap from the magnet poles, take away the Waste A tube (containing buffer and untrapped cells in this case); record the volume of Waste A.

4.9 Put a clean 15 mL centrifuge tube at the end of the trap for collecting labeled cells (Sample A).

4.10 Pump the isolation buffer (around 1 ml) into the system, and collect the samples from the magnet trap outlet. Move up and down the syringe to wash the magnetic trap throughout inside. The buffer containing labeled cells will be collected for future analysis. Record the volume of Sample A.

Step 5: Collect the captured labeled cells in Sample A by collecting 20 μL into a pipette, and count the captured cells' concentration in a hemacytometer. Also count the cells from waste fluid as well. Analyze both suspensions using the Hyperflux velocimeter to check the number of magnetic particles and cells as described in the text.

Appendix B

operation procedure for cell labeling and mixing

Step 1: Prepare Materials (same as step 1 in appendix 1)

Step2: Attach magnetic beads with antibody. (same as step 2 in appendix 1)

Step 3: Label cells with magnetic particles

Accordingly, we define the piston dealing with cell sample to be piston A and the piston dealing with reagent to be piston B using two piston pumps as in Appendix 1.

Set the value of the piston pumps as follows:

Piston A: volume is $36\mu L$, flow velocity is $1.2\mu L$/min

This translates to 1.7 mL and 0.056 mL/min using a 6 mL syringe.

Piston B: volume is $180\mu L$, flow velocity is $6\mu L$/min

This translates to 8.3 mL and 0.277 mL/min using a 12 mL syringe.

3.1 Take 0.5 ml of cell suspension from each original culture bottle. Collect 20 l into a pipette and put under hemacytometer and count for cells in central area. (However, at low concentration, it may be difficult to detect tumor cells) Dilute the cell suspension to concentration desired (>104 cells/ml), and keep the volume of cells at 8.3ml.

3.2 Take a spare syringe (35ml) filled with 10 15ml of PBS. Connect the syringe to the tubing of the static mixer and magnetic trap.

3.3 Hold up the static mixer vertically, push buffers into the system slowly, make sure all bubbles are removed during the process, and stop when both static mixer and magnetic trap are filled with buffer. Be sure both are free of bubbles. Use a stopper to seal the outlet of the magnetic trap.

3.4 Remove the syringe with buffer, and connect the mixer with syringe A and B, fix the magnetic trap into the magnetic holder. Fix syringes on piston pumps.

3.5 Put a tube at the outlet of magnet trap as waste receptacle. Remove the stopper.

3.5 Start running the pump, and wait for 30 minutes

3.6 Put a stopper onto the mixer outlet, remove syringes from the pumps, and connect the 12 mL syringe with buffers to the mixer, insert the 12 mL syringe into pump A, remove the stopper.

3.7 Pump 7ml of buffer into the system slowly using the same pump speed as was used for cells.

3.8 Put stopper on the outlet of the magnetic trap, remove the magnet trap from magnet poles, take away the beaker A (containing the mixture of cells, reagent and buffer) for later cell counting and examination by microscope and Hyperflux velocimeter. Clean up; put a clean 15 mL centrifuge tube (or other bio-container) at the outlet of the trap for collecting labeled cells.

3.9 Pump buffer (more than 3ml) into the system, and collect the samples from the magnetic trap's outlet. The buffer containing labeled cells will be collected for Hyperflux^{tm} analysis.

Appendix C

Operational procedure for cell mixing and separation with whole blood

Step 1: Prepare materials

1.1 Prepare immunomagnetic beads. For cell labeling process, the concentration of cells is less than 10^7 cells/ml, and according to the Dynabeads' manual, when working with lower volumes than $1*10^7$ cells or 1 mL blood, use the same volumes as for $1*10^7$ cells or 1 mL blood.

1.2 For the isolation buffer, we use PBS with 1% BSA (Bovine serum albumin) and 1% EDTA as the solution. The solution is stored in the refrigerator.

1.3 The amount of antibody required is 1 microgram/10^7 cells. In our test, considering the activity loss during the frost-defrost cycle, the amount of antibody used is increased. The original concentration of antibody is 0.5mg/ml, so 3 microliters of original antibodies is used for each sample.

1.4 The whole blood used in the test is obtained from a 500ml whole bovine blood sample, provided by Animal Tech, Tyler, TX. To keep the blood from coagulating, 1% of EDTA is added into the blood sample for storage.

1.5 When it was found that blood cells will affect the detection of tumor cells, a lysing agent is used to remove the undesired blood cells. The lysing agent solution consisting of 8% NH4Cl, 0.8% NaHCO3, and 0.3% EDTA is used. The agent is mixed with buffer (PBS) at a ratio of 1:10, and during the separation process, the agent dwelled for 10 minutes in the trap and the RBC debris is rinsed before removing the trap from the magnets.

Step2: Attach magnetic beads with antibody (same as step 2 in appendix 1).

Step 3. Label cells with magnetic particles. Accordingly, we define the piston dealing with the cell sample to be piston A and the piston dealing with reagent to be piston B. Set the values of the piston pumps as follows:

Piston A: volume is $36\mu L$, flow velocity is $1.2\mu L$/min

This translates to 1.7 mL and 0.056 mL/min using a 6 mL syringe.

Piston B: volume is $180\mu L$, flow velocity is $6\mu L$/min

This translates to 8.3 mL and 0.277 mL/min using a 12 mL syringe.

3.1. Take 0.5ml of cell suspension from each origin culture bottle. Collect $20\mu L$ into a pipette and put under the hemacytometer and count cells in the central area. However, at low concentration, it may be difficult to detect tumor cells. Dilute the cell suspension with whole blood to the concentration desired, and keep the volume of cells at 8.3ml.

3.2 Take a spare syringe (35ml) filled with 10 15ml of PBS. Connect the syringe with the tubing of the static mixer and magnetic trap.

3.3 Hold up the static mixer vertically, push buffers into the system slowly, make sure all bubbles are removed during the process, and stop when both static mixer and magnet trap are filled with buffer. Be sure both are free of bubbles. Use a stopper to seal the outlet of the magnetic trap.

3.4 Remove the syringe with buffer, and connect the mixer with syringe A and B, fix the magnetic trap into the magnet holder. Fix syringes on piston pumps.

3.5 Put a tube at the outlet of the magnetic trap as waste receptacle. Remove the stopper.

3.5 Start the pumps and wait for 30 minutes

3.6. Put a stopper onto the mixer's outlet, remove syringes from the pumps, and connect the 12 mL syringe with buffer to the mixer, insert the 12 mL syringe into pump A, and remove the stopper.

3.7 Pump 7ml of buffer into the system slowly using the same pump speed as was used for cells.

3.8 Pump 10 ml lysing solution into the magnetic trap. Let it dwell for 10 minutes in the trap then rinse the RBC debris free before removing the trap from the magnets.

3.9. Put a stopper on the outlet of the magnetic trap, remove the magnetic trap from the magnet poles, take away the beaker A (containing the mixture of cells, reagent and buffer) for later cell counting and examination by microscope and Hyperflux velocimeter. Clean up; put a clean 15 mL centrifuge tube (or other bio-container) at the outlet of the trap for collecting labeled cells.

3.10 Pump buffer (more than 3ml) into the system, and collect the samples from the magnetic trap's outlet. The buffer containing labeled cells will be collected for Hyperfluxtm analysis.